Division of Packaging Logistics

Division of Solid Mechanics

ISRN LUTMDN/TMFL-09/5064

OUTSIDE vs. INSIDE CREASING
- A PARAMETER STUDY

Master's Thesis by

Jennie Lillienberg and Emma Lörd

Supervisors

Magnus Just, Tetra Pak
Annika Olsson, Div. of Packaging Logistics
Matti Ristinmaa, Div. of Solid Mechanics

Printed by MEDIA-TRYCK, Lund, Sweden

For information, address:
Division of Packaging Logistics, Lund University, Box 118, SE-221 00 Lund, Sweden
Homepage: http://www.plog.lth.se

Division of Solid Mechanics, Lund University, Box 118, SE-221 00 Lund, Sweden
Homepage: http://www.solid.lth.se

Abstract

Creasing of paperboard is an essential operation to obtain a well defined shape and strength of a package. The creasing tool consists of one male and one female creasing plate. The male plate presses the paperboard into the female plate and introduces damage in the creasing zone. Today the standard creasing operation at Tetra Pak is that the male creasing plate presses the top ply (print side) of the paperboard, and female is pressed against bottom ply (back side). This is called outside creasing, and the opposite is called inside creasing.

This master's thesis has the purpose of studying the differences between inside and outside creasing with respect to how the paperboard behaves during bending and creasing. Since this area is hardly explored the purpose is to make a broad study about the differences of inside versus outside creasing. Many parameters will be measured and computer simulations will be used to get a better understanding of the parameters involved.

The experimental tests are divided into three different parts: 1) Straight creases are made using a flat bed laboratory creasing tool, 2) A bottom crease pattern is made using a flat bed laboratory creasing tool, 3) The pattern of a Tetra Brik 250ml Base package is made in pilot plant and tested on paperboard and packaging material.

MODDE, software using the method Design of Experiments, is used during two of the experimental parts in order to reduce the number of experiments. Straight creases are simulated using Abaqus built in material models for the continuum model and cohesive interface model for delamination. The creasing operation is simulated with rigid creasing plates while the folding operation is simulated using constraints and boundary conditions.

In the experimental part, for straight creases, there is a significant difference between inside and outside creasing on a few of the responses investigated, but all tests show that change of paperboard, crease tool and crease depth have a bigger impact on the responses than the crease side. However cracks occur on inside creasing at a lower crease depth than outside creasing. From the other two experimental parts, no significant difference between inside and outside creasing could be found, and also here change of paperboard, crease tool and crease depth have a bigger influence on the responses and crack propagation. The simulations do not give a univocal result since they are all too similar independent of crease depth and web tension something that do not correspond with the experimental results. However the delamination behavior in the simulations and the experimental tests are similar, the delamination behavior is very different in the inside and outside creasing but this fact is not shown in the investigated responses.

Preface

This is a master's thesis made in cooperation between Material Treatment at Tetra Pak and the divisions of Packaging Logistics and Solid Mechanics at Lund University in the fall of 2008.

First of all we would like to thank our supervisors; Magnus Just at Tetra Pak for his never ending patience with our questions, Johan Tryding our unofficial supervisor at Tetra Pak for his enthusiasm about our work, Annika Olsson at the division of Packaging Logistics and Matti Ristinmaa at the division of Solid Mechanics for support and knowledge in theoretical questions.

We also like to thank Johan Nilsson for introducing us to Design of Experiment and MODDE, Mikael Nygårds for giving us a simulation model and help us in the start up with simulations, Per-Göran Heide for helping us with setting up and using the high speed camera, Tomas Linné for doing all the hard work in the lab and last but not least we would like to thank Vladimir Ponjavic and the rest of the department of Material Treatment for helping and supporting us. Especially thanks to all the people whose desks we used in their absence. ☺

Lund in December 2008

Jennie Lillienberg and Emma Lörd

Table of Contents

1 Introduction 1

1.1 Background 1

1.2 Objective 3

1.3 Focus and delimitations 3

2 Method 5

2.1 Methodology 5

2.2 Work procedure 6

2.2.1 Design of Experiments - DOE 8

3 Theory 14

3.1 Paperboard 14

3.2 Finite Element Method 14

3.2.1 Equations of motion 15

3.2.2 Weak formulation - Principle of virtual power 16

3.2.3 Nonlinear Finite Element Method 18

3.2.4 Solution of Nonlinear Equilibrium Equations - Newton-Raphson Method 21

3.3 Material model of paperboard 23

3.3.1 Continuum model 24

3.3.2 Cohesive model 26

4 Experimental work 28

4.1 Experimental tools and parameters 28

4.1.1 Laboratory creasing tool 28

4.1.2 Creasability tester 30

4.1.3 Topography 31

4.1.4 Photography setup 33

4.1.5 Lab evaluation of the paperboard's properties 33

4.2 First experimental part: straight creases 34

4.2.1 In parameters 34

4.2.2 Procedure 34

4.3 Second experimental part: bottom crease pattern 36

4.3.1 In parameters 36

4.3.2 Procedure 36

4.4 Third experimental part: 250 Base crease pattern 37

4.4.1 In parameters 37
4.4.2 Procedure 37

5 Computer simulation 40

5.1 Abaqus 40

5.2 Model 40
5.2.1 Creasing 41
5.2.2 Folding 41

5.3 Procedure 42
5.3.1 Creasing 42
5.3.2 Folding 43

6 Results 44

6.1 Experimental 44
6.1.1 Straight creases 44
6.1.2 Bottom crease pattern 48
6.1.3 250 Base crease pattern 49

6.2 Computer simulation 51

7 Discussion 54

7.1 Experimental 54
7.1.1 Straight creases 54
7.1.2 Bottom crease pattern 55
7.1.3 250 Base crease pattern 55

7.2 Computer simulation 56

8 Conclusions 59

9 Recommendations of further investigation 60

10 References 61

List of Appendices 63

1 Introduction

1.1 Background

In the 1940's a development process, with the purpose of creating a package for milk that required a minimum of material and maximum of hygiene, started. The result was the tetrahedron-shaped carton. This lead to the foundation of Tetra Pak in the early 1950's by Ruben Rausing as a subsidiary of Åkerlund & Rausing. Over the next decades the company grew to an international company with filling machines and packaging material factories all over the world, with an ever expanding packaging portfolio with products such as Tetra Brik and Tetra Rex. In 1993 the Tetra Laval group was created and today, 2008, consists of three industrial groups: Tetra Pak, DeLaval and Sidel. Today Tetra Pak offers a complete processing and packaging system for their customers. Still the most important product in a Tetra Pak package is milk and cream but a wide range of other products are process treated and aseptically packed, for example juices, tea drinks, soy drinks, tomato products and wine [1].

This master's thesis is performed at the department Material Treatment at Tetra Pak that develop and maintain the converting process of the packaging material such as converting openings, creasing and cutting.

To assure a high quality package with a defined shape every time, a crease pattern (Figure 1.1) is important when folding a package at high speed. Creasing of paperboard is an essential operation to obtain a well defined shape and strength of a package. The creasing tool consists of one male creasing plate and one female. The male plate presses the paperboard into the female plate and introduces damage in the creasing zone. Today the standard creasing operation at Tetra Pak is that the male creasing plate presses the top ply (print side) of the paperboard, and female is pressed against the bottom ply (back side). This is called outside creasing, and the opposite is called inside creasing (Figure 1.2).

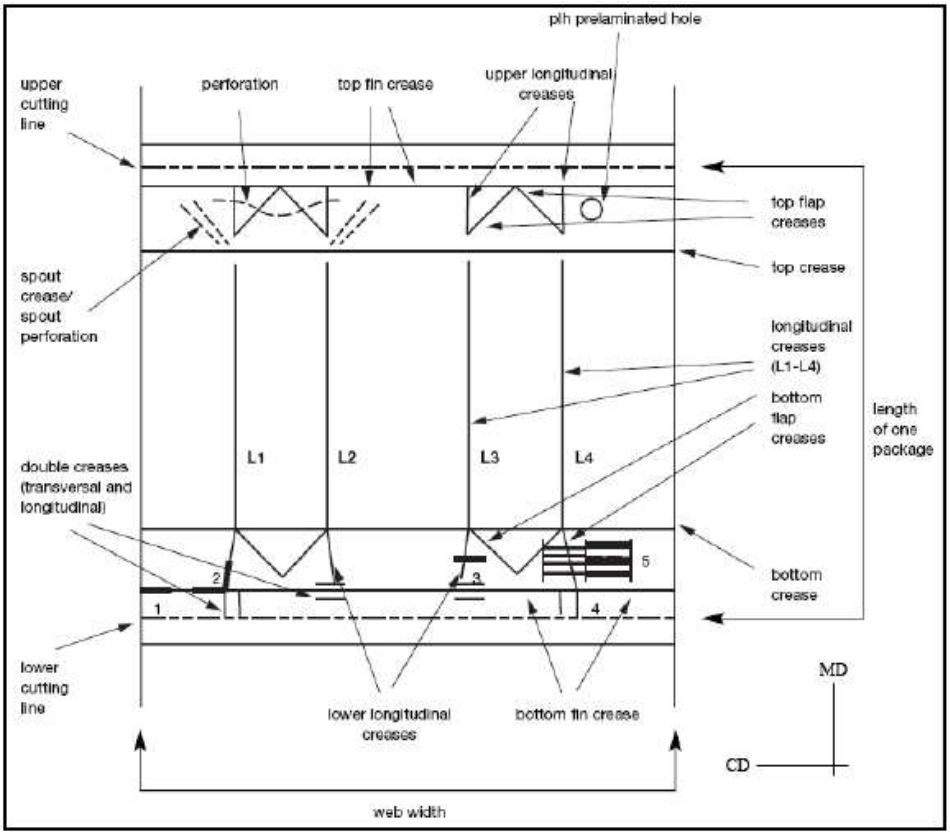

Figure 1.1. A schematic drawing of the Tetra Brik creasing pattern [8]

Since outside creasing is the standard creasing method at Tetra Pak many studies have been performed within this area. Out of all Tetra Pak factories only two factories, Monte Mor and Ponta Grossa in Brazil, use inside creasing to an almost full extent and inside creasing is there part of the concept.

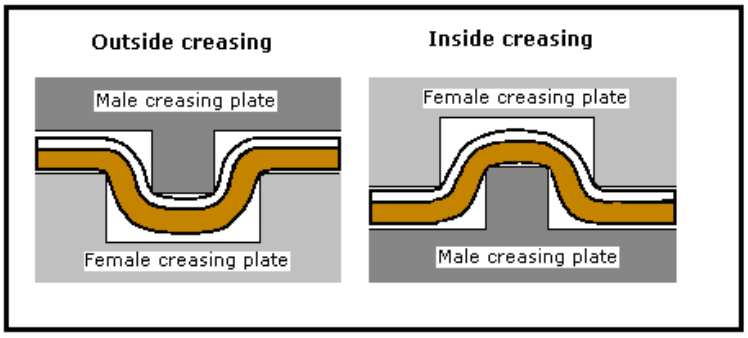

Figure 1.2. Illustration of outside and inside creasing (white is the bleached print side of the paperboard)

Only a certain amount of tests have been performed within the area of inside creasing and they haven't really given a clear picture of what happens with the paperboard and what the difference is compared to outside creasing. Panel tests have showed that customers find packages with inside creasing more attractive because they are perceived as having a more defined shape and to be easier to grip [3, 6, 7].

1.2 Objective

This master's thesis has the purpose of studying the differences between inside and outside creasing with respect to how the paperboard behaves during bending and creasing. Since this area is hardly explored the purpose is to make a broad study about the differences of inside verses outside creasing. Many parameters will be measured such as maximum forces, energy, remaining deformation and angles. The surface of the paperboard will be examined closely to see for example the height and depth of the creases and cracks in the material. Also computer simulations will be used to get a better understanding of the parameters involved.

1.3 Focus and delimitations

The number of experiments required in the experimental part is defined by the number of parameters evaluated, and require that all parameters are combined to each other; this rapidly expand the number of experiments. To obtain a manageable number of test combinations and parameters, some restrictions and delimitations are made in this master's thesis. During the first experimental tests the following restrictions are made:

- Paperboard from three paperboard suppliers
- Two paperboard qualities: thin paperboard, used for portion packages, and thick paperboard, used for family packages, from all paperboard suppliers.
- Two crease sides, inside and outside
- Three web tensions (the force used to pull the paperboard web)
- Three crease depths
- Three straight crease tool geometries each for thin and thick paperboard

Restrictions for the second experimental part:

- Paperboard from two paperboard suppliers
- One paperboard quality: thin paperboard

- Two crease sides, inside and outside
- One web tension
- Two crease depths for each paperboard and each crease side
- Two tool geometries, bottom crease pattern

Restrictions for the third experimental part:

- Paperboard from two paperboard suppliers
- One paperboard quality: thin paperboard
- Two crease sides, inside and outside
- One web tension
- Two crease depths for each paperboard and each crease side
- One tool geometry, Tetra Brik 250ml Base crease pattern (will henceforth be called 250 Base crease pattern)

Also in the simulations there are some restrictions due to the model used. Restrictions for the simulation:

- One material model for the paperboard
- Two crease sides, inside and outside
- Three web tensions
- Three crease depths
- One straight crease tool

2 Method

2.1 Methodology

The methodology sets the frames of how a study should be carried out and is chosen in the beginning of the work. Which method to choose, depends on the goals and character of the study. There are many different kinds of studies and most of them can be classified depending on how much one knows about a certain area, before the study [13].

Exploratory studies have a main purpose of finding as much information as possible about a pre-decided problem area that one lacks information about. Since this type of study often has the goal to get more knowledge within the problem area, many different techniques are used to collect information.

Sometimes knowledge already exists within the problem area. A *descriptive study* is limited to examine some aspects of the phenomenon one is interested in. The descriptions of these aspects are detailed and thorough. Often only one technique is used to collect information.

When the knowledge within a problem area is extensive and theories are already developed, the method to use is a *study of setting and testing hypothesis*. This means that one can assume that something is true and then test if it's accurate. There's a risk that other factors, other than the factors in the hypothesis, will affect the result of the test. Because of this it is very important how the study is built up. The technique for collecting information should be as precise as possible.

The three types of studies above are mostly performed as separate studies but within large projects two or all three types can exist [12]. The purpose of this master's thesis is to explore how inside and outside creasing behaves. Not many studies have been performed within this area and this work has the purpose of expanding the knowledge; this is why the study used is exploratory.

Research can be quantitative and qualitative and can be seen as how one chooses to analyze the collected information. Qualitative research uses verbal analyzing methods like words and detailed descriptions, while quantitative analyzing methods use data that one can count or measure. This master's thesis mostly analyzes quantitative data like force, displacements etc. but some data are qualitative like describing how the material looks like through a microscope [13].

2.2 Work procedure

Based on the objective and delimitations of the master's thesis the project plan is established. In the very beginning of the master's thesis a literature study is carried out. Development reports, books and articles concerning creasing and paperboard are studied and read through in order to get a theoretical input of the area, these will then serve as reference material.

Further, computer simulations in combination with experimental tests are conducted in order to evaluate inside and outside creasing from both an analytical and experimental perspective. Hence simulations are carried out by use of the finite-element software Abaqus.

The experimental tests are divided into three different parts:

1) A laboratorial part, where straight creases, both the inside and the outside, are made on paperboard using a flat bed laboratory creasing tool.

2) A laboratorial part, where a bottom crease pattern (similar to the creases on the bottom of a package) is used to make creases with the laboratory creasing tool. These tests are performed in order to study if there is a difference between creases in the machine direction (MD) and the cross machine direction (CD).

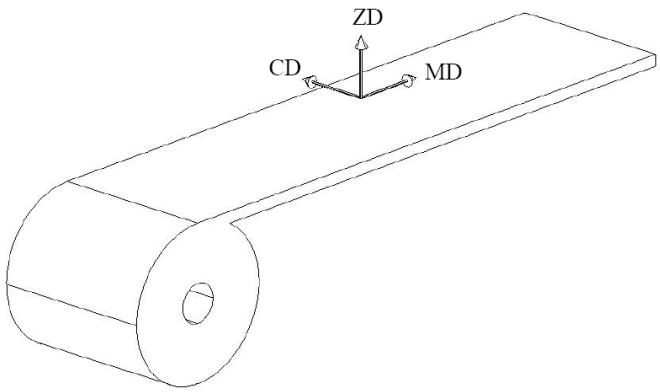

Figure 2.1. Illustrating the different directions in the paperboard [18].

3) A part where the paperboard is creased with the pattern of a Tetra Brik 250ml Base package in the Tetra Pak pilot plant. The paperboard is then laminated with the lamination specification of an aseptic juice package, see Figure 2.2.

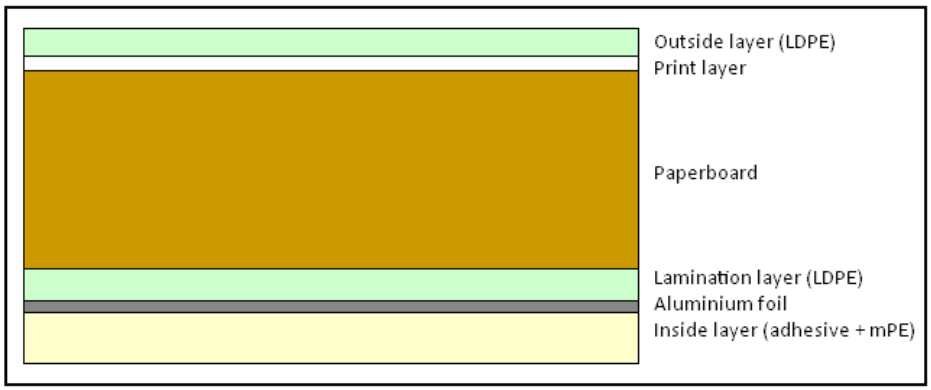

Figure 2.2. Package material of a Tetra Brik Aseptic juice package

Creases from all of the experimental parts are folded using a Lorentzen & Wettre creasability tester and studied closely using different methods:

a. Topography for measuring surface deformation of a crease

b. Laboratorial tests to find properties of the paperboard such as z-strength, bending stiffness and thickness of the paperboard.

c. Photos of the creasing and folding process in the first laboratorial part in order to study delamination of the paperboard.

To obtain a manageable number of test combinations, some restrictions and delimitations are made, as stated earlier. Even though these restrictions are made, there are still too many combinations of tests to be able to perform them all. Since all of the factors and combinations are desirable, a software MODDE, using a technique called Design of Experiments, is used to select a diverse and representative set of experiments in which all factors are independent of each other despite being varied simultaneously. The result is a causal predictive model showing the importance of all factors and their interactions. The model can be summarized as informative contour plots highlighting the optimum combination of factor settings. Design of Experiments is used in the first and last experimental part when straight creases are made and when a 250 Base crease pattern is used in the pilot plant. Design of Experiments is described in the following subchapter 2.2.1.

From the first analysis of MODDE a certain number of factors are chosen to be further investigated during the second laboratorial part, where bottom creases are made using the flatbed creasing tool.

The experimental results are compared to each other and to the computer simulations. The results are illustrated in tables, plots and figures.

2.2.1 Design of Experiments - DOE

Design of Experiments, DOE, is used to ensure that the selected experiments produce the maximum amount of relevant information. It is important to recognize that a model is an approximation, which simplifies the study of the reality. A model will never be 100% perfect, but can still be very useful.

A common approach in DOE is to define an interesting standard reference experiment and then perform new, representative experiments around it (see Figure 2.3). These new experiments are laid out in a symmetrical fashion around the standard reference experiment. Hence, the standard reference point is called the center-point.

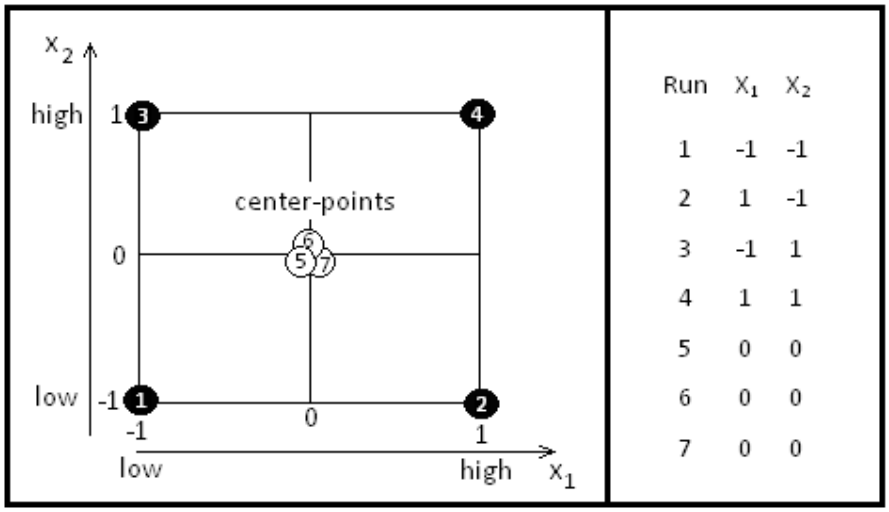

Run	X_1	X_2
1	-1	-1
2	1	-1
3	-1	1
4	1	1
5	0	0
6	0	0
7	0	0

Figure 2.3. Distribution of a full factorial design with two factors

In Figure 2.3 the experiments of a full factorial design can be seen with two factors, x_1 and x_2. Each dot represents an experiment and the three center-points are representative middle values of each factor.

There are basically three types of problems to which DOE is applicable.

1. Screening - is used to obtain the most influential factors, and to determine the ranges in which these should be investigated. This is a fairly straightforward aim, so screening requires few experiments in relation to the number of factors.

2. Optimization - is about defining which combination of the important factors will result in optimal operating conditions. Since optimization is more complex than screening, optimization designs require more experiments per factor.

3. Robustness testing - is used to determine the sensitivity of a product or production procedure to small changes in the factor settings. Such small changes usually correspond to fluctuations in the factors occurring during a "bad day" for production, or the customer not following product usage instructions.

The screening method is the one used in this master's thesis and is the only one of the three methods that is described further.

A problem formulation is very important and is carried out to make the intentions of an underlying experimental investigation completely clear, for all involved parties. There are a number of things to discuss and agree about, and it is necessary to consider six points.

1) The experimental objective – defines what kind of investigation is required. One should ask: *why is an experiment done*, *for what purpose* and *what is the desired result*? This master's thesis uses screening as the experimental objective since the interest is to find out which factors are the dominating ones, and what their optimal ranges are. To screening the Pareto principle applies well, which means that 80% of the effects on the responses are caused by 20% of the investigated factors.

2) Definition of factors – is about defining the variables which exert an influence on the system or the process, due to changes in their levels. The factors can be divided into controllable/ uncontrollable factors and quantitative/qualitative factors. A quantitative factor is a factor which may change according to a continuous scale and a qualitative factor can only assume certain discrete values. This point also involves setting the range of the quantitative factors and the exact value of the qualitative.

3) Specification of responses – is a process where one select responses that are relevant according to the problem formulation. It is often necessary to have many responses to well describe the properties of a product or the performance characteristics of a process. Responses can be quantitative or qualitative. A quantitative response is a metric with a distinct value, where as a qualitative response is about describing how well the response is perceived on a scale of 1-5, where 1 could be worthless and 5 could be

excellent. The responses in this master's thesis that are applied on Design of Experiments only have quantitative responses.

4) Selection of model – is an integral part of the problem formulation and about selecting an appropriate regression model. There are three main types of polynomial models:

Linear	$y = b_0 + b_1 x_1 + b_2 x_2 + ... + e$
Interaction	$y = b_0 + b_1 x_1 + b_2 x_2 + b_{12} x_1 x_2 + ... + e$
Quadratic	$y = b_0 + b_1 x_1 + b_2 x_2 + b_{11} x_1^2 + b_{22} x_2^2 + b_{12} x_1 x_2 + ... + e$

The variable b is a regression coefficient, x is a factor defined earlier in the problem formulation and e is the residual. The linear model can algebraically be seen as $\mathbf{y} = \mathbf{Xb} + \mathbf{e}$. Since the quadratic polynomial model is the most complex it requires more experiments than the others. An interaction model requires fewer experiments and a linear model even less. If the experimental objective is screening either a linear or an interaction model is pertinent. An interaction model is recommended if the number of experiments is easy to handle, but the experiments of this master's thesis have many factors which makes the linear model appropriate.

5) Generation of design – is the next step of the problem formulation and is intimately linked to the chosen model. The MODDE software will consider the number of factors, their levels and nature (quantitative, qualitative …) and the selected experimental objective, and propose a recommended design, which will well suit the given problem [9]. The design chosen by MODDE for the experimental work in the first experimental part is a design called D-Optimal. D-Optimal means that the design maximizes the information in the selected set of experimental runs with respect to a stated model. Given a model, the D-Optimal algorithm selects N experimental runs from the candidate set, which is the set of all potentially good runs, as to maximize the information in the matrix **X**. The extended design matrix **X** is created from the N experimental runs expanded with columns for the constant and cross terms according to the model [21], see Figure 2.4. During the third experimental part a full factorial design is used.

Run	Constant	X_1	X_2	$X_1 X_2$
1	1	-1	-1	1
2	1	1	-1	-1
3	1	-1	1	-1
4	1	1	1	1
5	1	0	0	0
6	1	0	0	0
7	1	0	0	0

$$\mathbf{X} = \begin{bmatrix} 1 & -1 & -1 & 1 \\ 1 & 1 & -1 & -1 \\ 1 & -1 & 1 & -1 \\ 1 & 1 & 1 & 1 \\ 1 & 0 & 0 & 0 \\ 1 & 0 & 0 & 0 \\ 1 & 0 & 0 & 0 \end{bmatrix}$$

*Figure 2.4. The extended matrix **X***

6) Creation of worksheet – is the last stage of the problem formulation. The worksheet is, in principle, very similar to a table containing the selected experimental design. It shows which experiments to perform and in which order [9]. In order to handle the noise of the experiments some center points are chosen, which often are three experiments with the same middle value settings.

When the worksheet is created is it possible to evaluate the performance of the experimental design prior to its execution by looking at the condition number. The condition number is the ratio of the largest and the smallest singular values of the X-matrix (eigenvalues of $\mathbf{X}^T\mathbf{X}$) and represents a measure of the orthogonality of the design. The optimal value of the condition number is 1 but a number < 3 is considered to be a good design. There are several plots and lists available to evaluate the model and one of these is the histogram plot. The *Histogram plot* is useful for studying the distributional shape of a response variable. If the responses are not approximately normally distributed like the Histogram of Screwness in Figure 2.5 it could indicate that one measurement is not like the others. It is not recommended to apply regression analysis to a response with this kind of distribution and the problem can be solved by a logarithmic transformation of the response.

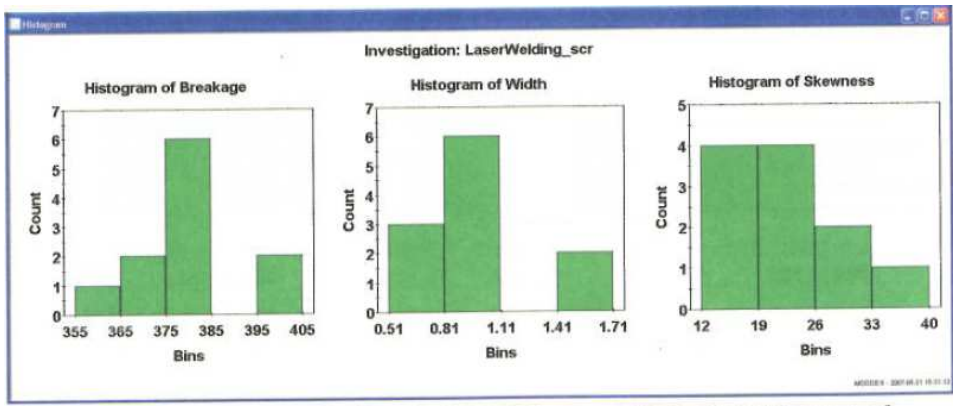

Figure 2.5. Example of a histogram plot

The next step of the analysis is to fit the model. When the model is fitted there are several plots and lists available to evaluate the result. One of the most important ones is the *Summary of Fit plot* seen in Figure 2.6 and through this plot the important parameters R^2 and Q^2 can be analyzed.

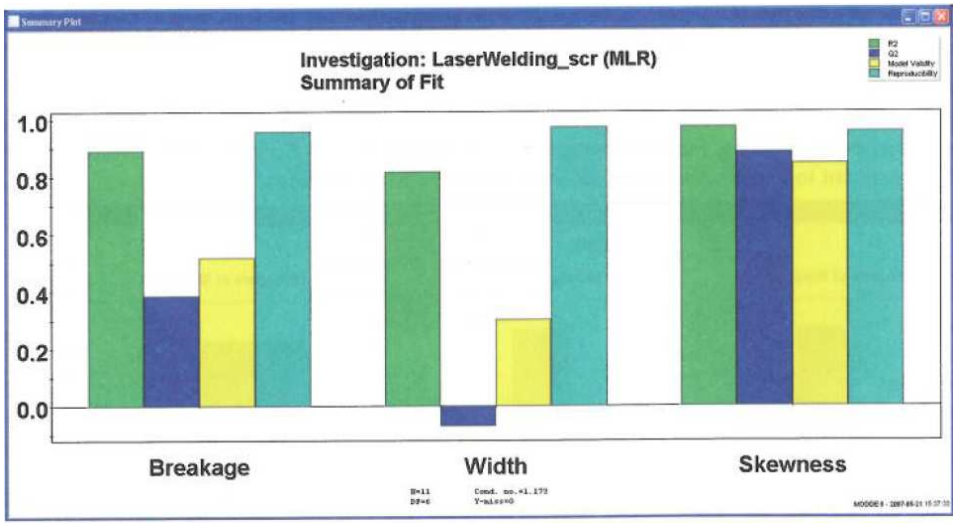

Figure 2.6. Example of a Summary of Fit plot

R^2 represents the green bars in Figure 2.6, is called the *goodness of fit* and is a measure of how well the regression model can be made to fit the raw data. R^2 varies between 0 and 1, where 1 indicates a perfect model and 0 no model at all. Q^2 represents the blue bars and is called the *goodness of prediction* which means that it estimates the predictive power of the model. This is a more realistic and useful performance indicator as it reflects the final goal of modeling – predictions of new

experiments. Q^2 has the upper bound 1 and lower limit minus infinity. For the model to pass this diagnostic test, both R^2 and Q^2 should be high and preferably not separated by more than 0.2-0.3. Generally speaking, Q^2 >0.5 should be regarded as a good model, and Q^2 >0.9 as excellent.

The yellow bar in the summary of fit plot is called *model validity* and reflects whether the right type of model was chosen from the beginning in the problem formulation. The higher the numerical value the more valid the model is, and a value above 0.25 suggests a valid model.

Finally, the turquoise bar in the summary of fit plot is called the *reproducibility*. The higher the numerical value the smaller the replicate error is in relation to the variability seen across the entire design. If the value of the reproducibility bar is small, below 0.5, it indicates a large pure error and poor control of the experimental procedure.

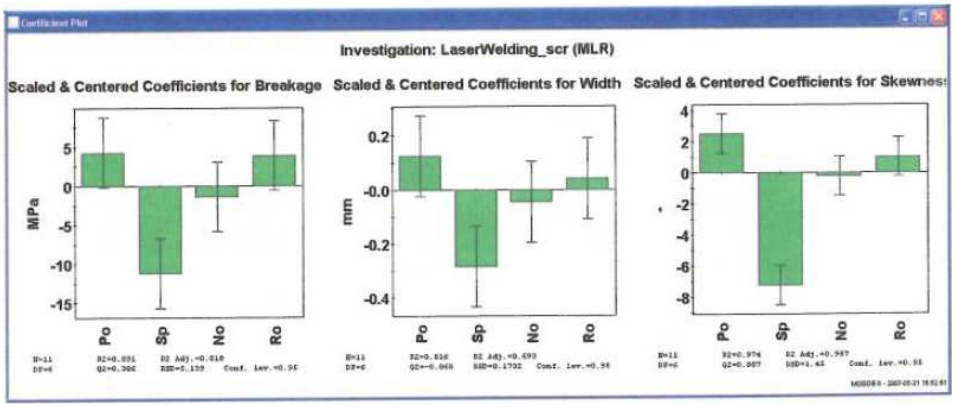

Figure 2.7. Example of a regression coefficient plot

To detect strong interactions between different responses and factors normally a *Regression coefficient plot* Figure 2.7 is used. The green bars reveal the real effects of the factors on each response. As can be seen in Figure 2.7 the factor **Sp** (Speed) has the strongest impact on all three responses, and it is interpreted as to when the speed is increased all three responses **Breakage**, **Width** and **Screwness** will decrease. The uncertainty of the coefficients is given by the confidence intervals and the size of these depends on the size of the noise.

3 Theory

3.1 Paperboard

Paperboard is made up of fibers that are mechanically deformed and bond to each other without help from other substances. Depending on how the fibers are deformed and oriented the paperboard gets a variety of properties. Paperboard is made up of several plies. The surface part is build up with chemical pulp and the middle part is build up with mechanical pulp. Sometimes the paperboard can also be several layers of chemical or mechanical pulp. The surface is often coated with clay to give a more even surface, better gloss and better printing qualities.

Mechanical pulp is wood that have been mechanically resolved. Different pulp qualities are produced by using different temperature and mechanical process. A big advantage with mechanical pulp is that more than 90 percent of the wood is used, this makes it cheap. But since the fibers get damaged the mechanical pulp results in a weak paperboard.

Chemical pulp is produced by boiling wood with water and chemical compounds so it can be resolved without force. Here only about 48 – 60 percent of the wood is used. But since the fibers are not damaged during the process they make a strong paperboard [15].

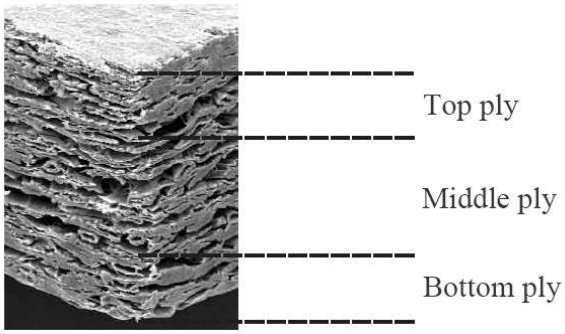

Figure 3.1. Paperboard showing different plies [*16*]

3.2 Finite Element Method

In the simulations the finite element method can be used to solve the problem numerically in an approximate manner [10]. The following text contains the theory of the finite element method and defines the material model used for paperboard. There exists a material model proposed by Xia using a continuum model and an interface model, where the continuum model describes the behavior within the ply,

and the interface model describes the delamination between the plies [19]. However, here Abaqus built in material models are used for the continuum model and cohesive interface model for delamination, since in this model have proven to give good and realistic curves and describes the delamination well [17].

3.2.1 Equations of motion

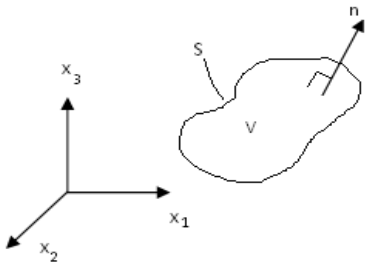

Figure 3.2. A body with volume V, surface S and normal vector n.

An arbitrary body has the volume *V*, the surface *S* and the outer normal unit vector **n**. The forces acting on the body are the traction vector ***t*** along the surface *S* and the body force ***b*** per unit volume in the region *V*. The displacements are denoted by ***u*** with the acceleration vector ***ü***. To get the equations of motion Newton's second law is used:

$$\int_S \boldsymbol{t} dS + \int_V \boldsymbol{b} dV = \int_V \rho \ddot{\boldsymbol{u}} dV \tag{1}$$

where ρ is the mass density. To reformulate Eq. (1), recall the divergence theorem of Gauss that says that for an arbitrary vector

$$\int_V div\boldsymbol{q} dV = \int_S \boldsymbol{q}^T \boldsymbol{n} dS \tag{2}$$

and per definition that

$$div\boldsymbol{q} = \frac{\partial q_1}{\partial x_1} + \frac{\partial q_2}{\partial x_2} + \frac{\partial q_3}{\partial q_3} = q_{i,i}; \qquad \boldsymbol{q}^T \boldsymbol{n} = q_i n_i \tag{3}$$

Hence the divergence theorem can be written [11]:

$$\int_V q_{i,i} dV = \int_S q_i n_i dS \tag{4}$$

Making use of the Cauchy stress, $\boldsymbol{T}$, defined as [14]:

$$\boldsymbol{t} = \boldsymbol{T}\boldsymbol{n} \tag{5}$$

Eq. (1) can now be reformulated using the divergence theorem and the Cauchy stress

$$\int_V (div\boldsymbol{T} + \boldsymbol{b} - \rho\ddot{\boldsymbol{u}}) dV = 0 \tag{6}$$

This equation holds for an arbitrary body and can be written as:

$$div\boldsymbol{T} + \boldsymbol{b} = \rho\ddot{\boldsymbol{u}} \tag{7}$$

These are the equations of motion of the body; Eq. (7) is often called the strong formulation since this equation contains the derivatives of the stress tensor [11].

3.2.2 Weak formulation - Principle of virtual power

To get the weak formulation one multiplies the equations of motion Eq. (7) with an arbitrary velocity (weight vector) $\boldsymbol{w}$ and integrates over the volume to obtain:

$$\int_V \boldsymbol{w}^T div\boldsymbol{T} dV + \int_V \boldsymbol{w}^T \boldsymbol{b} dV = \int_V \rho \boldsymbol{w}^T \ddot{\boldsymbol{u}} dV \tag{8}$$

Using the Green-Gauss theorem, divergence theorem and the Cauchy theorem the first part of equation can be written as:

$$\int_V \boldsymbol{w}^T div\boldsymbol{T} dV = \int_S \boldsymbol{w}^T \boldsymbol{t} dS - \int_V \nabla \boldsymbol{w} : \boldsymbol{T} dV \tag{9}$$

Inserting into Eq. (8) renders:

$$\int_S \boldsymbol{w}^T \boldsymbol{t} dS - \int_V \nabla \boldsymbol{w} : \boldsymbol{T} dV + \int_V \boldsymbol{w}^T \boldsymbol{b} dV = \int_V \rho \boldsymbol{w}^T \ddot{\boldsymbol{u}} dV \tag{10}$$

Introducing a symmetric tensor:

$$\hat{\boldsymbol{D}} = \frac{1}{2}(\nabla \boldsymbol{w} + (\nabla \boldsymbol{w})^T) \tag{11}$$

gives the principle of virtual power also known as the weak form.

$$\int_V \rho \boldsymbol{w}^T \ddot{\boldsymbol{u}} dV + \int_V \hat{\boldsymbol{D}} : \boldsymbol{T} dV - \int_S \boldsymbol{w}^T \boldsymbol{t} dS - \int_V \boldsymbol{w}^T \boldsymbol{b} dV = 0 \tag{12}$$

The weak form is one of the most important principles within solid mechanics, since it does not only form the basis for the finite element method but also for several other numerical methods and is also central for a number of theorems in solid mechanics [11, 14].

This formulation is based on the current configuration something that is not known and therefore it is better to write it in the reference configuration. All quantities that are described in the reference configuration will be denoted with a subscript o. Start with converting the body forces:

$$\int_V \boldsymbol{w}^T \boldsymbol{b} dV = \int_{V^\circ} \boldsymbol{w}^T \boldsymbol{b}^\circ dV^\circ \tag{13}$$

Changing the traction forces will need to more work using Cauchy's theorem, Nanson's formula:

$$\boldsymbol{n} ds = \boldsymbol{J} \boldsymbol{F}^{-T} \boldsymbol{n}^\circ ds^\circ \tag{14}$$

Where $d\boldsymbol{s}$ is the incremental area vector, **J** is the Jacobian that can be written as $J = \frac{dV}{dV^\circ}$, **F** is the deformation tensor defined by $\boldsymbol{F} = \nabla_\circ \boldsymbol{x}$. Finally introducing the definition of the first Piola-Kirchhoff stress tensor, **P** as

$$\boldsymbol{P} = \boldsymbol{J} \boldsymbol{T} \boldsymbol{F}^{-T} \tag{15}$$

gives:

$$\int_S \boldsymbol{w}^T \boldsymbol{t} dS = \int_S \boldsymbol{w}^T \boldsymbol{T} \boldsymbol{n} dS = \int_{S^\circ} \boldsymbol{w}^T \boldsymbol{J} \boldsymbol{T} \boldsymbol{F}^{-T} \boldsymbol{n}^\circ dS^\circ = \int_{S^\circ} \boldsymbol{w}^T \boldsymbol{P} \boldsymbol{n}^\circ dS^\circ = \int_{S^\circ} \boldsymbol{w}^T \boldsymbol{t}^\circ dS^\circ \tag{16}$$

The first term in the weak form can be rewritten as:

$$\int_V \rho \boldsymbol{w}^T \ddot{\boldsymbol{u}} dV = \int_{V^\circ} \rho^\circ \boldsymbol{w}^T \ddot{\boldsymbol{u}} dV^\circ \tag{17}$$

The remaining term need a little more work to be transformed. Hence we note that

$$\nabla \boldsymbol{w} = \hat{\boldsymbol{F}} \boldsymbol{F}^{-1} \tag{18}$$

where

$$\hat{\boldsymbol{F}} = \nabla_{\circ} \boldsymbol{w} \tag{19}$$

Hence Eq. (11) can be written as:

$$\hat{\boldsymbol{D}} = \frac{1}{2}(\hat{\boldsymbol{F}}\boldsymbol{F}^{-1} + \boldsymbol{F}^{-T}\hat{\boldsymbol{F}}^{T}) = \boldsymbol{F}^{-T}\hat{\boldsymbol{E}}_{\Diamond}\boldsymbol{F}^{-1} \tag{20}$$

where $\hat{\boldsymbol{E}}_{\Diamond}$ is a square matrix:

$$\hat{\boldsymbol{E}}_{\Diamond} = \frac{1}{2}(\boldsymbol{F}^{T}\hat{\boldsymbol{F}} + \hat{\boldsymbol{F}}^{T}\boldsymbol{F}) \tag{21}$$

Now the second term in the weak form can be rewritten:

$$\int_{V} \hat{\boldsymbol{D}} : \boldsymbol{T} dV = \int_{V} (\boldsymbol{F}^{-T}\hat{\boldsymbol{E}}_{\Diamond}\boldsymbol{F}^{-1}) : \boldsymbol{T} dV = \int_{V} \hat{\boldsymbol{E}}_{\Diamond} : (\boldsymbol{F}^{-1}\boldsymbol{T}\boldsymbol{F}^{-T}) dV = \int_{V^{\circ}} \hat{\boldsymbol{E}}_{\Diamond} : \boldsymbol{S}_{\Diamond} dV^{\circ} \tag{22}$$

where the second Piola-Kirchoff stress tensor is defined as:

$$\boldsymbol{S}_{\Diamond} = \boldsymbol{F}^{-1}\boldsymbol{P} = J\boldsymbol{F}^{-1}\boldsymbol{T}\boldsymbol{F}^{-T} \tag{23}$$

The weak form is now converted to the reference configuration [14]:

$$\int_{V^{\circ}} \rho \boldsymbol{w}^{T}\ddot{\boldsymbol{u}} dV^{\circ} + \int_{V^{\circ}} \hat{\boldsymbol{E}}_{\Diamond} : \boldsymbol{S}_{\Diamond} dV^{\circ} - \int_{S^{\circ}} \boldsymbol{w}^{T}\boldsymbol{t}^{\circ} dS^{\circ} - \int_{V^{\circ}} \boldsymbol{w}^{T}\boldsymbol{b}^{\circ} dV^{\circ} = 0 \tag{24}$$

3.2.3 Nonlinear Finite Element Method

Since paperboard is a nonlinear anisotropic material one has to use the nonlinear finite element method. Here the equations in the finite element method are formulated. They are based on the weak from in Eq. (12) and Eq. (24).

Here the variables are defined in matrix form:

$$\boldsymbol{E} = \begin{bmatrix} E_{xx} \\ E_{yy} \\ E_{zz} \\ 2E_{xy} \\ 2E_{xz} \\ 2E_{yz} \end{bmatrix}; \quad \boldsymbol{S} = \begin{bmatrix} S_{xx} \\ S_{yy} \\ S_{zz} \\ S_{xy} \\ S_{xz} \\ S_{yz} \end{bmatrix}; \quad \ddot{\boldsymbol{u}} = \begin{bmatrix} \ddot{u}_x \\ \ddot{u}_y \\ \ddot{u}_z \end{bmatrix}; \quad \boldsymbol{w} = \begin{bmatrix} w_x \\ w_y \\ w_z \end{bmatrix}; \quad \boldsymbol{t}^{\circ} = \begin{bmatrix} t_x^{\circ} \\ t_y^{\circ} \\ t_z^{\circ} \end{bmatrix}; \quad \boldsymbol{b}^{\circ} = \begin{bmatrix} b_x^{\circ} \\ b_y^{\circ} \\ b_z^{\circ} \end{bmatrix}$$

Green-Lagrange's strain may be written as:

$$\boldsymbol{E} = \begin{bmatrix} \frac{\partial u_x}{\partial x^\circ} \\ \frac{\partial u_y}{\partial y^\circ} \\ \frac{\partial u_z}{\partial z^\circ} \\ \frac{\partial u_x}{\partial y^\circ} + \frac{\partial u_y}{\partial x^\circ} \\ \frac{\partial u_y}{\partial z^\circ} + \frac{\partial u_z}{\partial y^\circ} \\ \frac{\partial u_x}{\partial z^\circ} + \frac{\partial u_z}{\partial x^\circ} \end{bmatrix} + \frac{1}{2} \begin{bmatrix} (\frac{\partial u_x}{\partial x^\circ})^2 + (\frac{\partial u_y}{\partial x^\circ})^2 + (\frac{\partial u_z}{\partial x^\circ})^2 \\ (\frac{\partial u_x}{\partial y^\circ})^2 + (\frac{\partial u_y}{\partial y^\circ})^2 + (\frac{\partial u_z}{\partial y^\circ})^2 \\ (\frac{\partial u_x}{\partial z^\circ})^2 + (\frac{\partial u_y}{\partial z^\circ})^2 + (\frac{\partial u_z}{\partial z^\circ})^2 \\ 2(\frac{\partial u_x}{\partial x^\circ}\frac{\partial u_x}{\partial y^\circ} + \frac{\partial u_y}{\partial x^\circ}\frac{\partial u_y}{\partial y^\circ} + \frac{\partial u_z}{\partial x^\circ}\frac{\partial u_z}{\partial y^\circ}) \\ 2(\frac{\partial u_x}{\partial y^\circ}\frac{\partial u_x}{\partial z^\circ} + \frac{\partial u_y}{\partial y^\circ}\frac{\partial u_y}{\partial z^\circ} + \frac{\partial u_z}{\partial y^\circ}\frac{\partial u_z}{\partial z^\circ}) \\ 2(\frac{\partial u_x}{\partial x^\circ}\frac{\partial u_x}{\partial z^\circ} + \frac{\partial u_y}{\partial x^\circ}\frac{\partial u_y}{\partial z^\circ} + \frac{\partial u_z}{\partial x^\circ}\frac{\partial u_z}{\partial z^\circ}) \end{bmatrix} \tag{25}$$

or shorter as:

$$\boldsymbol{E} = \nabla_l \boldsymbol{u} + \frac{1}{2}\boldsymbol{A}(\boldsymbol{u})\nabla_u \boldsymbol{u} \tag{26}$$

and the weak form may be rewritten:

$$\int_{V^\circ} \rho \boldsymbol{w}^T \ddot{\boldsymbol{u}} dV^\circ + \int_{V^\circ} \hat{\boldsymbol{E}}^T \boldsymbol{S} dV^\circ - \int_{S^\circ} \boldsymbol{w}^T \boldsymbol{t}^\circ dS^\circ - \int_{V^\circ} \boldsymbol{w}^T \boldsymbol{b}^\circ dV^\circ = 0 \tag{27}$$

Using Eq. (26) [14]:

$$\hat{\boldsymbol{E}} = \nabla_l \boldsymbol{u} + \boldsymbol{A}(\boldsymbol{u})\nabla_u \boldsymbol{u} \tag{28}$$

The boundary conditions of the body are expressed in the displacement vector **u** along the boundary surface S_u and the traction vector ***t*** along the boundary surface S_t. As can be seen in Figure 3.3.

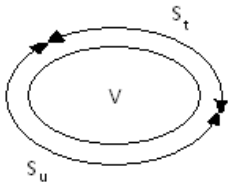

Figure 3.3. Boundary conditions S_t and S_u

The basis of the finite element method is to express the displacement vector $\boldsymbol{u}$ with the approximation:

$$\boldsymbol{u} = \boldsymbol{N}\boldsymbol{a} \tag{29}$$

where $\boldsymbol{N}$ is the global shape functions and $\boldsymbol{a}$ is the nodal displacements of the body. The displacement vector $\boldsymbol{u}$ depends on both position and time while the global shape functions only depend on position:

$$\boldsymbol{u}=\boldsymbol{u}(x_i,t); \quad \boldsymbol{N}=\boldsymbol{N}(x_i); \quad \boldsymbol{a}=\boldsymbol{a}(t) \tag{30}$$

This gives the acceleration

$$\ddot{\boldsymbol{u}} = \boldsymbol{N}\ddot{\boldsymbol{a}} \tag{31}$$

The arbitrary weight vector $\boldsymbol{w}$ is chosen with Galerkin's method in the same way as the displacement $\boldsymbol{u}$.

$$\boldsymbol{w} = \boldsymbol{N}\boldsymbol{c} \tag{32}$$

Here $\boldsymbol{c}$ is an arbitrary vector that is independent of position since $\boldsymbol{w}$ is arbitrary and $\boldsymbol{N}$ is defined above [11].

From Eq. (28) and using the matrices from Eq. (25), one can get:

$$\hat{\boldsymbol{E}} = (\boldsymbol{B}_0 + \boldsymbol{B}_u)\boldsymbol{c} = \boldsymbol{B}\boldsymbol{c} \tag{33}$$

where

$$\boldsymbol{B}_0 = \nabla_l \boldsymbol{N}\ , \ \ \boldsymbol{B}_u = \boldsymbol{A}(\boldsymbol{u})\boldsymbol{H} \ \text{ and } \ \ \boldsymbol{H} = \nabla_u \boldsymbol{N} \tag{34}$$

Inserting Eq. (32) and Eq. (33) in the weak form Eq. (27) [14]:

$$\boldsymbol{c}^T\left[(\int_{V^\circ} \rho^\circ \boldsymbol{N}^T\boldsymbol{N}dV^\circ)\ddot{\boldsymbol{a}} + \int_{V^\circ} \boldsymbol{B}^T\boldsymbol{S}dV^\circ - \int_{S^\circ} \boldsymbol{N}^T\boldsymbol{t}^\circ dS^\circ - \int_{V^\circ} \boldsymbol{N}^T\boldsymbol{b}^\circ dV^\circ \right] = 0 \tag{35}$$

Since this holds for arbitrary $\boldsymbol{c}$ matrices, it can be written:

$$\boldsymbol{M}\ddot{\boldsymbol{a}} + \int_{V^\circ} \boldsymbol{B}^T\boldsymbol{S}dV^\circ = \boldsymbol{f} \tag{36}$$

where $\boldsymbol{M}$ is the mass matrix.

$$\boldsymbol{M} = \int_{V^\circ} \rho^\circ \boldsymbol{N}^T \boldsymbol{N} dV^\circ \tag{38}$$

and $\boldsymbol{f}$ is the external forces.

$$\boldsymbol{f} = \int_{S^\circ} \boldsymbol{N}^T \boldsymbol{t}^\circ dS^\circ + \int_{V^\circ} \boldsymbol{N}^T \boldsymbol{b}^\circ dV^\circ \tag{39}$$

Eq. (36) is derived straight from the equations of motion without knowing the particular problem hence it holds for any problem. When the accelerations $\ddot{\boldsymbol{a}}$ are zero Eq. (36) is reduced to the equilibrium equations:

$$\boldsymbol{\psi}(\boldsymbol{a}) = \boldsymbol{0} \tag{40}$$

where

$$\boldsymbol{\psi}(\boldsymbol{a}) = \int_{v^\circ} \boldsymbol{B}^T \boldsymbol{S} dV^\circ - \boldsymbol{f} \tag{41}$$

These equations form the base in the Newton-Raphson method [11].

3.2.4 Solution of Nonlinear Equilibrium Equations - Newton-Raphson Method

To solve a nonlinear problem the Newton-Raphson method uses the linearization of a function about a point. This is done by guessing a starting value x^0, at the corresponding point A on the curve the tangent is determined and this tangent is extrapolated to get a new estimate x^1 that is used to find the point B on the curve that provides the next estimate x^2 and so on.

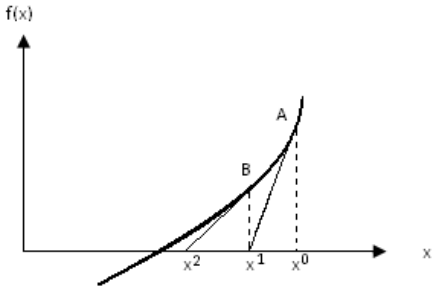

Figure 3.4. Newton-Raphson method for a one dimensional problem.

Assuming that the approximation $\boldsymbol{a}^{i-1}$ to the solution $\boldsymbol{a}$ have been determined. A Taylor series expansion of $\boldsymbol{\psi}$ about $\boldsymbol{a}^{i}$ using only the linear part is:

$$\boldsymbol{\psi}(\boldsymbol{a}^{i}) = \boldsymbol{\psi}(\boldsymbol{a}^{i-1}) + (\frac{\partial \boldsymbol{\psi}}{\partial \boldsymbol{a}})^{i-1}(\boldsymbol{a}^{i} - \boldsymbol{a}^{i-1}) \tag{42}$$

This represents the tangent to the curve at point $\boldsymbol{a}^{i-1}$. Since $\boldsymbol{\psi}(\boldsymbol{a}^{i}) = \boldsymbol{0}$ Eq. (42) becomes:

$$\boldsymbol{0} = \boldsymbol{\psi}(\boldsymbol{a}^{i-1}) + (\frac{\partial \boldsymbol{\psi}}{\partial \boldsymbol{a}})^{i-1}(\boldsymbol{a}^{i} - \boldsymbol{a}^{i-1}) \tag{43}$$

To continue, we need the derivate $\partial\boldsymbol{\psi}/\partial\boldsymbol{a}$ also known as the Jacobian, having fixed external forces the equation becomes:

$$\frac{\partial \boldsymbol{\psi}}{\partial \boldsymbol{a}} = \int_{V^\circ} \boldsymbol{B}^T \frac{d\boldsymbol{S}}{d\boldsymbol{a}} dV^\circ + \int_{V^\circ} \frac{d\boldsymbol{B}^T}{d\boldsymbol{a}} \boldsymbol{S} dV^\circ \tag{44}$$

Hence it can be shown that:

$$\frac{d\boldsymbol{S}}{d\boldsymbol{a}} = \boldsymbol{D}_t \boldsymbol{B} \tag{45}$$

Inserting Eq. (44) into Eq. (45) gives

$$\frac{\partial \boldsymbol{\psi}}{\partial \boldsymbol{a}} = \boldsymbol{K}_t \quad \text{where} \quad \boldsymbol{K}_t = \int_{V^\circ} \boldsymbol{B}^T \boldsymbol{D}_t \boldsymbol{B} dV + \int_{V^\circ} \boldsymbol{H}^T \boldsymbol{R} \boldsymbol{H} dV^\circ \tag{46}$$

where $\boldsymbol{R} = \begin{bmatrix} \boldsymbol{S}_\diamond & 0 \\ 0 & \boldsymbol{S}_\diamond \end{bmatrix}$ and $\boldsymbol{K}_t$ is the tangent stiffness matrix of the body. Hence Eq. (43) takes the form of:

$$(\boldsymbol{K}_t)^{i-1}(\boldsymbol{a}^{i} - \boldsymbol{a}^{i-1}) = -\boldsymbol{\psi}(\boldsymbol{a}^{i-1}) \tag{47}$$

In a Newton-Raphson approach one start from a state *n* where equilibrium is fulfilled and all stresses, strains, displacements and loadings are known. The external loadings are then changed to $\boldsymbol{f}_{n+1}$ and the goal is to find the equivalent stresses, strains and displacements. To get the starting conditions we know the out of balance forces $\boldsymbol{\psi}(\boldsymbol{a}^{i-1})$

$$\boldsymbol{\psi}(\boldsymbol{a}^{i-1}) = \int_V \boldsymbol{B}^T \boldsymbol{S}^{i-1} dV^\circ - \boldsymbol{f}_{n+1} \tag{48}$$

and taking the most recent known values as starting point.

$$\boldsymbol{a}^0 = \boldsymbol{a}_n; \qquad \boldsymbol{S}^0 = \boldsymbol{S}_n; \qquad (\boldsymbol{K}_t)^0 = (\boldsymbol{K}_t)_n \tag{49}$$

This gives the first iteration

$$(\boldsymbol{K}_t)_n(\boldsymbol{a}^1 - \boldsymbol{a}_n) = \boldsymbol{f}_{n+1} - \int_V \boldsymbol{B}^T \boldsymbol{S}_n dV^\circ \tag{50}$$

When the out of balance forces $\boldsymbol{\psi}(\boldsymbol{a}^{i-1})$ approach zero the finite element software stop the iterations at a certain value specified in the software since the balance forces will not reach exactly zero. At this small value of $\boldsymbol{\psi}(\boldsymbol{a}^{i-1})$ one accept the solution $\boldsymbol{a}^{i-1}$.

$$\boldsymbol{a}_{n+1} = \boldsymbol{a}^{i-1}; \qquad \boldsymbol{\varepsilon}_{n+1} = \boldsymbol{\varepsilon}^{i-1}; \quad \boldsymbol{S}_{n+1} = \boldsymbol{\varepsilon}^{i-1} \tag{51}$$

Every Newton-Raphson iteration is costly, since the $\boldsymbol{K}_t$-matrix needs to be established in every step. This means that the modified Newton-Raphson often is used instead. Here the $\boldsymbol{K}_t$-matrix is only recalculated once every load step. The above equations are used in Abaqus in an updated format, i.e. an updated Lagrange formulation. The updated formulation takes advantage of the fact that if the reference configuration is updated continuously in every iteration to become equal to the current configuration the equation system can be simplified [11].

3.3 Material model of paperboard

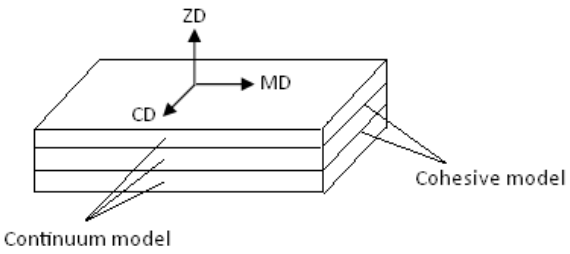

Figure 3.5. Material directions shown in the paperboard.

The material directions in the paperboard are defined as machine direction (MD), cross machine direction (CD) and out-of-plane direction (ZD) as can be seen in Figure 3.5.

3.3.1 Continuum model

An anisotropic material has different properties in MD, CD and ZD. Here the material is approximated with an orthotropic model, hence there are nine elastic constants, Young's moduli: E_x, E_y, E_z, shear moduli: G_{xy}, G_{xz}, G_{yz} and Poisson's ratios: $\nu_{xy}, \nu_{xz}, \nu_{yz}$.

Abaqus uses a rotated Jaumann rate of Cauchy stress ($\overset{\circ}{\boldsymbol{\sigma}}$) to define the constitutive law. To obtain this stress rate a rotational stress rate is first introduced:

$$\dot{\boldsymbol{\sigma}}^R = \overset{\bullet}{(\boldsymbol{Q}^T \boldsymbol{\sigma} \boldsymbol{Q})} \tag{52}$$

where $\boldsymbol{Q}$ is the rotation, letting the Jaumann stress rate to be related to the rotational stress rate:

$$\boldsymbol{Q}\dot{\boldsymbol{\sigma}}^R\boldsymbol{Q}^T = \overset{\circ}{\boldsymbol{\sigma}} = \dot{\boldsymbol{\sigma}} - \boldsymbol{w}\boldsymbol{\sigma} - \boldsymbol{\sigma}\boldsymbol{w}^T \tag{53}$$

allows the evolution law for **Q** to be defined as:

$$\dot{\boldsymbol{Q}} = \boldsymbol{w}\boldsymbol{Q} \tag{54}$$

Above the spin tensor **w**, was introduced and is defined as

$$\boldsymbol{w} = \frac{1}{2}(\nabla \boldsymbol{v} - \nabla \boldsymbol{v}^T) \tag{55}$$

where $\boldsymbol{v}$ is the velocity vector. To define plasticity it is assumed that the rate of deformation $\boldsymbol{d}$ can be decomposed into an elastic part $\boldsymbol{d}^e$ and a plastic part $\boldsymbol{d}^p$.

$$\boldsymbol{d} = \frac{1}{2}(\nabla \boldsymbol{v} + \nabla \boldsymbol{v}^T) = \boldsymbol{d}^e + \boldsymbol{d}^p \tag{56}$$

A rotated format can then be identified as

$$\boldsymbol{d}^{\boldsymbol{R}} = \boldsymbol{Q}^T \boldsymbol{d} \boldsymbol{Q} = (\boldsymbol{d}^e)^R + (\boldsymbol{d}^p)^R \tag{57}$$

With the above quantities the relation for the elastic problem is given as

$$\dot{\boldsymbol{\sigma}}^R = \boldsymbol{\mathcal{L}}^R (\boldsymbol{d}^e)^R \tag{58}$$

where the constitutive matrix takes the form

$$\boldsymbol{\mathcal{L}}^R = \begin{bmatrix} \frac{1-\nu_{yz}\nu_{zy}}{E_y E_z \Delta} & \frac{\nu_{yx}+\nu_{zx}\nu_{yz}}{E_y E_z \Delta} & \frac{\nu_{zx}+\nu_{yx}\nu_{zy}}{E_y E_z \Delta} & 0 & 0 & 0 \\ \frac{\nu_{xy}+\nu_{xz}\nu_{zy}}{E_z E_x \Delta} & \frac{1-\nu_{zx}\nu_{xz}}{E_z E_x \Delta} & \frac{\nu_{zy}+\nu_{zx}\nu_{xy}}{E_z E_x \Delta} & 0 & 0 & 0 \\ \frac{\nu_{xz}+\nu_{xy}\nu_{yz}}{E_x E_y \Delta} & \frac{\nu_{yz}+\nu_{xz}\nu_{yx}}{E_x E_y \Delta} & \frac{1-\nu_{xy}\nu_{yx}}{E_x E_y \Delta} & 0 & 0 & 0 \\ 0 & 0 & 0 & G_{xy} & 0 & 0 \\ 0 & 0 & 0 & 0 & G_{xz} & 0 \\ 0 & 0 & 0 & 0 & 0 & G_{yz} \end{bmatrix} \tag{59}$$

with

$$\Delta = \frac{1-\nu_{xy}\nu_{yx}-\nu_{yz}\nu_{zy}-\nu_{zx}\nu_{xz}-2\nu_{xy}\nu_{yz}\nu_{zx}}{E_x E_y E_z} \tag{60}$$

The plastic behavior is described with an orthotropic model. The evolution law for the plastic strains is [25]:

$$(\boldsymbol{d}^p)^R = \dot{\boldsymbol{\lambda}} \frac{\partial f}{\partial \boldsymbol{\sigma}^R} \tag{61}$$

where f is the yield function and $f \le 0$, $\dot{\boldsymbol{\lambda}} \ge 0$ and $f\dot{\boldsymbol{\lambda}} = 0$ should be fulfilled [25].

The particular yield function used in the simulations is given by the Hill's stress potential:

$$f(\sigma) = \ldots$$
$$\ldots\sqrt{F(\sigma_y^R - \sigma_z^R)^2 + G(\sigma_z^R - \sigma_x^R)^2 + H(\sigma_x^R - \sigma_y^R)^2 + 2L\tau_{yz}^{R\,2} + 2M\tau_{zx}^{R\,2} + 2N\tau_{xy}^{R\,2}} - \sigma_0 \tag{62}$$

Where

$$F = \frac{\sigma_0^2}{2}\left(\frac{1}{\overline{\sigma}_y^2} + \frac{1}{\overline{\sigma}_z^2} - \frac{1}{\overline{\sigma}_x^2}\right)$$

$$G = \frac{\sigma_0^2}{2}\left(\frac{1}{\bar{\sigma}_z^2} + \frac{1}{\bar{\sigma}_x^2} - \frac{1}{\bar{\sigma}_y^2}\right)$$

$$H = \frac{\sigma_0^2}{2}\left(\frac{1}{\bar{\sigma}_x^2} + \frac{1}{\bar{\sigma}_y^2} - \frac{1}{\bar{\sigma}_z^2}\right)$$

$$L = \frac{3}{2}\left(\frac{\tau_0}{\bar{\tau}_{yz}}\right)^2$$

$$M = \frac{3}{2}\left(\frac{\tau_0}{\bar{\tau}_{xz}}\right)^2$$

$$N = \frac{3}{2}\left(\frac{\tau_0}{\bar{\tau}_{xy}}\right)^2$$

Here $\sigma_0, \bar{\sigma}_x, \bar{\sigma}_y, \bar{\sigma}_z, \bar{\tau}_{xy}, \bar{\tau}_{yz}, \bar{\tau}_{xz}$ is specified by the user as potentials [11].

3.3.2 Cohesive model

The cohesive material used in the interfaces is the cohesive material defined in Abaqus. The elastic behavior is defined by tractions (*t*). For uncoupled behavior the tractions depend only on the nominal strains defined as

$$\begin{bmatrix} t_x \\ t_y \\ t_z \end{bmatrix} = \begin{bmatrix} K_{xx} & & \\ & K_{yy} & \\ & & K_{zz} \end{bmatrix} \begin{bmatrix} \varepsilon_x \\ \varepsilon_y \\ \varepsilon_z \end{bmatrix} \tag{63}$$

Where $\varepsilon_i = \frac{\delta_i}{T_o}$; *i* = *x,y,z*, T_0 is the original thickness of the cohesive element and δ_i are the separations. The stability criterion requires this $K_{xx} > 0$, $K_{yy} > 0$ and $K_{zz} > 0$. The damage is initiated when the maximum nominal stresses reaches a value of one. This can be written as:

$$\max\left\{\frac{\langle t_x \rangle}{t_x^0}, \frac{t_y}{t_y^0}, \frac{t_z}{t_z^0}\right\} = 1 \tag{64}$$

The tractions are then given via the relation

$$t_i = (1-d)t_0 \qquad 0 \le d \le 1, \quad i = x,y,z \tag{65}$$

Where *d* denotes the damage evolution describing the material stiffness degradation. When *d*=1 the material have lost it's carrying capacity.

The damage evolution is exponential:

$$d = 1 - \frac{\delta_m^0}{\delta_m^{\max}}\left(1 - \frac{1 - e^{-\alpha\left(\frac{\delta_m^{\max} - \delta_m^0}{\delta_m^f - \delta_m^0}\right)}}{1 - e^{-\alpha}}\right) \tag{66}$$

Where α is the exponential law parameter, $\delta_m^{\max}$ is the maximum value of the effective displacement during load history, the effective displacement (δ_m) is define below and the effective displacement at complete failure (δ_m^f) and the effective displacement at the initiation of damage (δ_m^0) can be seen in Figure 3.6 [20].

$$\delta_m = \sqrt{\langle \delta_x \rangle^2 + \delta_y^2 + \delta_z^2} \tag{67}$$

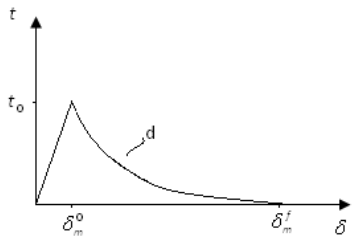

Figure 3.6. Damage evolution

4 Experimental work

As stated earlier the experimental tests are divided into three different parts:

- Laboratorial tests when making straight creases by using a flat bed creasing machine.
- Laboratorial tests when making creases with the pattern of bottom creases by using a flat bed creasing machine.
- Tests in the pilot plant when making creases with the full scale pattern of a Tetra Brik Base, 250ml package using a rotational crease tool.

4.1 Experimental tools and parameters

4.1.1 Laboratory creasing tool

The laboratory creasing tool is mounted into a MTS 858 Table Top System. The male die holder is restricted to only move in the z-direction by rails mounted on the U-bolt and the female die is mounted on a 15kN load cell (Figure 4.1).

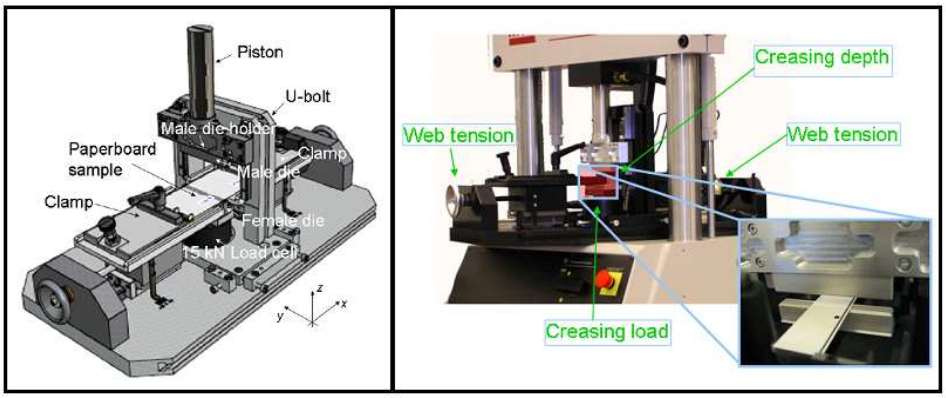

Figure 4.1. The laboratory creasing tool setup unit. Left: 3D-CAD [2], Right: Photography [5]

A schematic sketch of the creasing tool in the xz-plane during creasing of the paperboard is shown in Figure 4.2. The male die has a rule sticking out from the base and can be chosen to have different heights and widths. The female die has a groove where the paperboard is pressed down by the rule during creasing. The groove can also have different depths and widths.

The machine direction (MD) of the paperboard is parallel to the x-direction in Figure 4.1. The paperboard is given a prescribed displacement and a load cell, mounted on the creasing tool, displays the web tension. The speed of the rule is set to be 1mm/s.

During the operation one load cell measures the out of plane crease force in the z-direction (ZD) and one load cell measures the in-plane force in the x-direction (MD). The relative distance between the male and the female die is denoted crease depth. The tests were made at a relative humidity of 50±2% and at a temperature of 23±1degree Celsius.

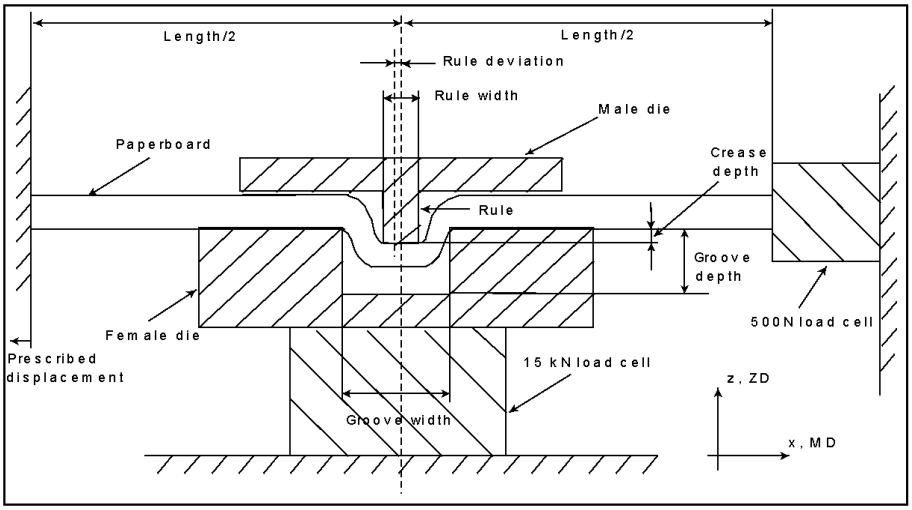

Figure 4.2. A principle 2D-sketch of the creasing tool [5]

The MTS-creaser makes it possible to control the web tension, creasing depth and the creasing speed, and to monitor web tension as function of time, creasing depth as function of time and creasing load as function of time [2]. By use of Matlab the crease force is plotted as a function of crease depth (Figure 4.3). The following parameters are established:

- Maximum force
- Energy: area below the curve
- Remaining deformation of the crease with applied web tension

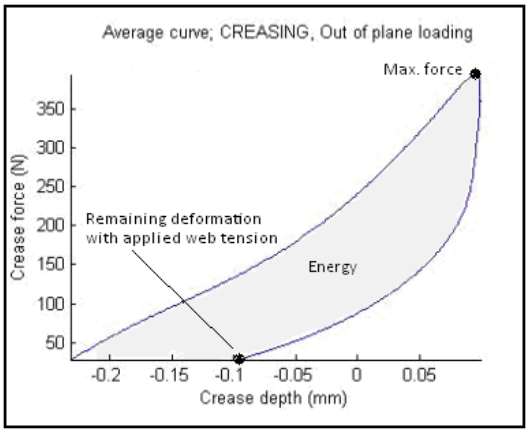

Figure 4.3. Creasing parameters

4.1.2 Creasability tester

To fold the creased paperboard a Lorentzen & Wettre creasability tester (L&W) is used (Figure 4.4). A clamp on the L&W fastens the specimen and when the clamp rotates from 0 to 120 degrees a load cell measures the bending force (Figure 4.5).

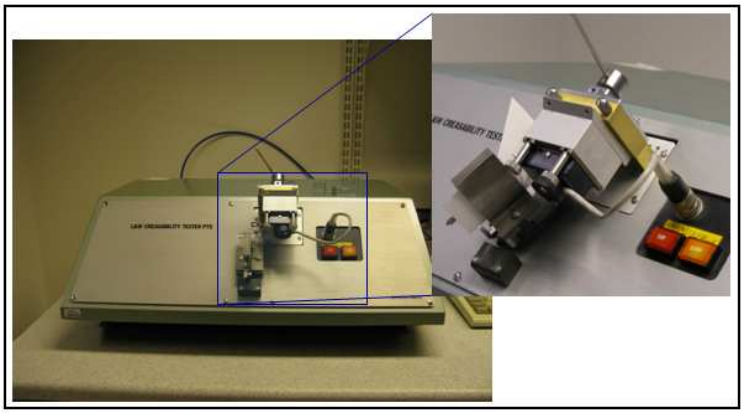

Figure 4.4. L&W Creasability tester [2]

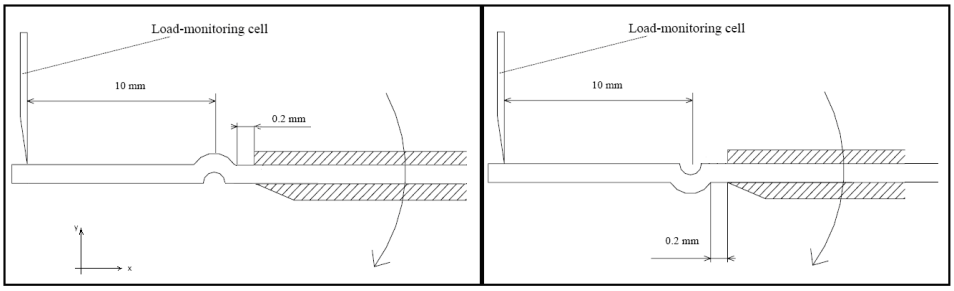

Figure 4.5. Principle sketch of the L&W creasability tester

Both creased and uncreased paperboard of each specimen are folded and by use of Matlab the relation between the bending force and the bending angle is plotted (Figure 4.6).

The following parameters are established:

- Maximum force at or before 30 degrees of the creased sample
- Energy, area below the curve of the creased sample
- Initial inclination of the creased sample (same as initial stiffness of the crease)
- Final angle after released bending force of the creased sample
- Relative Crease Strength – RCS

The RCS value is the relation between the maximum force at or before 30 degrees of the creased sample divided by the maximum force at or before 30 degrees of the uncreased sample. It is desirable with a RCS value as low as possible.

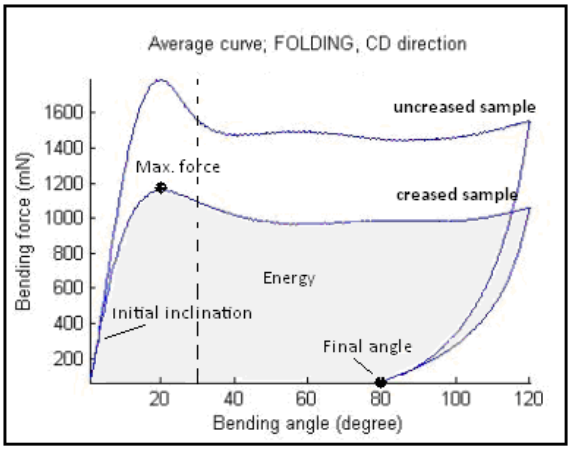

Figure 4.6. Folding parameters

4.1.3 Topography

To study the surface of the creased paperboard an optical 3D measuring system called MikroCAD, GFM is used. This machine is a computer-assisted optical surface measuring system and is used for 2D and 3D profile measurements, as well as roughness measurements of small and microscopic parts. The functional structure of the optical 3D sensor is shown in the principle picture Figure 4.7.

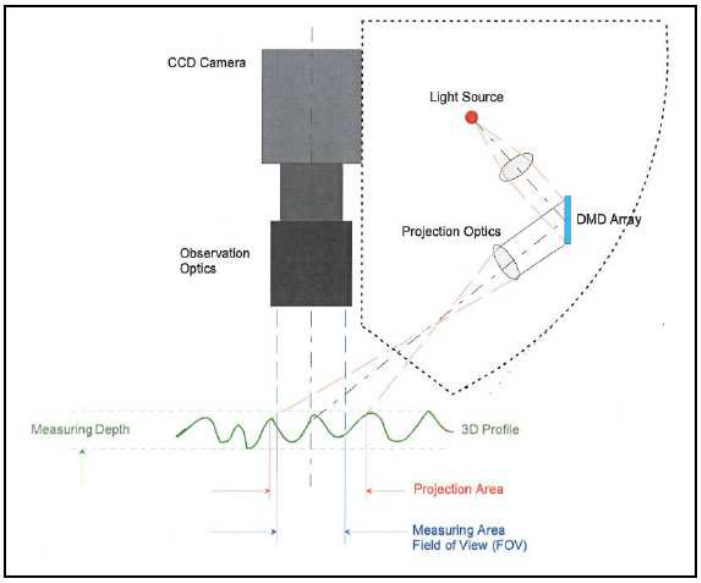

Figure 4.7. Principle sketch of optical 3D sensor [22]

Stripes with sinusoidal intensity of brightness are projected onto the surface of the paperboard and the projection is recorded with a well defined triangulation angle by a CCD camera. The topography of the crease is calculated from the stripes position and the values of all registered individual image points. To analyze the topography it is split in 30 lines and can then be plotted, see Figure 4.8. The MikroCAD can also be used as a microscope and it is possible to detect if there are cracks along the crease.

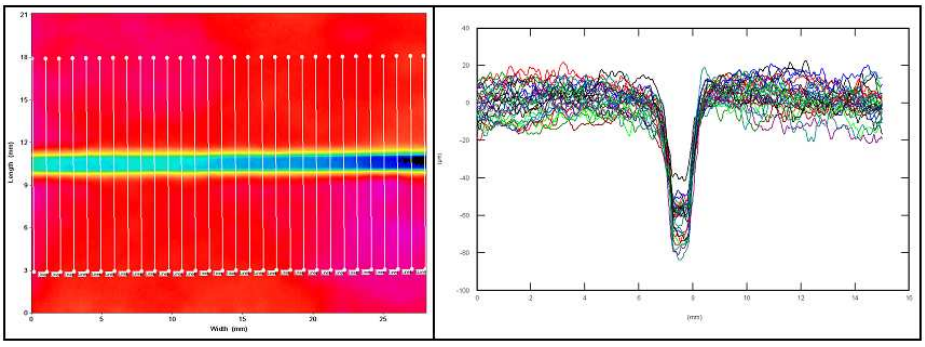

Figure 4.8. Topography split in 30 lines (left), plot of the cross section with all 30 lines (right)

Matlab is used to plot an average curve of the 30 lines, see Figure 4.9. The topography is performed on both sides of the creased paperboard which gives one plot of a “bump” and one of a “dip” (Figure 4.10). The remaining deformation of both sides of the crease can be established from the Matlab plots.

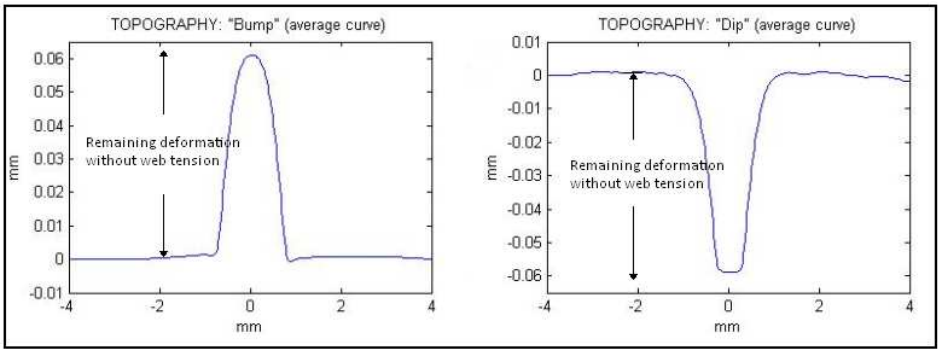

Figure 4.9. Topography parameters

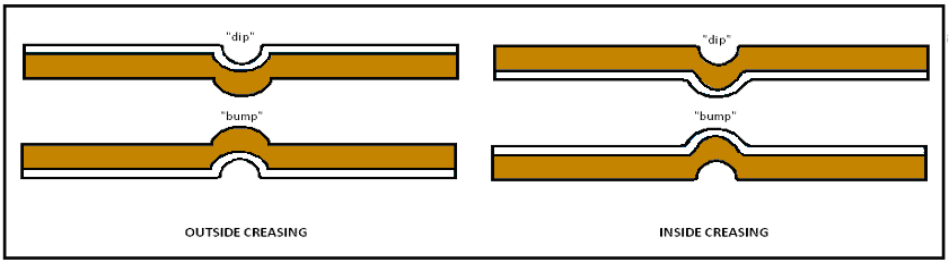

Figure 4.10. Visual illustration of "dip" and "bump"

4.1.4 Photography setup

To film the process of creasing and folding a high speed camera is rigged close to the paperboard. The filming makes it possible to evaluate the whole process when creasing and folding both from the inside and the outside and to see if the behavior differs between the two.

4.1.5 Lab evaluation of the paperboard's properties

The paperboards are sent to the lab for material analysis for evaluation of the paperboard properties. The tests performed on the paperboards are:

- GRAMMAGE: Grammage (g/m²)
- THICKNESS: Thickness (µm)
- TENSILE PROPERTIES: Tensile strength MD and CD (kN/m)
  Tensile strength ratio (%)
  Tensile stretch MD and CD (%)
  Tensile stiffness MD and CD (kN/m)
  E-Modulus MD and CD (MPa)
  Tensile Energy Absorption MD and CD (J/ m²)
- BENDING FORCE: Bending force MD and CD (mN)

Bending force GM (mN)
Bending force index
Bending force ratio

- DENSITY: Density (kg/m³)
- SCOTT BOND: Scott Bond (J/m²)
- Z-TENSILE STRENGTH: Z-tensile strength (kPa)

4.2 First experimental part: straight creases

4.2.1 In parameters

Crease depth: 0.1mm, 0.2mm, 0.3mm

Web tension: 1kN/m, 1.5kN/m, 2kN/m

Crease side: Inside, Outside

Paperboard: A, B, C (thin paperboards)
D, E, F (thick paperboards)

Crease geometry: Straight1, Straight2, Straight3 (to use with thin paperboard)
Straight4, Straight5, Straight6 (to use with thick paperboard)

4.2.2 Procedure

The samples for the tests with straight creases have a width of 38mm and a length of 110mm (Figure 4.11). In the MTS creasing tool the distance between the clamps are 80mm. Each test in the MTS creasing tool consists of 15 samples and out of the 15 samples, five samples are folded using the L&W creasability tester and ten samples are measured in the MikroCAD. The number of samples is chosen to get reliable results.

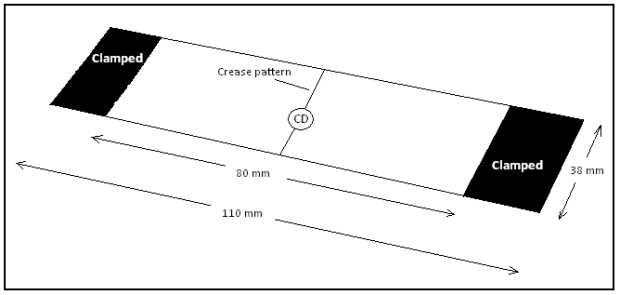

Figure 4.11. Sample for straight crease test

Even though the number of parameters have been reduced it is not possible to perform all combinations of tests within this master's thesis. MODDE is a software using Design of Experiments explained earlier and by the use of this software the number of tests will be considerably less.

The MODDE evaluation is split in two parts, one for the thinner paperboards A-C and one for the thicker paperboards D-F. For each part there are five factors:

- Two quantitative: crease depth and web tension
- Three qualitative: crease side, paperboard and crease geometry.

The responses chosen to evaluate the first experimental part are from the creasing process: maximum force, the remaining deformation of the paperboard ("dip") with applied web tension and the energy (Figure 4.3). From the folding process the responses chosen are: maximum force at or before 30 degrees, initial stiffness of the creased paperboard, RCS and final angle after released bending force (Figure 4.6). The evaluation from the topography gives the remaining deformation of the crease with no web tension, both the "dip" and the "bump" (Figure 4.9). By the use of the MikroCAD it is also possible to see if there are any cracks in the crease area of the paperboard.

The final MODDE worksheets with all experiments for both the thinner paperboard setup and the thicker paperboard setup are found in Appendix A.1 and Appendix A.3. The condition number for these setups is in both cases equal to 2.11 which is less than 3 and can be considered as a good model.

A Matlab software gives six plots: crease force as a function of crease depth (one plot with all tests and one average plot), bending force as a function of bending angle (one plot with all tests and one average plot) and also plots of the average cross section of the crease, both the "dip" and "bump" from the MikroCAD. The software also states the numerical values of the wanted responses, based on calculations from the average plots. The numerical values of the responses are put into the MODDE worksheet and the results can be evaluated by use of the histogram plot, the summary of fit plot and coefficient plot.

The creasing process and the folding process are also filmed in purpose to examine if inside creasing behaves different from outside creasing.

4.3 Second experimental part: bottom crease pattern

4.3.1 In parameters

Crease depth: Vary crease depth until crack limit of the paperboard is reached. Start with crease depth 0.2mm.

Web tension: 1kN/m

Crease side: Inside, Outside

Paperboard: A, B

Crease geometry: Bottom1, Bottom2

4.3.2 Procedure

The samples for the crease tests with bottom crease pattern have a width of 100mm and a length of 180mm (Figure 4.12). In the MTS creasing tool the distance between the clamps are 160mm. The crease pattern shown in Figure 4.12 has creases in both machine direction (MD), cross machine direction (CD) and diagonal direction (DD). In the L&W creasability tester samples for tests in MD has a width of 15mm and samples for tests in CD has a width of 25mm. These samples are cut out from the 100 by 180 sample, their locations are shown in Figure 4.12.

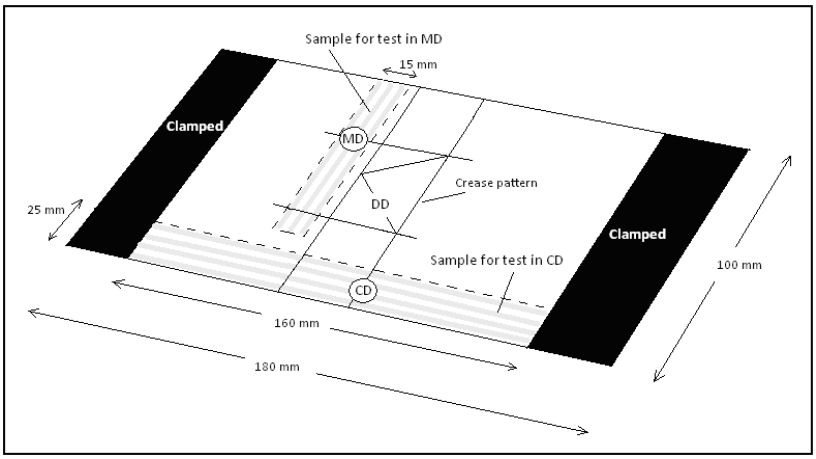

Figure 4.12. Sample for tests with bottom crease pattern

From the results of the first experimental part a decision was taken to investigate at which crease depth cracks appear in the paperboard and what the RCS value is, in

both MD and CD, for those samples. Each test in the MTS creasing tool consists of ten samples and of these five are folded using the L&W creasability tester.

The procedure of the second experimental part is to start creasing to the depth of 0.2mm and then study if there are any cracks developed in the ten samples. If the crack limit is not reached a new test is preformed with the crease depth increased by 0.05mm. This is repeated until the crack limit is reached. If the crack limit is reached in the first test, the test is repeated with the crease depth decreased by 0.05mm. This is repeated until cracks no longer are visible.

The samples are to be folded by the L&W creasability tester in both MD and CD. The RCS value is calculated and the result is displayed in a table.

4.4 Third experimental part: 250 Base crease pattern

4.4.1 In parameters

Crease depth:	Perform the test at crease depth 0.05mm and 0.1mm below the crack limit
Web tension:	1.3kN/m
Crease side:	Inside, Outside
Paperboard:	A, B
Crease geometry:	Crease pattern of a Tetra Brik 250ml Base
Lamination specification:	Aseptic juice package

4.4.2 Procedure

During this last experimental part the paperboard is converted in the Tetra Pak pilot plant. MODDE and Design of Experiments is used throughout this last experimental part and the worksheet can be seen in Appendix F.1 for paperboard and Appendix F.3 for packaging material.

The MODDE evaluation is split in two parts, one for paperboards and one for packaging material. For each part there are three factors:

- One uncontrollable quantitative: crease depth
- Two qualitative: crease side and paperboard

The responses chosen to evaluate the third experimental part are from the folding process: maximum force at or before 30 degrees, initial stiffness of the creased paperboard, RCS and final angle after released bending force. The condition number for these setups is in both cases equal to 1.414 which is considered to be a good model.

The creasing process is performed at the printing press “Briggen” where the paperboard is creased when going through a rotational creasing tool, see Figure 4.13. On the rollers of the rotational creasing tool, male and female crease plates are assembled to represent the creasing tool. Two paperboards are tested, A and B, and two rolls are used for each of the paperboards. The rolls have the width 430mm.

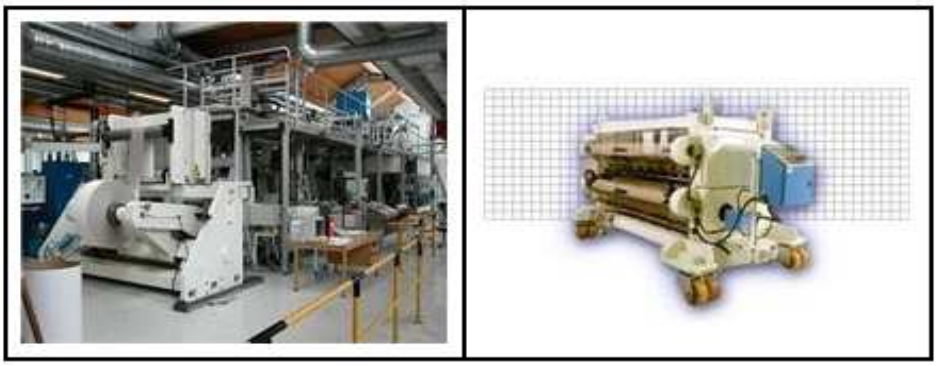

Figure 4.13. Briggen (left), rotational creasing tool (right)

The creasing procedure starts by trying to find at which crease depth the paperboard cracks for an outside creasing for both paperboard A and B. The crease depth is then decreased until no cracks appear, i.e. 0.05mm from the crack limit. Half of the paperboard roll is creased at this crease depth and the rest of the roll is creased with a crease depth 0.10mm from the crack limit. When both paperboard A and B have been creased with outside creasing the crease plates are switched to inside creasing mode. The process performed of outside creasing is then repeated with inside for paperboard A and B.

Samples of paperboard are collected of the creased paperboard before the paperboard is sent to be laminated with the specification of an aseptic juice package. Samples are then collected from the packaging material. The samples of the paperboard and packaging material can be seen in Figure 4.14.

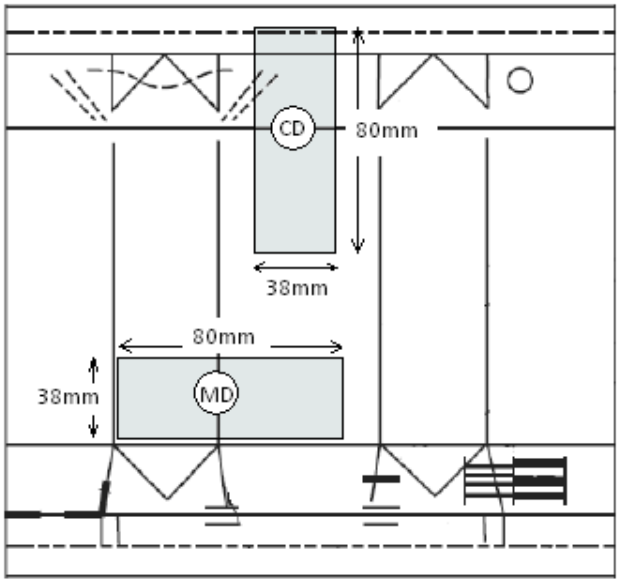

Figure 4.14. Samples for 250 Base crease pattern

Five samples of each setting for both paperboard and packaging material are folded using the L&W creasability tester. The bending force is plotted as a function of bending angle and the average curves of inside and outside creasing are plotted in the same plot so they can be compared to each other.

5 Computer simulation

5.1 Abaqus

Abaqus is a finite element analysis software used to solve a variety of problems both nonlinear and linear. The analysis has three different stages. In the preprocessing the model and the physical problem are defined using Abaqus/CAE, parts can also be imported from other CAD software. This file is sent to the simulation step to be processed with Abaqus/Standard or Abaqus /Explicit. Here the numerical problem is solved and the results are stored in files ready to be post-processed. Abaqus/standard is an implicit solver while Abaqus/Explicit solves the problem explicit. The post-processing is done in Abaqus/CAE and is visualized by color contour plots, animations and X-Y plots. [20]

5.2 Model

The paperboard model is a three dimensional model with an offset of 0.1mm to save computer power and time during simulation. The paperboard is locked in the offset direction hence it can be resembled with a two dimensional model. The height is 390µm containing three plies divided by two interfaces; the model is expected to delaminate in the interfaces. The top and bottom ply are mechanical ply and the middle ply is chemical ply. The exact material parameters can be seen in Appendix J. The interfaces are made up by cohesive elements and both the chemical and mechanical plies are continuum elements described in Material model of paperboard, chapter 3.3. There are only interface elements in the creasing area since the paperboard is expected to delaminate in this region. The length of the paperboard is 80mm since this is the length between the clamps in the experimental setup.

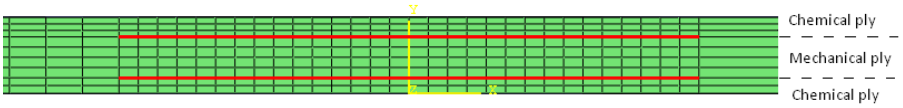

Figure 5.1: Paperboard with two interfaces marked red, showing the different plies.

The continuum element mesh is made up by C3D8R elements; this means an 8-node linear brick element with reduced integration and hourglass control. The cohesive elements are COH3D8; 8-node three dimensional cohesive elements. The mesh is denser in the crease region to better capture the deformation while it is coarser in the regions where the clamp should be since smaller deformations are expected here.

5.2.1 Creasing

The crease setup is the same for both inside and outside creasing since the bottom and top ply have the same material properties and it is easier to change the fold direction than changing the crease tools. The simulated crease tool has the same dimensions as Straight4 in the first experimental setup. Both the male and female dies are made up by rigid bodies. In the tangential direction a friction coefficient of 0.5 is used on the female die, the male die has no tangential behavior hence no friction. In the normal direction both the male and the female die have a pressure-overclosure that is exponential with a pressure of 0.5MPa and clearance of 0.0001mm for the female die and 0.001mm for the male die.

5.2.2 Folding

The best correlation with the experimental behavior is found, according to Appendix K, when the folding model is made up by constraints and boundary conditions instead of a real clamp and load cell. The node sets marked in red in Figure 5.2 are encastred so they cannot move in any direction as if there was a clamp. 10mm from the center of rotation (purple reference point) a set of nodes labeled load cell (yellow in Figure 5.2) is tied to the reference point in the center of rotation with a constraint. Hence if the reference point in the center of rotation moves so does the load cell nodes, this is how the paperboard is folded.

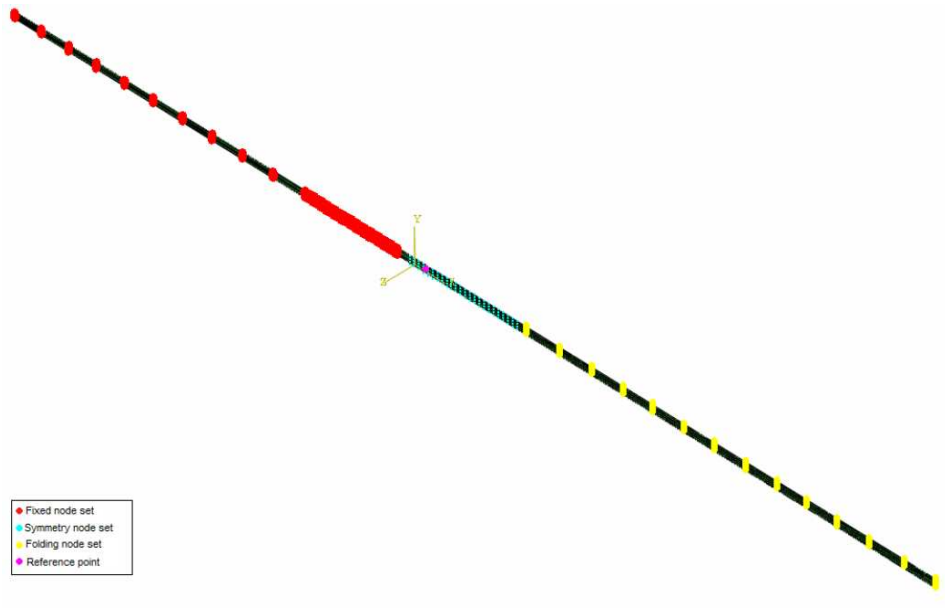

Figure 5.2. Illustration of the boundary conditions

5.3 Procedure

The creasing and folding procedure contains five steps:

1. Apply web tension
2. Male die punch
3. Male die remove
4. Remove web tension
5. Fold

5.3.1 Creasing

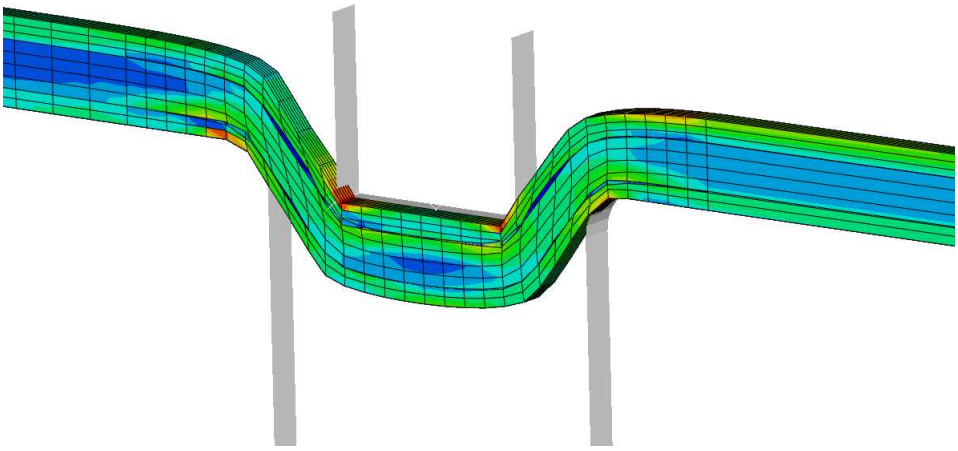

Figure 5.3. Simulating the creasing

The first four steps are the creasing procedure. In the first step the web tension is applied. This is done by boundary conditions displacing the yellow end nodes in Figure 5.2, in the lengthwise direction of the paperboard to stretch it. The second step is when the male die creases the paperboard by being displaced in the y-direction (Figure 5.3) and in step three the male die is moved back up. In step four the yellow end nodes are moved back to their original position. To compare the simulation with the experimental values the reaction force in the male die is used and recalculated, this is done by multiplying the force from the simulation with 380, since the width of the simulated paperboard is 0.1mm and the experimental paperboard is 38mm.

5.3.2 Folding

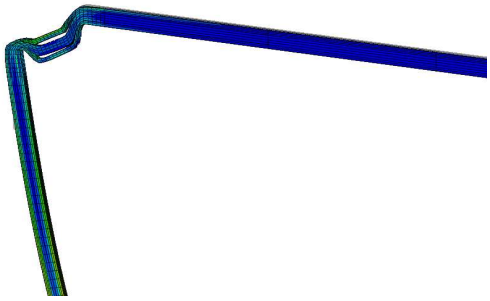

Figure 5.4. Folding after outside creasing

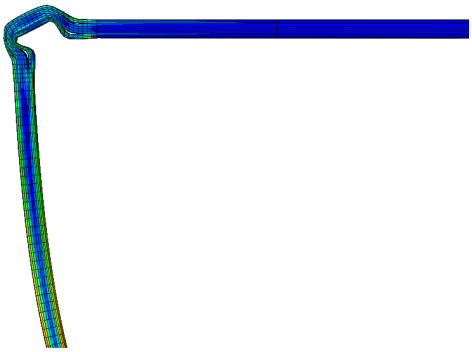

Figure 5.5. Folding after inside creasing

The last step is the fold procedure; if the model was able to unfold there would be one more step, but the model does not converge. In the fold step the fold reference point is rotated 120 deg in either positive or negative direction to give an outside (Figure 5.4) or an inside (Figure 5.5) folding. The value that is compared to the experimental value is the moment in the center of rotation, this need to be recalculated to get the force using:

$$F = \frac{Mw_{\exp}}{lw_{sim}}$$

Where M is the bending moment from the simulations in Nmm per 0.1mm width, w_{exp}=38mm is the width of the experimental paperboard, w_{sim}=0.1mm is the width of the simulated paperboard and l=10mm is the lever. Due to some problem either with calculations or the values received from Abaqus the bending force is scaled down with 1/10 to fit the plot, otherwise the values are not reasonable.

6 Results

6.1 Experimental

6.1.1 Straight creases

The lab evaluation of the paperboards properties showed that the values lie within the specification.

The MODDE worksheet consists of 26 tests and can be seen in Appendix A.1 for the thinner paperboards A-C and Appendix A.3 for thicker paperboards D-F. The numerical values put into MODDE worksheet can be seen in Appendix A.2 for thin paperboard and Appendix A.4 for thick paperboard. When the MODDE worksheet, with all the numerical values, is fitted the summary of fit plot can be used to analyze how well the model fits the results.

The summary of fit plot for thin paperboard can be seen in Figure 6.1. The bars in the summary of fit plot; goodness of fit (R^2), goodness of prediction (Q^2) as well as reproducibility are all excellent according the theoretical limits, stated in subchapter 2.2.1 Design of Experiments - DOE. The bars R^2 and Q^2 are all very high and the difference between them is less than 0.2-0.3 as recommended.

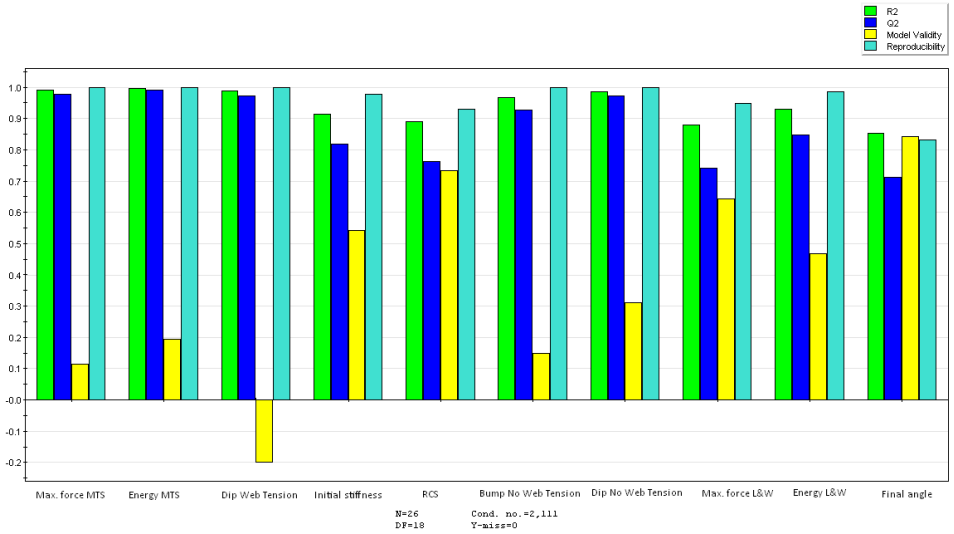

Figure 6.1. Summary of Fit plot for tests performed with thin paperboard, straight creases

The summary of fit plot for thick paperboard can be seen in Figure 6.2. The R^2, Q^2 and the reproducibility bars are just as for thin paperboard excellent according the theoretical limits.

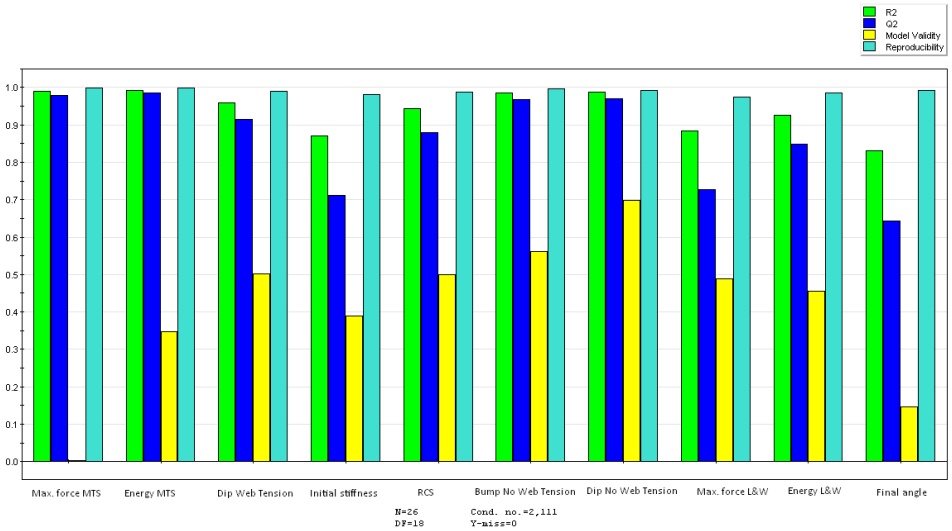

Figure 6.2. Summary of Fit plot for tests performed with thick paperboard, straight creases

Looking at the coefficient plots in Appendix B for the thin paperboards only three responses show a significant difference at 95% confidence level between outside and inside creasing. These are maximum force and energy as well as the remaining deformation ("dip") with applied web tension, all three from the creasing process. None of these responses are measurable in the real production line. The responses with no significant difference between inside and outside creasing for thin paperboard are: the remaining deformation with no applied web tension, both "dip" and "bump", from the topography, initial stiffness, maximum force at or before 30 degrees, energy and final angle from the folding process as well as RCS.

The results in Appendix C for the thicker paperboards D-F are quite different from the thinner paperboards. Here more factors appear to show significant difference at 95% confidence level between inside and outside creasing. These factors are maximum force and energy from the creasing process, maximum force at or before 30 degrees, energy and the initial stiffness from the folding process as well as the RCS. The responses with no significant difference between inside and outside creasing are: final angle from the folding process and the remaining deformation with no applied web tension, both "dip" and "bump" from the topography.

Representative coefficient plots for thin and thick paperboard are displayed in Figure 6.3 with the response being RCS.

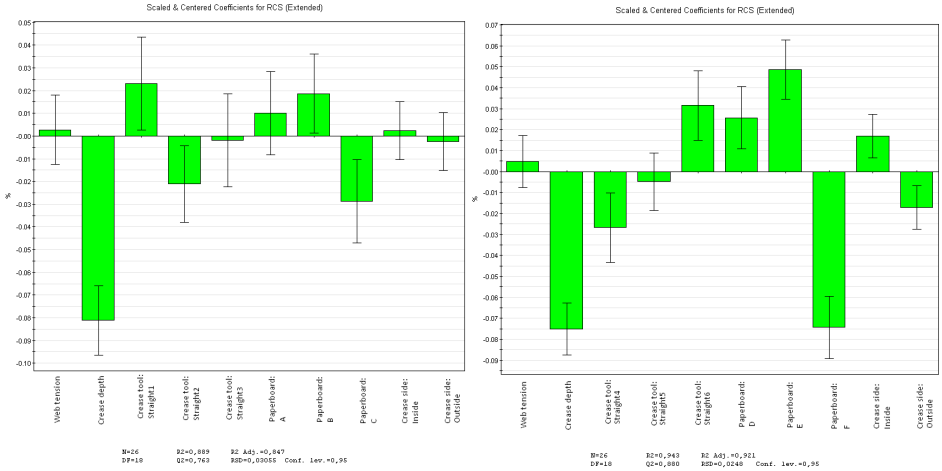

Figure 6.3. Coefficient plot for the response RCS, straight creases: thin paperboard (left), thick paperboard (right)

The coefficient plot for thin paperboard in Figure 6.3 shows that the RCS value is not significantly depending on the crease side. There is a tendency for inside creasing to increase the RCS value compared to outside creasing but the factors paperboard, crease tool and crease depth have a greater impact on the response.

The coefficient plot for thick paperboard in Figure 6.3 shows that the RCS value is significantly depending on the crease side. As with thin paperboard there is a tendency for inside creasing to increase the RCS value compared to outside creasing and here too the factors paperboard, crease tool and crease depth have a greater impact on the response.

Sequences of photos were extracted from the filming of the creasing and folding process. All creasing photos are displayed in Appendix D and all folding photos in Appendix E. Representative photos can be seen in Figure 6.4 and Figure 6.5.

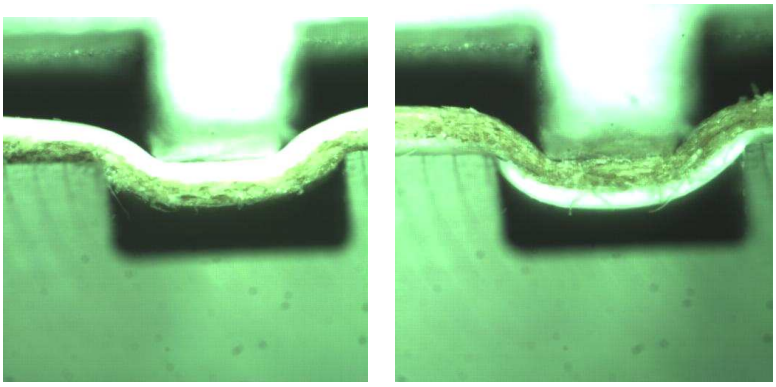

Figure 6.4. Photos of the creasing process with straight creases, paperboard D: outside creasing (left), inside creasing (right)

It is difficult to see if the paperboard behaves differently when comparing outside and inside creasing and when studying the photos in Figure 6.4; their behavior look similar.

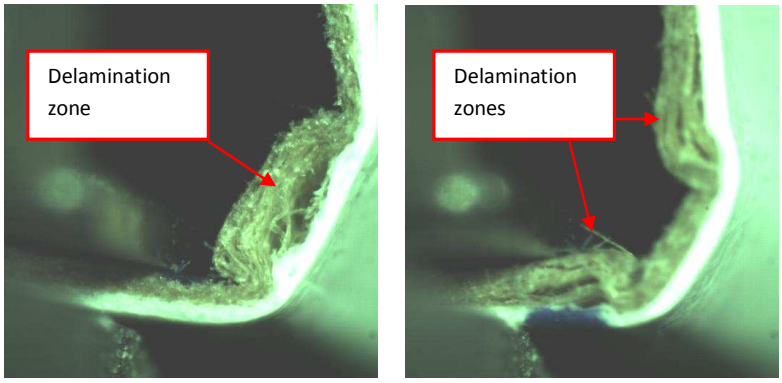

Figure 6.5. Photos of the folding process with straight creases, paperboard D: outside creasing (left), inside creasing (right)

When looking at the photos of the folding process in Figure 6.5 it is apparent that inside crease paperboard folds and delaminates very differently from outside creased paperboard. All photos in Appendix E show the same behavior.

During the first experimental part cracks were discovered in some specimens. The cracks only occur on some tests and only on inside creasing. For all paperboards except A there are cracks on inside creasing at the crease depth of 0.30 mm, independent of crease tool and other factors. Cracks are not acceptable and are therefore investigated further when looking at bottom creases.

6.1.2 Bottom crease pattern

The lab evaluation of the paperboards properties showed that the values lie within the specification.

The results from the tests of bottom creases can be seen in Table 6.1. The table displays the RCS value in the machine direction (MD) and the cross machine direction (CD) and if any cracks are visible. The geometrical mean RCS value is defined as: $RCS_{GM} = \sqrt{RCS_{MD} \times RCS_{CD}}$.

Table 6.1. Results of tests on Bottom crease pattern

Crease tool	Crease side	Crease depth	PAPERBOARD A				PAPERBOARD B			
		[mm]	RCS MD	RCS CD	RCS GM	Crack	RCS MD	RCS CD	RCS GM	Crack
Bottom1	Inside	0.10	-	-	-	-	0.70	0.62	0.66	No
		0.15	0.62	0.60	0.61	No	0.62	0.54	0.58	Yes
		0.20	0.57	0.52	0.54	Yes	0.52	0.50	0.51	Yes
		0.25	-	-	-	-	-	-	-	-
	Outside	0.10	-	-	-	-	0.69	0.57	0.63	No
		0.15	-	-	-	-	0.62	0.54	0.58	Yes
		0.20	0.49	0.50	0.50	No	0.54	0.50	0.52	Yes
		0.25	0.48	0.52	0.50	Yes	-	-	-	-
Bottom2	Inside	0.10	-	-	-	-	0.66	0.66	0.66	No
		0.15	-	-	-	-	0.60	0.60	0.60	Yes
		0.20	0.55	0.59	0.57	No	-	-	-	-
		0.25	0.46	0.46	0.49	Yes	-	-	-	-
	Outside	0.10	-	-	-	-	0.68	0.63	0.65	No
		0.15	0.60	0.57	0.58	No	0.63	0.58	0.60	Yes
		0.20	0.58	0.53	0.55	Yes	0.56	0.51	0.53	Yes
		0.25	-	-	-	-	-	-	-	-

The red numbers mean that cracks were found on the samples. After closer examining and folding the specimens there were two samples that initially seemed to not have any cracks but when folded and examined closely, cracks were found. These two samples are marked with a red No in Table 6.1.

Table 6.1 shows that for paperboard B outside creasing gives a slightly lower RCS than with inside creasing independent if crease tool Bottom1 or Bottom2 is used. When using paperboard A it is a bit more complicated. Crease tool Bottom1 in combination with paperboard A shows that the RCS value is lower when using

outside creasing than it is with inside creasing. Bottom2 in combination with paperboard A shows that inside creasing gives a lower RCS than with outside creasing.

6.1.3 250 Base crease pattern

The lab evaluation of the paperboards properties showed that the values lie within the specification.

The MODDE worksheet consists of ten tests and can be seen in Appendix F.1 for paperboard samples and Appendix F.3 for samples of packaging material. The numerical values put into MODDE worksheet can be seen in Appendix F.2 for paperboard and Appendix F.4 for packaging material.

The summary of fit plot for paperboard and packaging material can be seen in Figure 6.6 and Figure 6.7. Most of the responses show a good and valid model with a good reproducibility. The bars R^2 and Q^2 are high and the difference between them is less than 0.2-0.3 as recommended. Exceptions are the final angle in MD and the RCS value in both CD and MD. These three responses indicate a poor goodness of prediction, but the yellow bars are high which indicate a valid model.

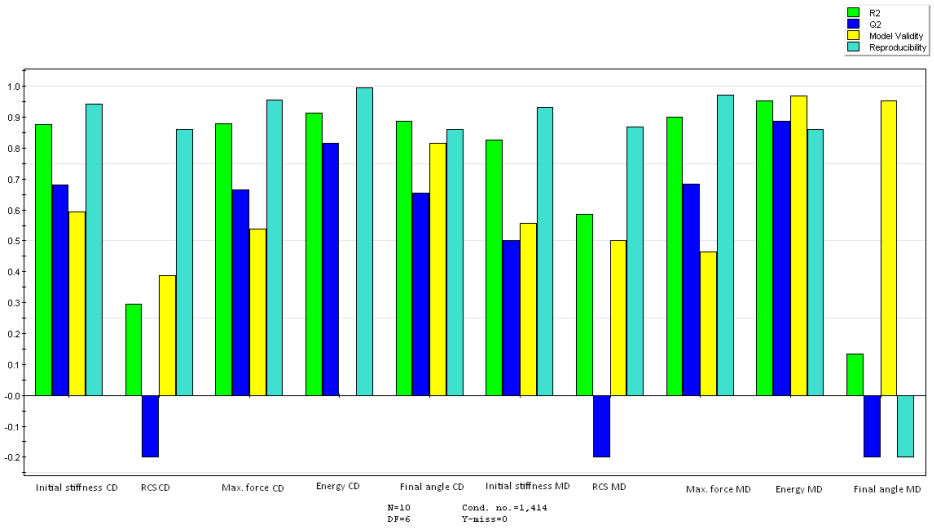

Figure 6.6. Summary of Fit plot for tests performed on paperboard, 250 Base crease pattern

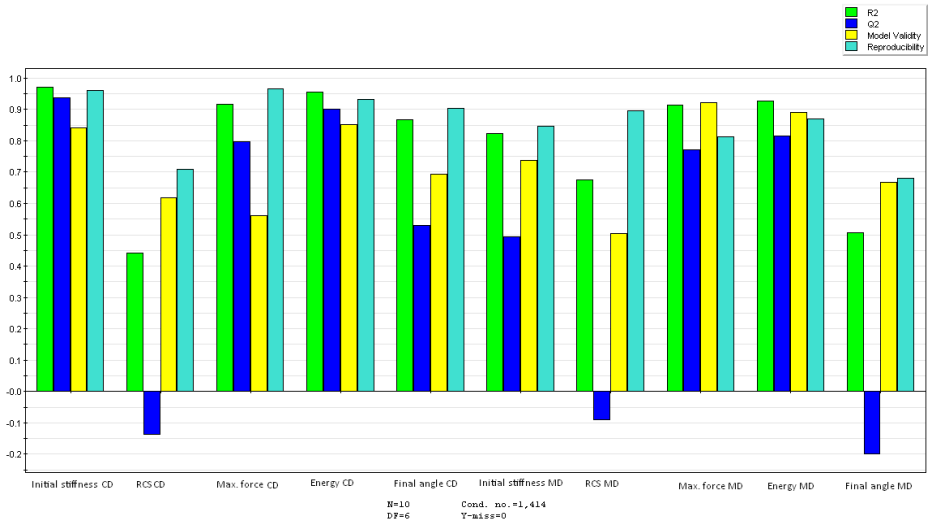

Figure 6.7. Summary of Fit plot for tests performed on packaging material, 250 Base crease pattern

The coefficient plots for paperboard and packaging material are all displayed in Appendix G and Appendix H showing that for all responses outside and inside creasing alone do not show significant difference at 95% confidence level. All responses for both paperboard and packaging material indicate that when paperboard B is used the values of all responses are increased compared to paperboard A.

Representative coefficient plots for paperboard and packaging material in Figure 6.8 for the response Energy CD.

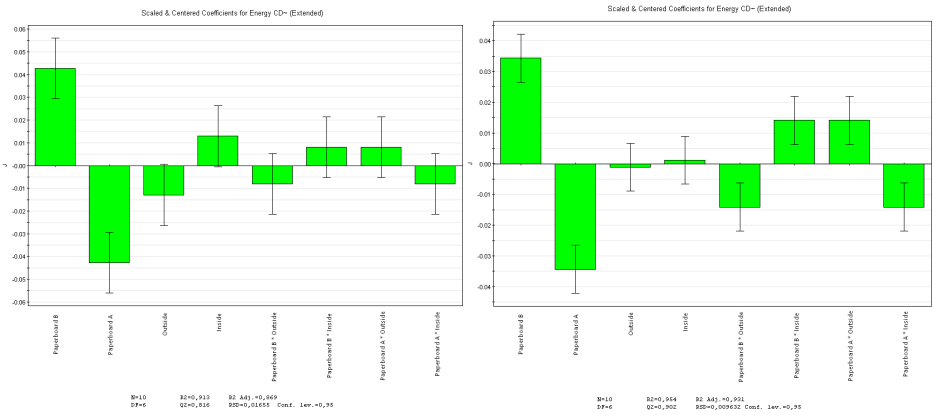

Figure 6.8. Coefficient plot for the response Energy CD for 250 Base crease pattern: paperboard (left), packaging material (right)

As can be seen in Figure 6.8 the crease side does not make a significant difference at 95 % confidence level and at the same time paperboard does make a significant difference. Both these observations are consistent with all other responses for both paperboard and packaging material. Paperboard B seems to increase the energy compared to when using paperboard A just as inside creasing indicate an increasing energy compared to outside creasing. Paperboard influences the energy and all other responses much more in than the crease side. It is also interesting to see that when paperboard and crease side are combined, paperboard B combined with outside creasing and paperboard A combined with inside creasing indicate a lower energy while paperboard B combined with inside creasing and paperboard A combined with outside creasing indicate an increased energy.

A graphic comparison between outside and inside creasing for paperboard A with the crease depth 0.23mm and paperboard B with the crease depth 0.13mm of both paperboard and packaging material in CD and MD can be seen in Appendix I. The plots show the average bending force plotted as a function of bending angle and to see the variation of the average plots the standard deviation is included. A representative plot can be seen in Figure 6.9.

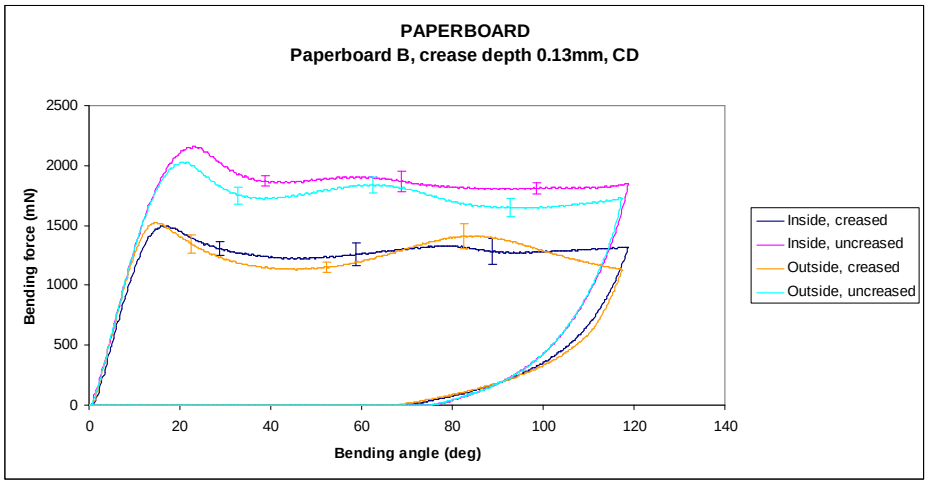

Figure 6.9. Representative plot of bending force as a function of bending angle, comparing inside and outside creased paperboard

6.2 Computer simulation

The results from the simulations compared to the experimental results can be seen in Appendix L where the simulation is plotted against the experimental result for the same setup. There are only five plots but there are six experiments made on this

crease tool. The sixth simulation using web tension 2kN/m and crease depth 0.3mm failed. The two plots found below in Figure 6.10 are the plots showing the best resemblance between simulation and experimental values.

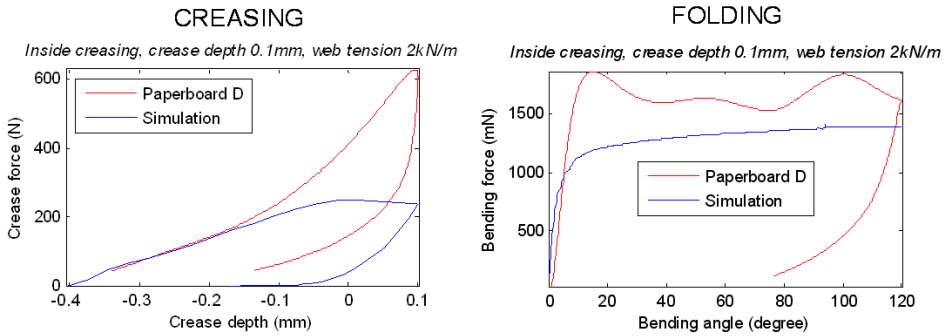

Figure 6.10. Comparing the simulation with experimental test, creasing (left), folding (right).

Appendix M shows a comparison between inside and outside creasing during folding for the computer simulations with the same crease settings. The creasing is not shown since the results are exactly the same for both cases. As can be seen in Figure 6.11 the inside and outside folding plots follow each other very well, inside creasing have a slightly higher bending force than outside creasing. This is conclusive for all three graphs.

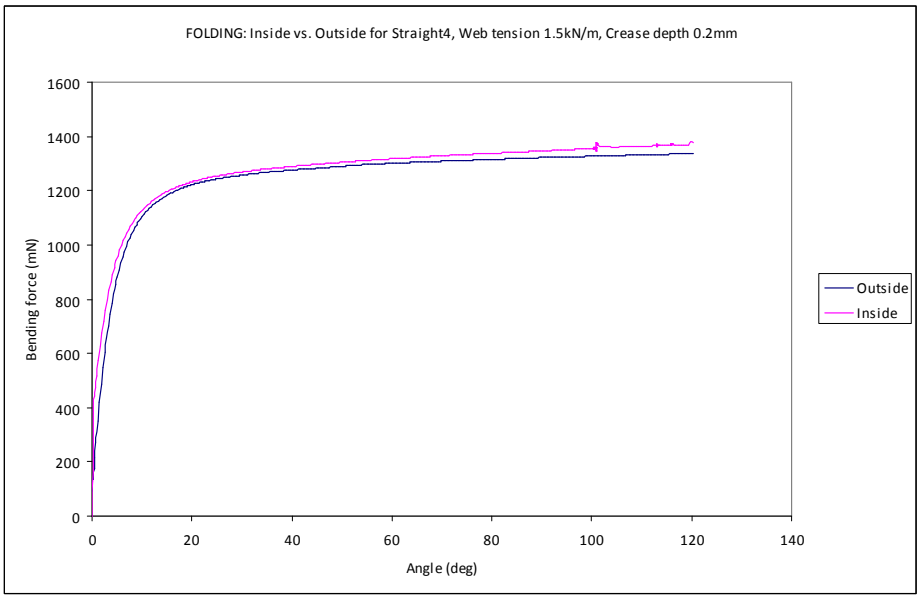

Figure 6.11. Comparing inside creasing with outside creasing in folding

The delamination and folding of the paperboard in simulation is very different for inside and outside creased paperboard as can be seen in Figure 6.12.

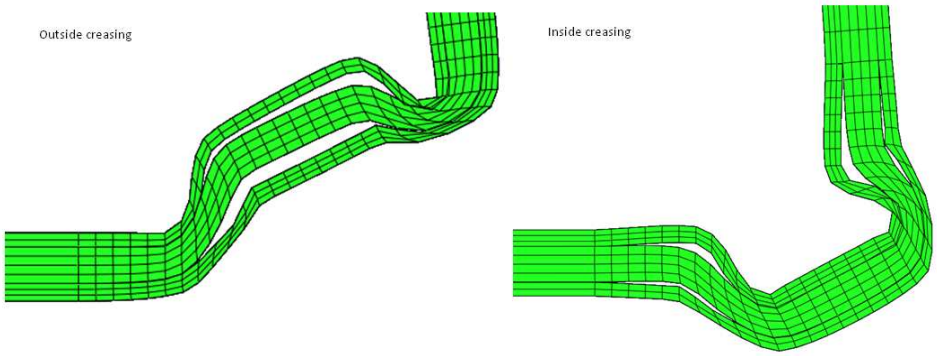

Figure 6.12. The delamination in the simulation during folding, outside creasing (left), inside creasing (right).

7 Discussion

7.1 Experimental

7.1.1 Straight creases

The results of the summary of fit plots for both thin and thick paperboard are very good which means that the model and the results are reliable. The model validity may seem low on some responses and is negative for the response remaining deformation with applied web tension (Dip Web Tension), but according to *Design of Experiments – Principles and Applications* [9] this is nothing to worry about when R^2, Q^2 and the reproducibility bars are as high as they are.

The coefficient plots for thin paperboard show that only the maximum force, energy and remaining deformation with applied web tension from the creasing process are significantly affected by the crease side. None of these are measurable in the real production line. The RCS value is an important measurement considering how well the creases are converted and when the paperboard is creased in the real production line. RCS is often the only factor used to study the creases. Neither outside nor inside creasing do significantly affect the RCS value according to the coefficient plots for thin paperboard. A interesting note is that even thought there in most cases are no significant difference between inside and outside creasing on the responses there is a tendency for the responses to increase with inside creasing.

The coefficient plots for thick paperboard show that only the maximum force and energy from the creasing process, maximum force at or before 30 degrees, energy and the initial stiffness from the folding process as well as the RCS are significantly affected by the crease side. The tests performed on thick paperboard imply an increasing RCS with inside creasing compared to outside creasing. This corresponds with results received from earlier tests done on the RCS value while investigating the difference between inside and outside creasing when evaluating the grip stiffness of packages [6]. All responses seem to increase with inside creasing compared to outside creasing.

The photos of the folding process of thick paperboard show that outside and inside creasing delaminate very differently. Even though the delaminations are very different they both seem to delaminate well and contribute to defined package corners. The corners of inside creasing might be perceived as a bit more defined than for outside creasing. Outside creasing gives rise to one large delamination zone while inside creasing has two smaller delamination zones. The fact that for example the energy and the maximum force at or before 30 degrees are higher for inside

creasing than for outside creasing might be explained by that it takes more energy to create a crack than for an existing crack to grow. Since the maximum force when folding is larger for inside creasing than for outside creasing this also means that the RCS value for inside creasing is higher than for outside creasing. That the RCS value for outside creased paperboard is lower than the inside creased paperboard does not necessary mean that its performance is worse. Maybe the RCS of an inside creased paperboard cannot be compared to the RCS of an outside creased paperboard? Maybe it is like comparing apples and oranges? There might be a need for one specification for outside RCS and on for inside RCS.

7.1.2 Bottom crease pattern

As have been stated in the results for bottom crease pattern the crack limit on the different paperboards A and B are very different. Paperboard B has a lower crack limit for inside creasing than for outside creasing. While for paperboard A the influence of the crease geometry have to be taken into account since the crack limit is opposite for Bottom1 and Bottom2. Hence the conclusion would be that there is more of a difference between the paperboards and crease geometries than between inside and outside creasing something that was shown in the experimental part with straight creases.

Investigating the RCS value that is preferred as low as possible one observes that the lowest RCS value over all is for paperboard A in combination with: crease geometry Bottom1, outside creasing on the crease depth 0.2mm. The second best setting overall and the best setting for paperboard B is also Bottom1 and outside creasing but with a decreased crease depth of 0.1mm. For crease geometry Bottom2 the best setting is using paperboard A with inside creasing on the crease depth of 0.2mm, this is also the best setting for inside creasing over all.

7.1.3 250 Base crease pattern

The summary of fit plot for tests performed on paperboard (Figure 6.6) show a poor model for the responses RCS CD, RCS MD and final angle MD. It is difficult to say why the goodness of prediction bar (Q^2) for RCS CD and MD is low but the poor Q^2 for the response final angle MD might depend on the scatter of the numerical values of the center points, see the numerical values of test 3, 6 and 8 for the final angle MD in Appendix F.2.

The summary of fit plot for test performed on packaging material (Figure 6.7) also show a poor model for the responses RCS CD, RCS MD and final angle MD, just as for the tests performed on pure paperboard. The response final angle MD's poor Q^2 cannot depend on the scatter of the numerical values of the center points since the

reproducibility bar is pretty high. It's difficult to say why the responses RCS CD, RCS MD and final angle MD show a poor model. We have noticed in Figure 6.9 and Appendix I that all tests have the same unfolding curve starting at 120deg and ending at 70deg independent of paperboard, packaging material, crease depth and crease direction. What this might depend on is hard to say but it could be something with the behavior of the L&W.

None of the coefficient plots for paperboard (Appendix G) or packaging material (Appendix H) are significantly affected by the crease side, but are significantly affected by the choice of paperboard. The coefficient plots show for both paperboard and packaging material that all responses are increased when paperboard B is used compared to paperboard A. Even though the crease side is insignificant there is an indication that the responses are increased with inside creasing compared to outside creasing. The coefficient plots for both paperboard and packaging material show that the choice of paperboard has a greater impact on the responses than the choice of crease side.

The representative plot in Figure 6.9 shows that the curves of the inside and outside creased samples are very similar. The difference between the uncreased samples is larger than between the creased samples, which is quite surprising. The fact that there is a larger difference between the uncreased samples than there is for the creased samples can conclude that there is no apparent difference between inside creasing and outside creasing on the measured parameters. When studying the rest of the plots in Appendix I they indicate the same result.

7.2 Computer simulation

The converting of the moment, obtained in the simulations of folding, to bending force that can be compared to the experimental values showed that our values of bending force are ten times bigger than the experimental values. Hence the simulated bending force was scaled down with 1/10. The reason for our values being so much bigger was not found but could be due to human error or have something to do with the values received from Abaqus. Several attempts were made to find a solution to the problem with several different persons doing the calculations and looking into the values attained.

In Figure 6.10 and Appendix L the simulations are compared with experimental results. In creasing the simulation most resemblance paperboard D as can be seen in Figure 6.10, unfortunately only one of the simulations can be compared with paperboard D since the other simulation that was comparable with paperboard D

failed. The failure was probably due to the fact that the settings where a combination of web tension 2kN/m and crease depth of 0.3mm, these are the highest settings so the simulation did not converge. The simulation follows the curve quite well in the beginning of the creasing but cannot capture the maximum force. This problem has also been noticed by Nygårds [4]. In the unloading of the creasing the simulation has the same behavior as the experimental, the curves seem to be parallel. In the folding the simulation curve does not follow the experimental curve as well as in the creasing. Neither does it show the maximum force, this corresponds with results retrieved by Hui [17]. The simulation curves are very even in their behavior when yield stress is reached this is not the case for the experimental curves that have a wavy curve above yield, this is likely dependent on the fact that our simulations are run in Abaqus/Standard, Abaqus/Explicit would probably show the "waves".

Comparing the simulation and experimental plots in both creasing and folding it is possible to see that there is a big difference between the simulations and experiments. This makes it hard to actually tell if the data we obtain from the simulation are useful. A better material model and setup have to be developed for the simulations to better capture the maximum forces.

When comparing the folding of inside and outside creased paperboard in Figure 6.11, the simulation for the folding of inside creased paperboard follows the folding of outside creased paperboard very closely, this is the same for all the graphs shown in Appendix M. Using crease tool Straight4 there is only a small increase in force needed to fold a inside crease compared to outside crease in all the different settings, the same tendency is found with the experimental tests. Hence there is no difference between inside and outside creasing in the simulations for the model used. A problem with the simulations is that they all look very much the same independent of different settings. The maximum force seems to be the same independent of web tension and crease depth, the maximum force in creasing is around 250N and the maximum bending force is around 1200mN, this is not the case for the experimental values where both the maximum crease and folding force change depending on web tension and crease depth. Therefore it is not alarming that the folding curves comparing inside and outside look the same.

Comparing the simulated delamination in Figure 6.12 with the photos in Figure 6.5 and Appendix E, of the delamination in the experimental setup, one can see that the delamination of the folding in the simulations look very much like the delamination

of the experimental tests. Hence the delamination is well simulated and the two interfaces seem to capture the behavior well.

There were several problems encountered during the simulation except for the ones already mentioned. Such as the unfold step did not work for most of the different folding models as can be seen in Appendix K, this could be due to the fact that there seemed to be damping in the material that was not expected, this was also a problem since the paperboard started to fold before there was a resistance to hold the paperboard down in the folding using a rotating clamp. This unaccounted damping might also be the reason the moving clamp curve look so different from the other curves in Figure K.7. Another problem in the simulation of the moving clamp is that the load cell goes into the material when folding to more than 90 deg.

8 Conclusions

- For the thin paperboards A-C considering the straight crease tool and the creasing process there is a significant difference between outside and inside creasing considering the responses: maximum force, energy and remaining deformation. Paperboard, crease tool and crease depth have a more significant influence on all the investigated responses than crease side.

- Considering straight creases with thick paperboard D-F the crease side has a significant impact on the responses maximum force and energy from the creasing process and maximum force, energy and initial stiffness and RCS from the folding process. As for thin paperboard the choice of crease tool, crease depth and paperboard have a greater impact on the responses than crease side.

- When investigating straight creases both thin and thick paperboard show a tendency to crack at a lower crease depth for inside creasing compared to outside creasing. This also applies for thin paperboard combined with 250 Base crease pattern.

- Photos of the creasing process when using thick paperboard show that inside and outside creasing behave very similarly. Studying the photos of the folding process show a big difference in delamination for inside and outside creasing.

- Test performed on thin paperboard when using a bottom crease pattern show that the paperboard and crease tool have a greater influence on the RCS value than the crease side.

- None of the responses are significantly affected by the crease side for thin paperboards and packaging material using 250 Base crease pattern. The choice of paperboard has a greater impact on all investigated responses compared to the crease side.

- The results from the simulation show that the delamination of inside and outside creased paperboard is very different which is consistent with the experimental delamination. Both crease and bending force of the simulation seem independent of crease depth and web tension which is not consistent with the experiments.

9 Recommendations of further investigation

In this master's thesis interesting parameters were selected to be investigated after discussion with our supervisors, other parameters might be of interest and give a different answer and might therefore be interesting to examine in the future. Earlier investigations have shown that there is a difference between inside and outside creasing considering the perception of grip stiffness, which may indicate that there exist some undiscovered parameters showing a difference in the shape of the package.

The RCS value as stated earlier is an important measure of how well the crease is converted. In this study RCS have not shown any univocal difference on inside and outside creasing, but delamination differences have been detected between the two which might indicate that the RCS value needs a complement for evaluating creases.

The simulation model needs a closer examination since it is unable to capture the behavior of the paperboard. There are several ways to fold the paperboard in the simulations, in this study only three were tried and other possibilities exist. The best would probably be if a simulation with a rotating clamp and stationary load cell worked since this is closer to the real experimental setup and might give a better correlation to the experimental values.

10 References

Tetra Pak internal:

1 Information brochure from Tetra Pak, (2005), *Tetra Pak – development in brief,* Code 9704en

2 Just, M. & Tryding, J., (2008), *Laboratory study of creased board*, Power Point Presentation Tetra Pak 080901

3 Karlsson, C., Gustafsson, A., Ljung, A., Andersson, M., Olevall, L. & Strandberg, E., (2008), *Production Report CR TBA Monte Mor 2007 w 38*, Development Report Tetra Pak nr DR0024638

4 Nygårds, M. (2008) *Creasing of paperboard*, STFI-Packforsk Report No.:395

5 Nygårds, M., Just, M. & Tryding, J., (2008), *Experimental and numerical studies of creasing of paperboard*, Preprint submitted to Elsevier

6 Olevall, L. & Tryding, J., (2007), *Reduced board stiffness by use of inside creasing – inhouse verification*, Development Report Tetra Pak nr DR0022031

7 Rosander, J., (2006), *Creasing Development TAA*, Development Report Tetra Pak nr DR0021173

8 Tryding, J. & Just, M., (2008), *Memo*, Tetra Pak Packaging Solutions – Base Materials

External literature:

9 Eriksson, L., Johansson, E., Kettaneh-Wold, N., Wikström, C. & Wold, S., (2008), *Design of Experiments – Principles and Applications*, 3rd ed., Umetrics

10 Ottosen, N. & Petersson, H., (1992), *Introduction to the finite element method*, Prentice Hall

11 Ottosen, N. S. & Ristinmaa, M., (2005), *The Mechanics of Constitutive Modeling*, Elsevier Ltd

12 Patel, R. & Davidson, B., (1994), *Forskningsmetodikens grunder: Att planera, genomföra och rapportera en undersökning*, 2nd ed., Studentlitteratur

13 Regnell, B. & Runeson, P., (2006), *Att genomföra examensarbete*, Studentlitteratur

14 Ristinmaa, M. & Ljung, C., (2002) *An introduction to stability analysis*, Department of Solid Mechanics, Lund University

Master's thesis:

15 Bristow, J. A., Fellers, C., Mohlin, U., Norman, B., Rigdahl, M. & Ödberg, L., (1991), *Pappersteknik*, Institutionen för Pappersteknik, Kungliga Tekniska Högskolan

16 Eliason, O. & Hansson, L., (2005) *Evaluating the 3dm Model – An Experimental and Finite Element Study*, Master's Thesis at Lund University

17 Huang, H., (2008), *Folding of Paperboard*, Master's Thesis at Royal Institute of Technology

18 Just, M. & Pålsson, M., (2003), *Roller nip influence on crease geometry and bending stiffness*, Master's Thesis at Lund University

19 Xia, Q. S. (2002) *Mechanics of inelastic deformation and delamination in paperboard*, Master's thesis at Massachusetts Institute of Technology

Manuals:

20 Abaqus v 6.8, (2008), *Documentation*, Dassault Systèmes

21 MODDE v 8.0, (2006), *User Guide and Tutorial for MODDE*, Umetrics

22 OSCAD 4.0, *Manual – Optical 3D Measuring Device MikroCAD compact,* GFMesstechnik GmbH

Interviews :

23 Nilsson, Johan. Development Engineer, Tetra Pak Lamination Technology, September 11th, 12thand 18th, and October 21st 2008

24 Nygårds, Mikael. Senior Research Associate, STFI – Packforsk, October 9th and 10th, 2008

25 Ristinmaa, Matti. Professor, Head of Division of Solid Mechanics, Lund University, November 20th, 2008

List of Appendices

Appendix A	Straight creases: *MODDE Worksheet*	64
Appendix B	Straight creases: *MODDE Coefficient plots, thin paperboard*	68
Appendix C	Straight creases: *MODDE Coefficient plots, thick paperboard*	73
Appendix D	Straight creases: *Photos of creasing process*	78
Appendix E	Straight creases: *Photos of folding process*	84
Appendix F	250 Base crease pattern: *MODDE Worksheet*	90
Appendix G	250 Base crease pattern: *MODDE Coefficient plots, paperboard*	92
Appendix H	250 Base crease pattern: *MODDE Coefficient plots, packaging material*	97
Appendix I	250 Base crease pattern: *Comparing inside and outside creasing*	102
Appendix J	Computer simulation: *Material Parameters*	106
Appendix K	Computer simulation: *Comparing simulation models*	107
Appendix L	Computer simulation: *Comparing simulation results with experimental results*	112
Appendix M	Computer simulation: *Comparing Inside vs. Outside creasing*	114

Appendix A Straight creases: *MODDE Worksheet*

A.1 Worksheet, thin paperboard

Test Number	Web tension	Crease Depth	Crease Tool	Paperboard	Crease Side
	[kN/m]	[mm]			
1	2	0.1	Straight3	B	Inside
2	1	0.1	Straight3	C	Inside
3	1	0.1	Straight3	A	Outside
4	2	0.3	Straight3	C	Inside
5	2	0.3	Straight3	B	Outside
6	1	0.3	Straight3	A	Outside
7	2	0.1	Straight1	A	Inside
8	1	0.1	Straight1	B	Outside
9	2	0.1	Straight1	C	Outside
10	2	0.3	Straight1	A	Inside
11	1	0.3	Straight1	C	Inside
12	1	0.3	Straight1	B	Outside
13	1	0.1	Straight2	B	Inside
14	2	0.1	Straight2	A	Outside
15	1	0.1	Straight2	C	Outside
16	1,5	0.2	Straight2	A	Outside
17	1,5	0.2	Straight2	A	Inside
18	1,5	0.2	Straight2	B	Outside
19	1,5	0.2	Straight2	B	Inside
20	1,5	0.2	Straight2	B	Outside
21	1,5	0.2	Straight2	B	Inside
22	2	0.3	Straight2	B	Inside
23	1	0.3	Straight2	A	Inside
24	2	0.3	Straight2	C	Outside
25	1,5	0.2	Straight2	A	Outside
26	1,5	0.2	Straight2	A	Outside

A.2 Numerical values of MODDE worksheet, thin paperboard

	CREASING			FOLDING					TOPOGRAPHY		
Test Number	Max. Force	Energy	Def. "dip"	Initial Stiffness	RCS	Max. Force	Energy	Final angle	Def. "bump"	Def. "dip"	Cracks
	[N]	[J]	[mm]	[mN/ deg]		[N]	[kJ]	[deg]	[mm]	[mm]	
1	393	45.7	0.15	71.7	0.59	1191	111.5	81.9	0.07	0.07	No
2	392	45.7	0.18	62.2	0.56	1176	100.6	78.8	0.08	0.09	No
3	391	39.4	0.13	59.5	0.58	1189	95.7	76.0	0.07	0.07	No
4	924	167.8	0.29	33.4	0.40	993	74.6	76.7	0.15	0.15	Yes
5	793	141.3	0.27	50.3	0.49	981	86.7	78.3	0.12	0.13	No
6	737	112.8	0.25	39.7	0.46	885	76.9	74.1	0.13	0.14	No
7	391	39.4	0.13	67.4	0.65	684	101.9	78.7	0.06	0.06	No
8	326	36.6	0.16	74.5	0.61	948	105.6	81.1	0.07	0.07	No
9	401	41.8	0.14	71.0	0.61	1167	101.4	79.0	0.07	0.07	No
10	858	132.0	0.23	41.7	0.49	1041	81.4	73.3	0.12	0.12	No
11	855	142.2	0.29	36.1	0.42	1044	74.2	74.5	0.16	0.16	Yes
12	759	126.4	0.28	45.4	0.45	949	79.8	77.5	0.14	0.15	No
13	388	47.3	0.18	65.7	0.64	949	108.1	80.7	0.08	0.08	No
14	391	40.9	0.13	58.6	0.58	892	94.7	77.1	0.06	0.06	No
15	389	44.8	0.17	55.9	0.52	893	89.6	76.1	0.08	0.08	No
16	585	74.6	0.19	49.3	0.53	857	85.4	74.3	0.09	0.09	No
17	632	83.1	0.2	50.4	0.54	793	87.2	75.5	0.09	0.09	No
18	571	82.3	0.21	55.2	0.53	839	91.2	78.5	0.10	0.10	No
19	632	92.4	0.23	50.7	0.49	1161	95.4	76.5	0.11	0.11	No
20	659	92.4	0.22	51.8	0.45	974	87.3	76.9	0.12	0.12	No
21	704	98.9	0.23	50.4	0.50	1094	90.4	78.6	0.11	0.11	No
22	876	161.6	0.29	31.9	0.36	943	75.6	76.6	0.14	0.14	Yes
23	864	135.6	0.27	36.9	0.43	960	77.7	72.9	0.14	0.14	No
24	907	157.5	0.26	42.8	0.39	766	76.2	75.7	0.15	0.15	No
25	590	74.6	0.19	46.0	0.49	818	83.5	75.9	0.09	0.09	No
26	582	73.5	0.19	46.2	0.50	729	82.9	76.0	0.09	0.09	No

A.3 Worksheet MODDE, thick paperboard

Test Number	Web tension	Crease Depth	Crease Tool	Paperboard	Crease Side
	[kN/m]	[mm]			
1	2	0.1	Straight4	D	Inside
2	1	0.1	Straight4	E	Outside
3	2	0.1	Straight4	F	Outside
4	2	0.3	Straight4	D	Inside
5	1	0.3	Straight4	F	Inside
6	1	0.3	Straight4	E	Outside
7	2	0.1	Straight5	D	Outside
8	1	0.1	Straight5	E	Inside
9	1	0.1	Straight5	F	Outside
10	1.5	0.2	Straight5	D	Outside
11	1.5	0.2	Straight5	D	Inside
12	1.5	0.2	Straight5	E	Outside
13	1.5	0.2	Straight5	E	Inside
14	1.5	0.2	Straight5	F	Outside
15	1.5	0.2	Straight5	F	Inside
16	2	0.3	Straight5	E	Inside
17	1	0.3	Straight5	D	Inside
18	2	0.3	Straight5	F	Outside
19	2	0.1	Straight6	E	Inside
20	1	0.1	Straight6	F	Inside
21	1	0.1	Straight6	D	Outside
22	2	0.3	Straight6	F	Inside
23	2	0.3	Straight6	E	Outside
24	1	0.3	Straight6	D	Outside
25	1.5	0.2	Straight5	D	Outside
26	1.5	0.2	Straight5	D	Outside

A.4 Numerical values of MODDE worksheet, thick paperboard

	CREASING			FOLDING					TOPOGRAPHY		
Test Number	Max. Force	Energy	Def. "dip"	Initial Stiffness	RCS	Max. Force	Energy	Final angle	Def. "bump"	Def. "dip"	Cracks
	[N]	[J]	[mm]	[mN/ deg]		[N]	[kJ]	[deg]	[mm]	[mm]	
1	628	78.0	0.20	98.7	0.62	1779	170.9	75.6	0.07	0.07	No
2	569	82.6	0.25	105.6	0.53	2040	187.6	76.9	0.10	0.10	No
3	777	118.0	0.25	94.2	0.42	2185	192.1	78.5	0.12	0.12	No
4	1296	229.3	0.30	65.0	0.44	1399	126.2	70.7	0.14	0.14	Yes
5	1449	329.2	0.42	62.7	0.29	1795	1498.9	79.3	0.27	0.25	Yes
6	1160	237.8	0.38	74.2	0.40	1505	145.5	75.5	0.18	0.20	No
7	519	64.7	0.19	82.4	0.57	1521	158.9	74.7	0.07	0.08	No
8	548	81.8	0.25	131.8	0.59	1689	218.1	80.0	0.10	0.11	No
9	618	93.1	0.26	98.8	0.42	1880	193.7	78.1	0.13	0.13	No
10	748	107.6	0.25	72.9	0.52	1716	143.5	73.2	0.11	0.12	No
11	809	121.7	0.26	87.6	0.53	1723	158.6	74.1	0.11	0.12	No
12	748	107.6	0.25	72.9	0.52	1475	143.5	73.2	0.12	0.13	No
13	817	140.3	0.30	99.4	0.50	1478	186.9	77.0	0.13	0.14	No
14	963	171.5	0.32	83.8	0.37	1550	175.0	77.2	0.17	0.16	No
15	1044	184.4	0.32	102.8	0.44	1632	205.6	78.4	0.17	0.17	No
16	1140	230.7	0.34	75.2	0.39	1296	165.1	77.6	0.16	0.17	Yes
17	1124	191.3	0.31	70.8	0.47	1402	137.8	71.4	0.15	0.16	No
18	1293	281.0	0.38	74.7	0.34	1380	161.7	79.0	0.22	0.21	No
19	544	79.1	0.22	149.6	0.64	1863	231.1	80.8	0.09	0.09	No
20	595	90.4	0.25	140.4	0.54	1886	234.3	80.7	0.13	0.13	No
21	425	53.1	0.21	84.8	0.59	2413	161.8	76.0	0.09	0.09	No
22	1216	255.0	0.37	88.2	0.39	1666	188.4	77.9	0.20	0.20	Yes
23	1025	198.7	0.34	97.2	0.44	1926	179.9	77.8	0.14	0.15	No
24	925	151.2	0.30	68.0	0.45	1359	133.5	72.4	0.14	0.16	No
25	748	104.8	0.25	72.3	0.50	1534	137.5	72.9	0.10	0.11	No
26	755	105.0	0.24	76.6	0.51	1777	143.7	73.5	0.10	0.12	No

Appendix B Straight creases: *MODDE Coefficient plots, thin paperboard*

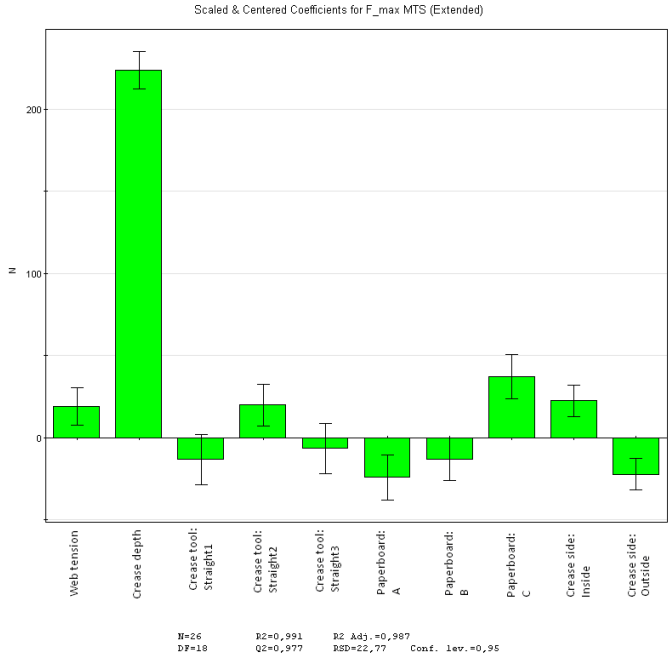

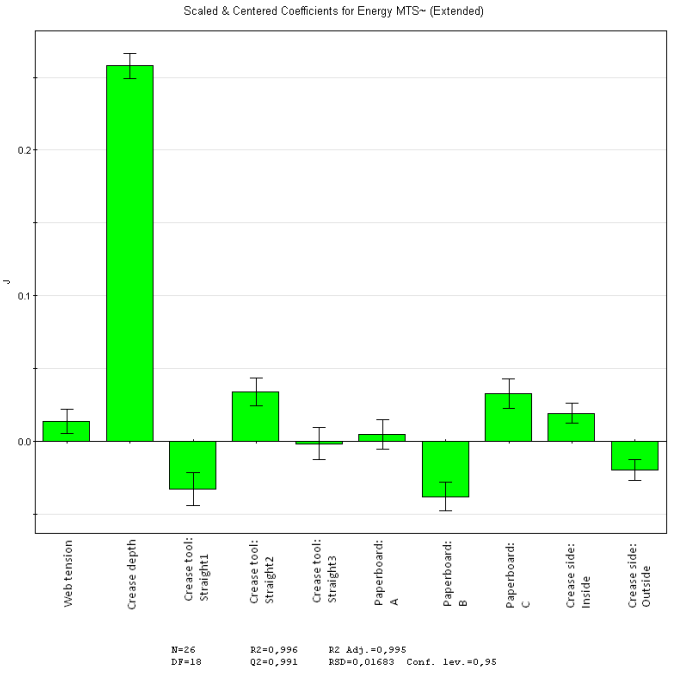

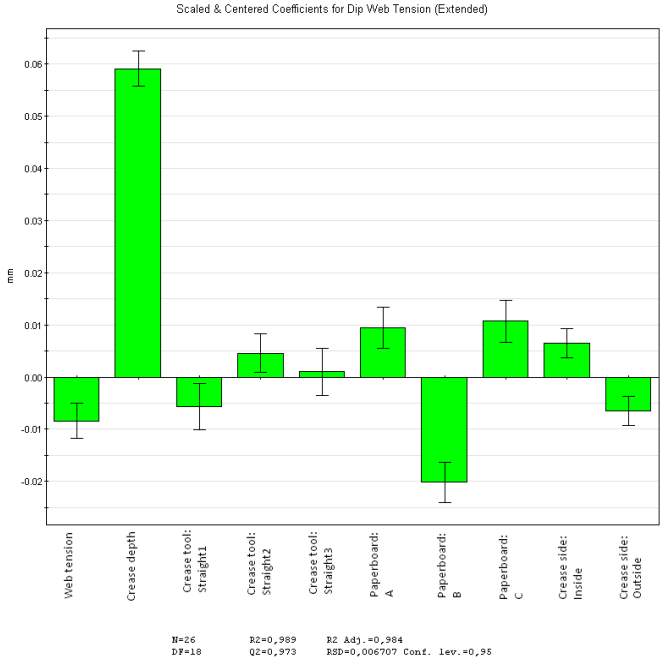
Scaled & Centered Coefficients for Dip Web Tension (Extended)
mm
0.06
0.05
0.04
0.03
0.02
0.01
0.00
-0.01
-0.02
Web tension
Crease depth
Crease tool: Straight1
Crease tool: Straight2
Crease tool: Straight3
Paperboard: A
Paperboard: B
Paperboard: C
Crease side: Inside
Crease side: Outside
N=26 R2=0,989 R2 Adj.=0,984
DF=18 Q2=0,973 RSD=0,006707 Conf. lev.=0,95

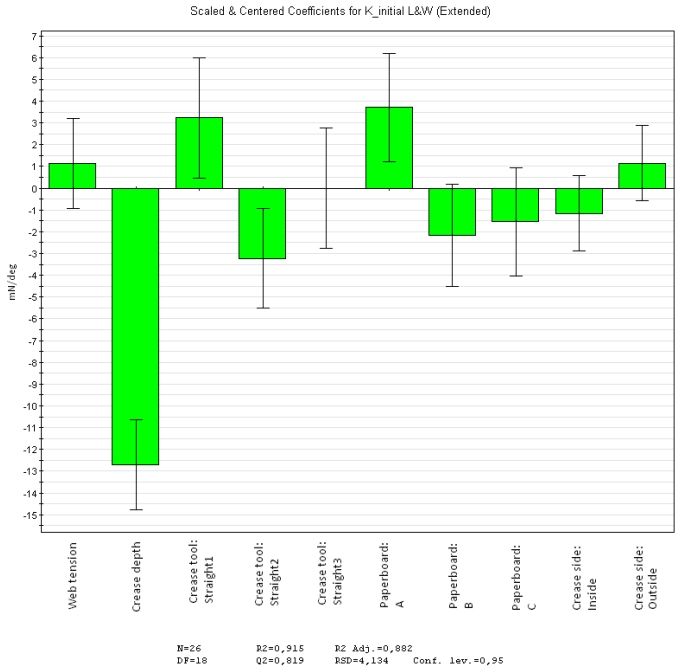
Scaled & Centered Coefficients for K_initial L&W (Extended)
mN/deg
7
6
5
4
3
2
1
0
-1
-2
-3
-4
-5
-6
-7
-8
-9
-10
-11
-12
-13
-14
-15
Web tension
Crease depth
Crease tool: Straight1
Crease tool: Straight2
Crease tool: Straight3
Paperboard: A
Paperboard: B
Paperboard: C
Crease side: Inside
Crease side: Outside
N=26 R2=0,915 R2 Adj.=0,882
DF=18 Q2=0,819 RSD=4,134 Conf. lev.=0,95

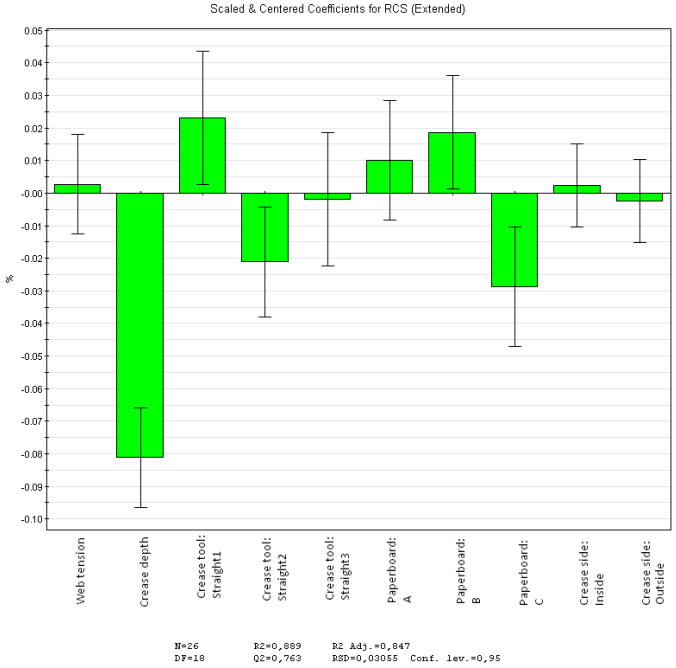
Scaled & Centered Coefficients for RCS (Extended)
%
0.05
0.04
0.03
0.02
0.01
-0.00
-0.01
-0.02
-0.03
-0.04
-0.05
-0.06
-0.07
-0.08
-0.09
-0.10
Web tension
Crease depth
Crease tool: Straight1
Crease tool: Straight2
Crease tool: Straight3
Paperboard: A
Paperboard: B
Paperboard: C
Crease side: Inside
Crease side: Outside
N=26 R2=0,889 R2 Adj.=0,847
DF=18 Q2=0,763 RSD=0,03055 Conf. lev.=0,95

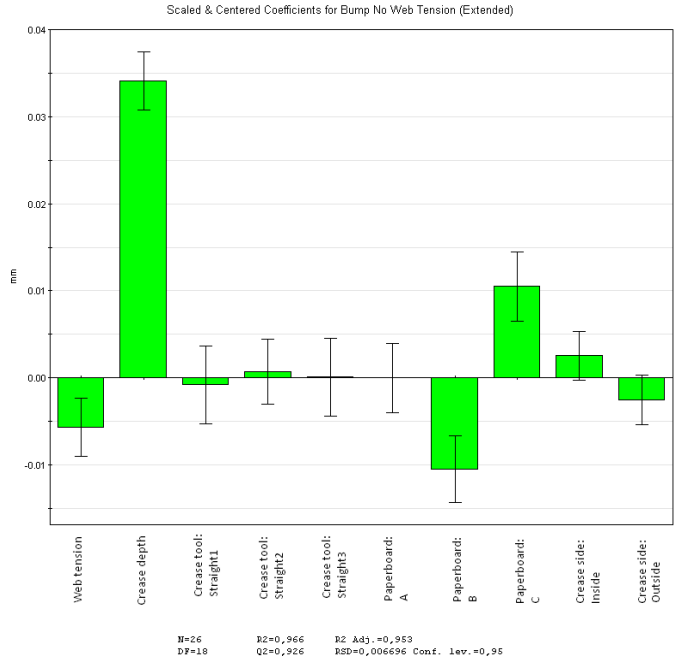
Scaled & Centered Coefficients for Bump No Web Tension (Extended)
mm
0.04
0.03
0.02
0.01
0.00
-0.01
Web tension
Crease depth
Crease tool: Straight1
Crease tool: Straight2
Crease tool: Straight3
Paperboard: A
Paperboard: B
Paperboard: C
Crease side: Inside
Crease side: Outside
N=26 R2=0,966 R2 Adj.=0,953
DF=18 Q2=0,926 RSD=0,006696 Conf. lev.=0,95

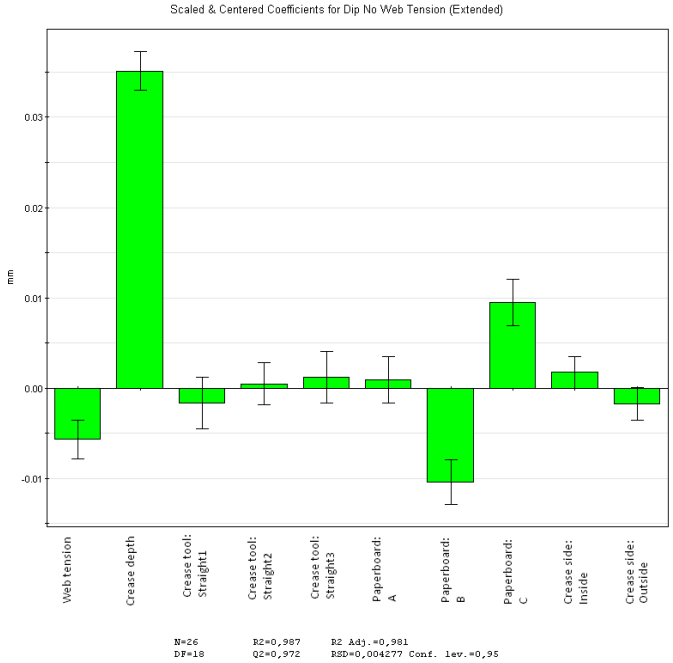
Scaled & Centered Coefficients for Dip No Web Tension (Extended)
mm
0.03
0.02
0.01
0.00
-0.01
Web tension
Crease depth
Crease tool: Straight1
Crease tool: Straight2
Crease tool: Straight3
Paperboard: A
Paperboard: B
Paperboard: C
Crease side: Inside
Crease side: Outside
N=26 R2=0,987 R2 Adj.=0,981
DF=18 Q2=0,972 RSD=0,004277 Conf. lev.=0,95

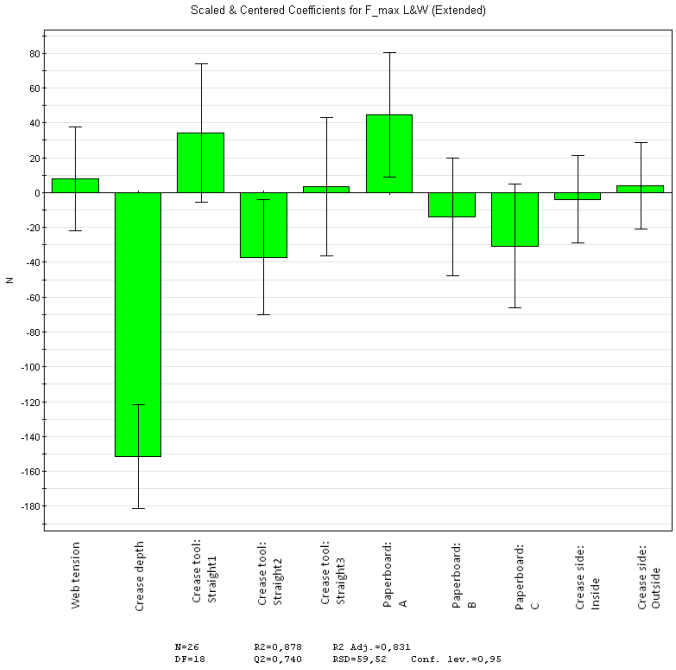
Scaled & Centered Coefficients for F_max L&W (Extended)
N
80
60
40
20
0
-20
-40
-60
-80
-100
-120
-140
-160
-180
Web tension
Crease depth
Crease tool: Straight1
Crease tool: Straight2
Crease tool: Straight3
Paperboard: A
Paperboard: B
Paperboard: C
Crease side: Inside
Crease side: Outside
N=26 R2=0,878 R2 Adj.=0,831
DF=18 Q2=0,740 RSD=59,52 Conf. lev.=0,95

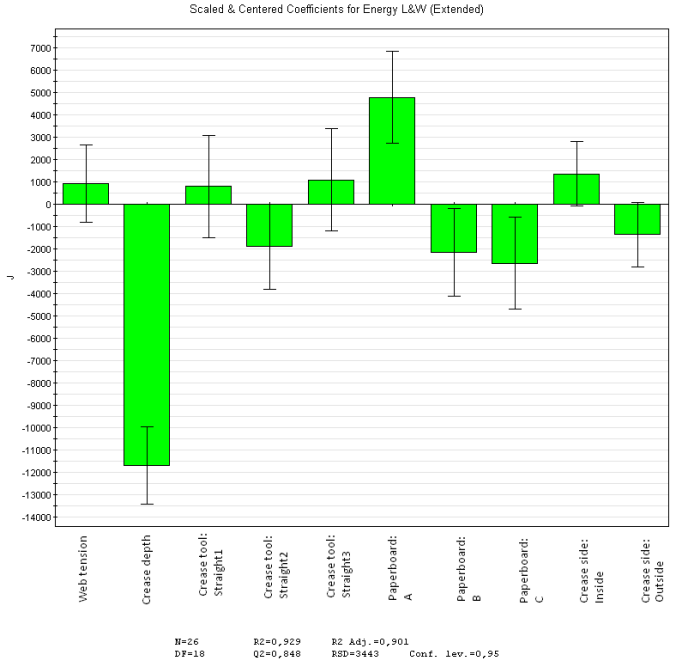
Scaled & Centered Coefficients for Energy L&W (Extended)
J
7000
6000
5000
4000
3000
2000
1000
0
-1000
-2000
-3000
-4000
-5000
-6000
-7000
-8000
-9000
-10000
-11000
-12000
-13000
-14000
Web tension
Crease depth
Crease tool: Straight1
Crease tool: Straight2
Crease tool: Straight3
Paperboard: A
Paperboard: B
Paperboard: C
Crease side: Inside
Crease side: Outside
N=26 R2=0,929 R2 Adj.=0,901
DF=18 Q2=0,848 RSD=3443 Conf. lev.=0,95

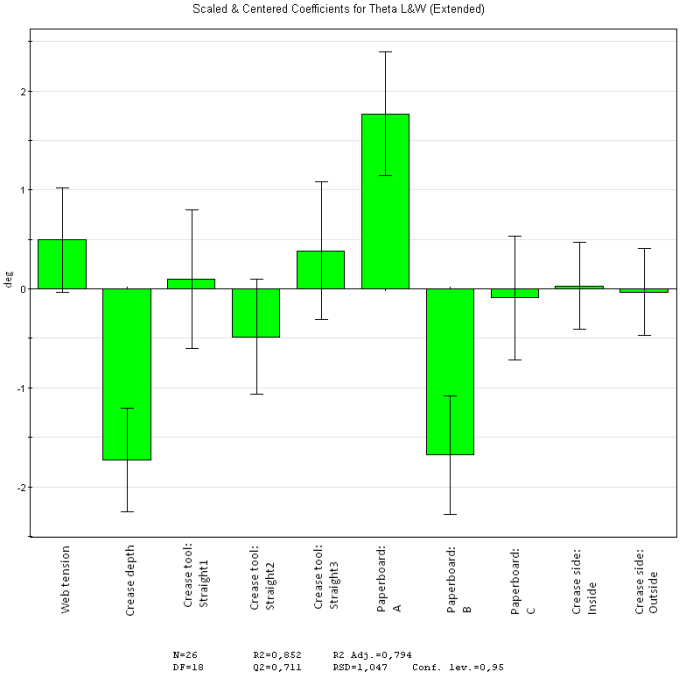
Scaled & Centered Coefficients for Theta L&W (Extended)
deg
2
1
0
-1
-2
Web tension
Crease depth
Crease tool: Straight1
Crease tool: Straight2
Crease tool: Straight3
Paperboard: A
Paperboard: B
Paperboard: C
Crease side: Inside
Crease side: Outside
N=26 R2=0,852 R2 Adj.=0,794
DF=18 Q2=0,711 RSD=1,047 Conf. lev.=0,95

Appendix C Straight creases: *MODDE Coefficient plots, thick paperboard*

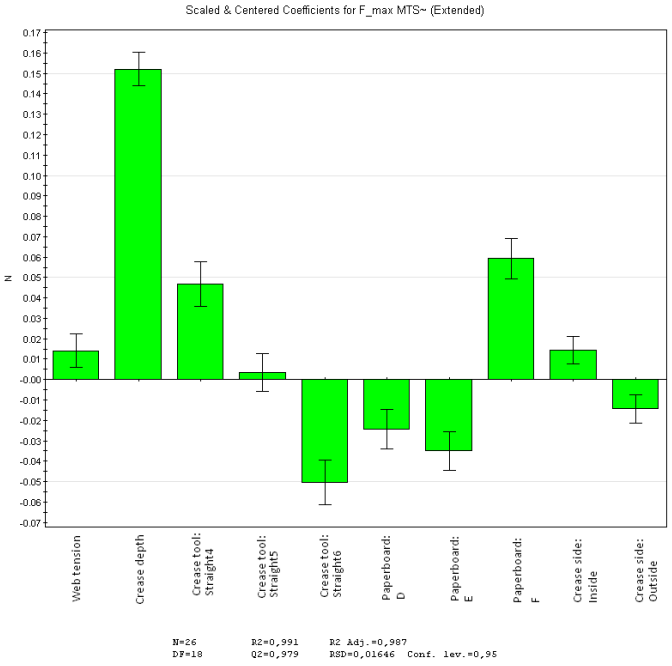

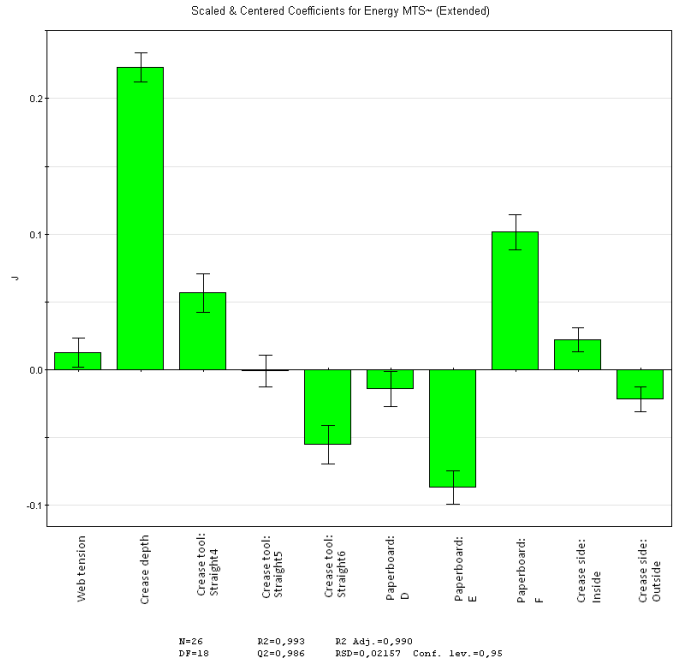

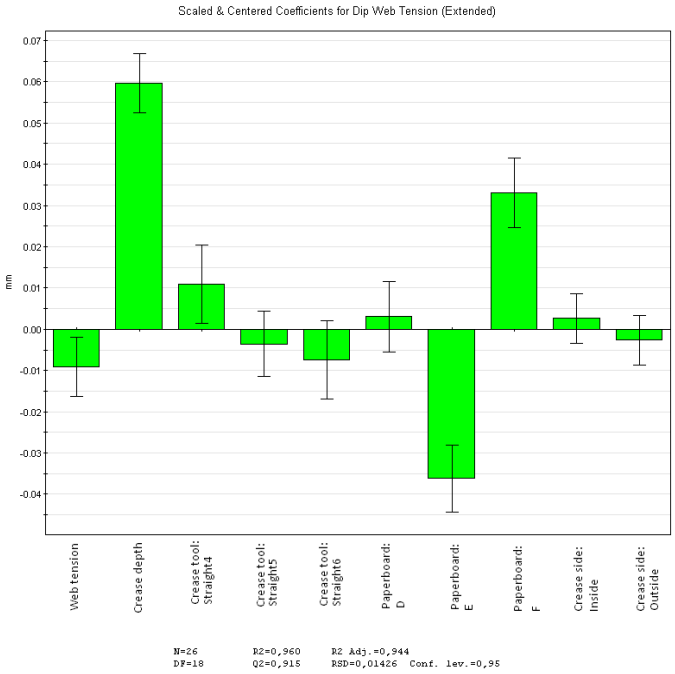
Scaled & Centered Coefficients for Dip Web Tension (Extended)
mm
0.07
0.06
0.05
0.04
0.03
0.02
0.01
0.00
-0.01
-0.02
-0.03
-0.04
Web tension
Crease depth
Crease tool: Straight4
Crease tool: Straight5
Crease tool: Straight6
Paperboard: D
Paperboard: E
Paperboard: F
Crease side: Inside
Crease side: Outside
N=26 R2=0,960 R2 Adj.=0,944
DF=18 Q2=0,915 RSD=0,01426 Conf. lev.=0,95

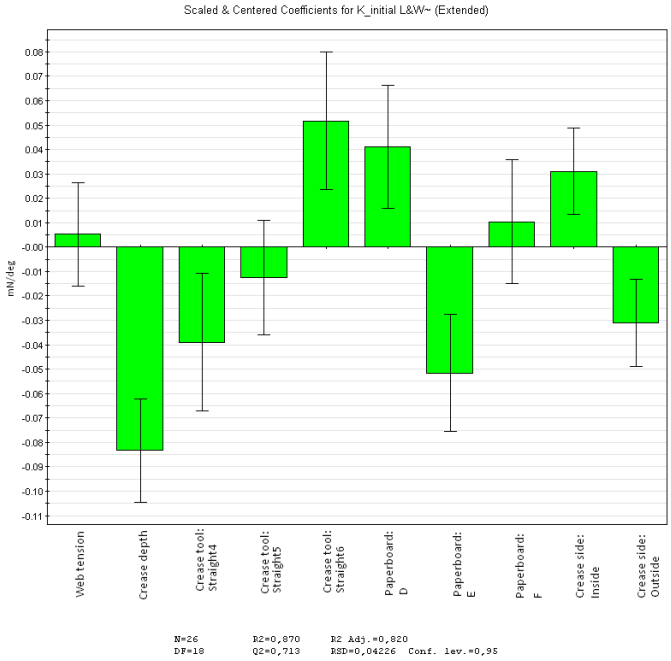
Scaled & Centered Coefficients for K_initial L&W~ (Extended)
mN/deg
0.08
0.07
0.06
0.05
0.04
0.03
0.02
0.01
0.00
-0.01
-0.02
-0.03
-0.04
-0.05
-0.06
-0.07
-0.08
-0.09
-0.10
-0.11
Web tension
Crease depth
Crease tool: Straight4
Crease tool: Straight5
Crease tool: Straight6
Paperboard: D
Paperboard: E
Paperboard: F
Crease side: Inside
Crease side: Outside
N=26 R2=0,870 R2 Adj.=0,820
DF=18 Q2=0,713 RSD=0,04226 Conf. lev.=0,95

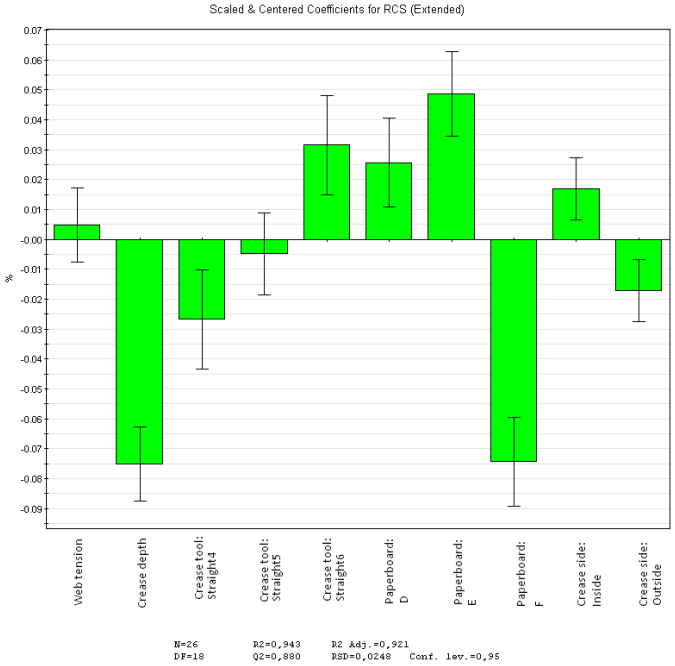
Scaled & Centered Coefficients for RCS (Extended)
%
0.07
0.06
0.05
0.04
0.03
0.02
0.01
0.00
-0.01
-0.02
-0.03
-0.04
-0.05
-0.06
-0.07
-0.08
-0.09
Web tension
Crease depth
Crease tool: Straight4
Crease tool: Straight5
Crease tool: Straight6
Paperboard: D
Paperboard: E
Paperboard: F
Crease side: Inside
Crease side: Outside
N=26 R2=0,943 R2 Adj.=0,921
DF=18 Q2=0,880 RSD=0,0248 Conf. lev.=0,95

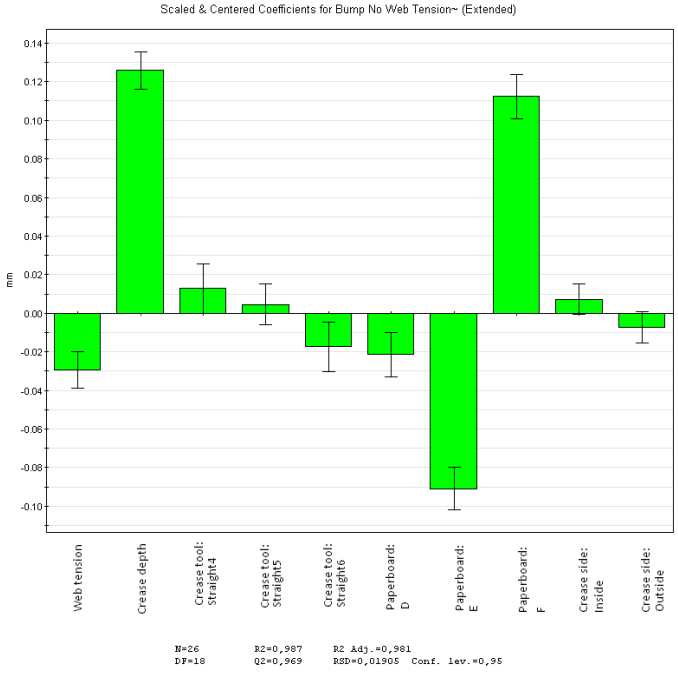
Scaled & Centered Coefficients for Bump No Web Tension~ (Extended)
mm
0.14
0.12
0.10
0.08
0.06
0.04
0.02
0.00
-0.02
-0.04
-0.06
-0.08
-0.10
Web tension
Crease depth
Crease tool: Straight4
Crease tool: Straight5
Crease tool: Straight6
Paperboard: D
Paperboard: E
Paperboard: F
Crease side: Inside
Crease side: Outside
N=26 R2=0,987 R2 Adj.=0,981
DF=18 Q2=0,969 RSD=0,01905 Conf. lev.=0,95

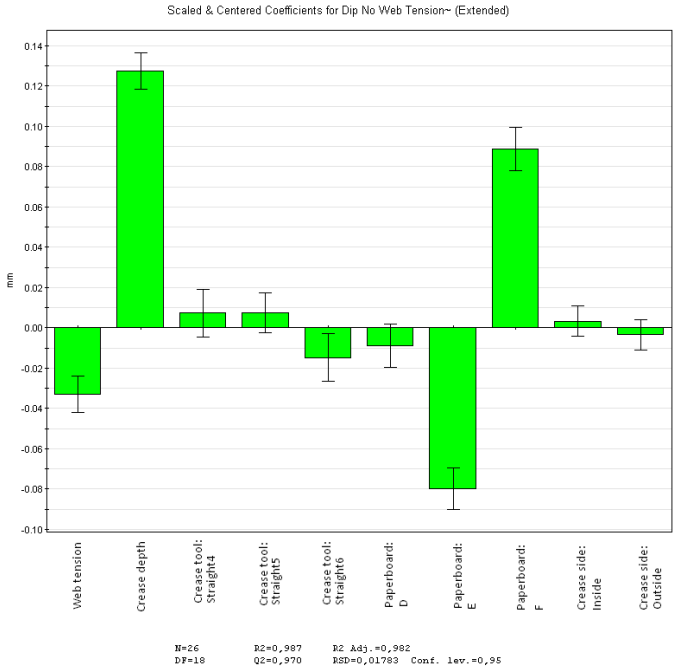
Scaled & Centered Coefficients for Dip No Web Tension~ (Extended)
mm
0.14
0.12
0.10
0.08
0.06
0.04
0.02
0.00
-0.02
-0.04
-0.06
-0.08
-0.10
Web tension
Crease depth
Crease tool: Straight4
Crease tool: Straight5
Crease tool: Straight6
Paperboard: D
Paperboard: E
Paperboard: F
Crease side: Inside
Crease side: Outside
N=26 R2=0,987 R2 Adj.=0,982
DF=18 Q2=0,970 RSD=0,01783 Conf. lev.=0,95

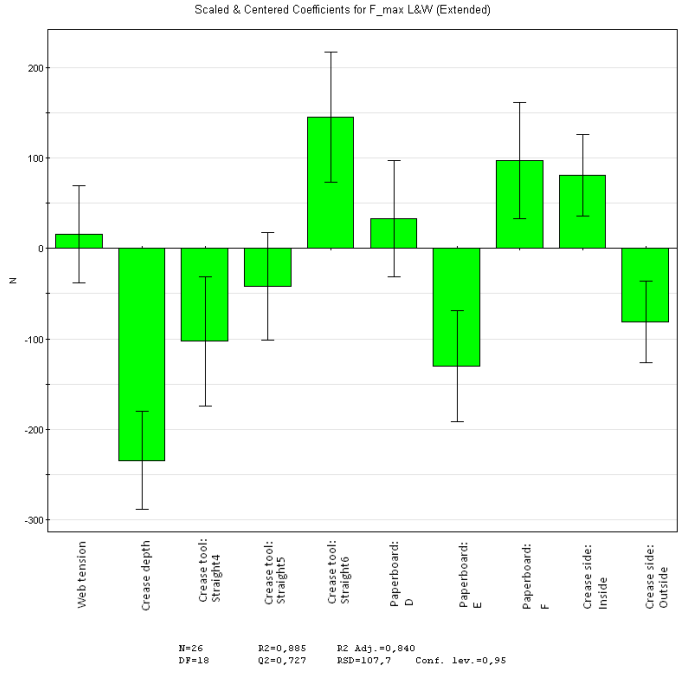
Scaled & Centered Coefficients for F_max L&W (Extended)
N
200
100
0
-100
-200
-300
Web tension
Crease depth
Crease tool: Straight4
Crease tool: Straight5
Crease tool: Straight6
Paperboard: D
Paperboard: E
Paperboard: F
Crease side: Inside
Crease side: Outside
N=26 R2=0,885 R2 Adj.=0,840
DF=18 Q2=0,727 RSD=107,7 Conf. lev.=0,95

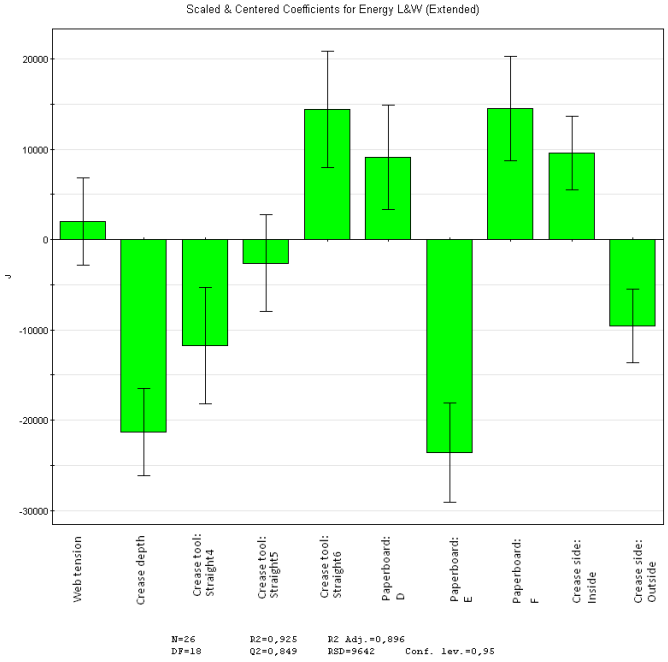
Scaled & Centered Coefficients for Energy L&W (Extended)
J
20000
10000
0
-10000
-20000
-30000
Web tension
Crease depth
Crease tool: Straight4
Crease tool: Straight5
Crease tool: Straight6
Paperboard: D
Paperboard: E
Paperboard: F
Crease side: Inside
Crease side: Outside
N=26 R2=0,925 R2 Adj.=0,896
DF=18 Q2=0,849 RSD=9642 Conf. lev.=0,95

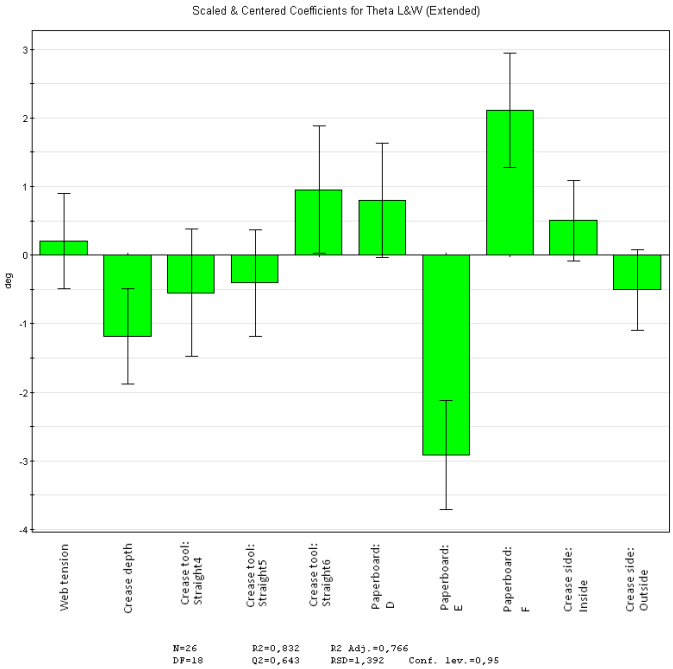
Scaled & Centered Coefficients for Theta L&W (Extended)
deg
3
2
1
0
-1
-2
-3
-4
Web tension
Crease depth
Crease tool: Straight4
Crease tool: Straight5
Crease tool: Straight6
Paperboard: D
Paperboard: E
Paperboard: F
Crease side: Inside
Crease side: Outside
N=26 R2=0,832 R2 Adj.=0,766
DF=18 Q2=0,643 RSD=1,392 Conf. lev.=0,95

Appendix D Straight creases: *Photos of creasing process*

D.1 Paperboard D, outside

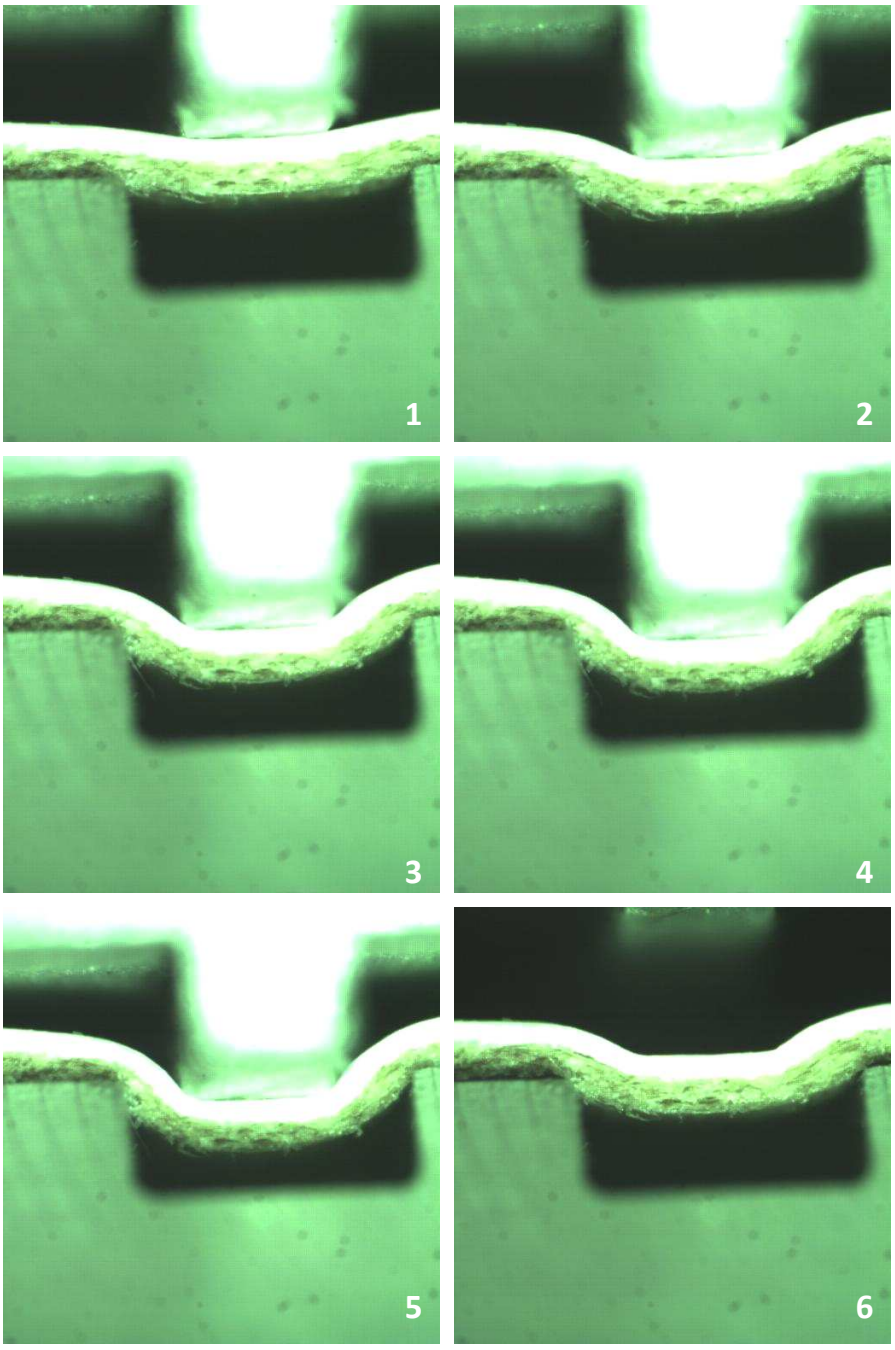

D.2 Paperboard D, inside

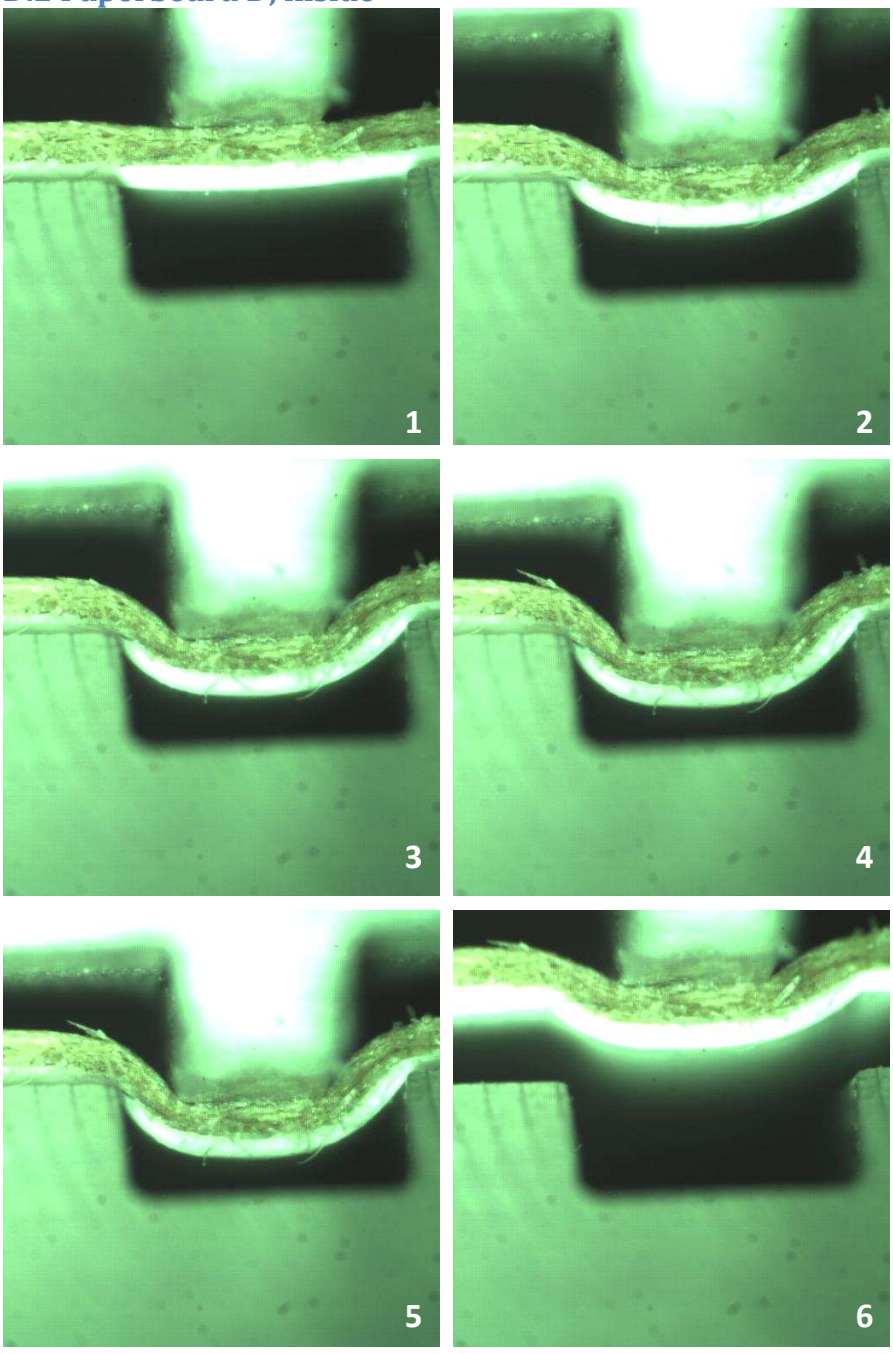

D.3 Paperboard E, outside

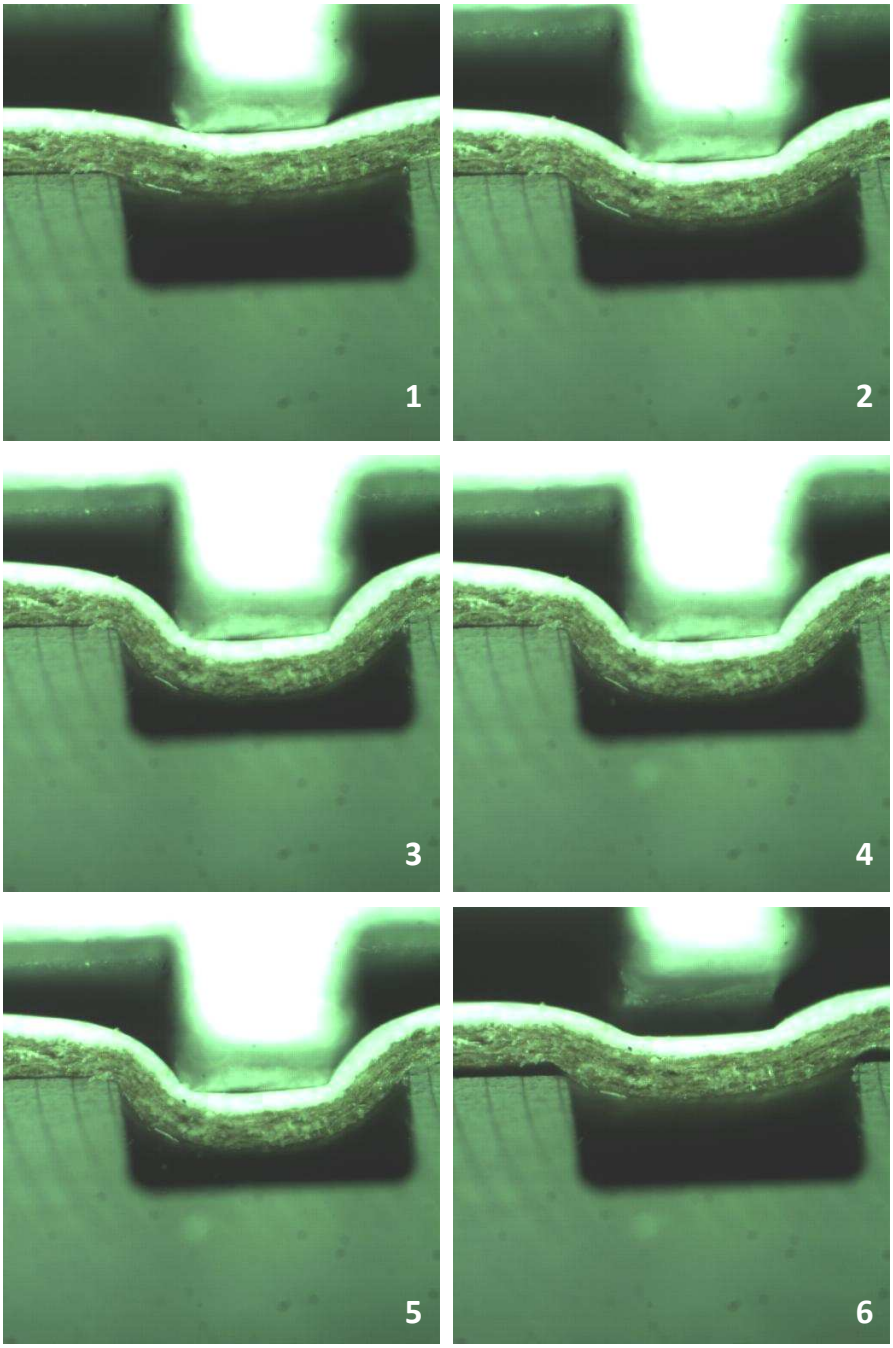

D.4 Paperboard E, inside

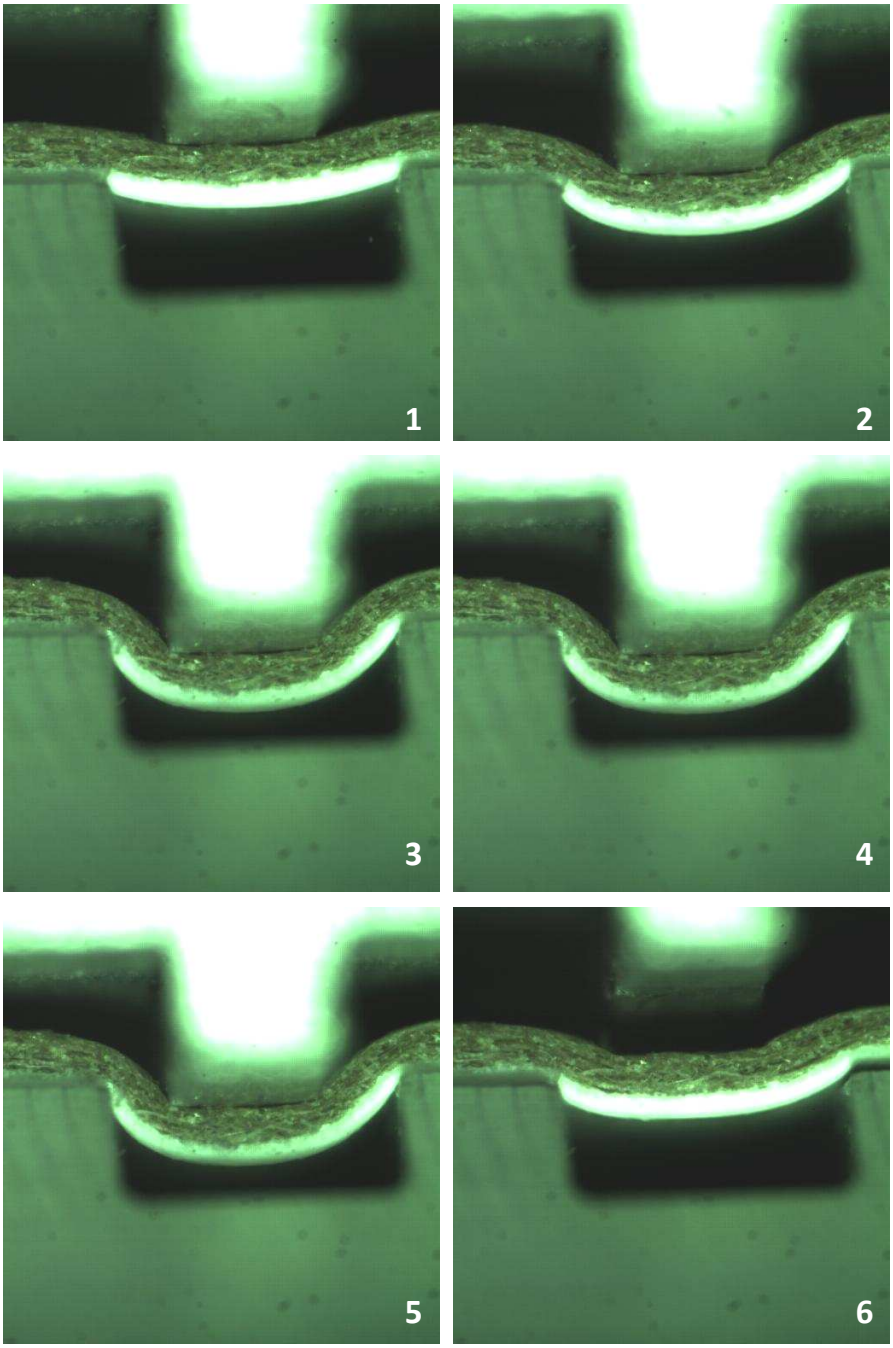

D.5 Paperboard F, outside

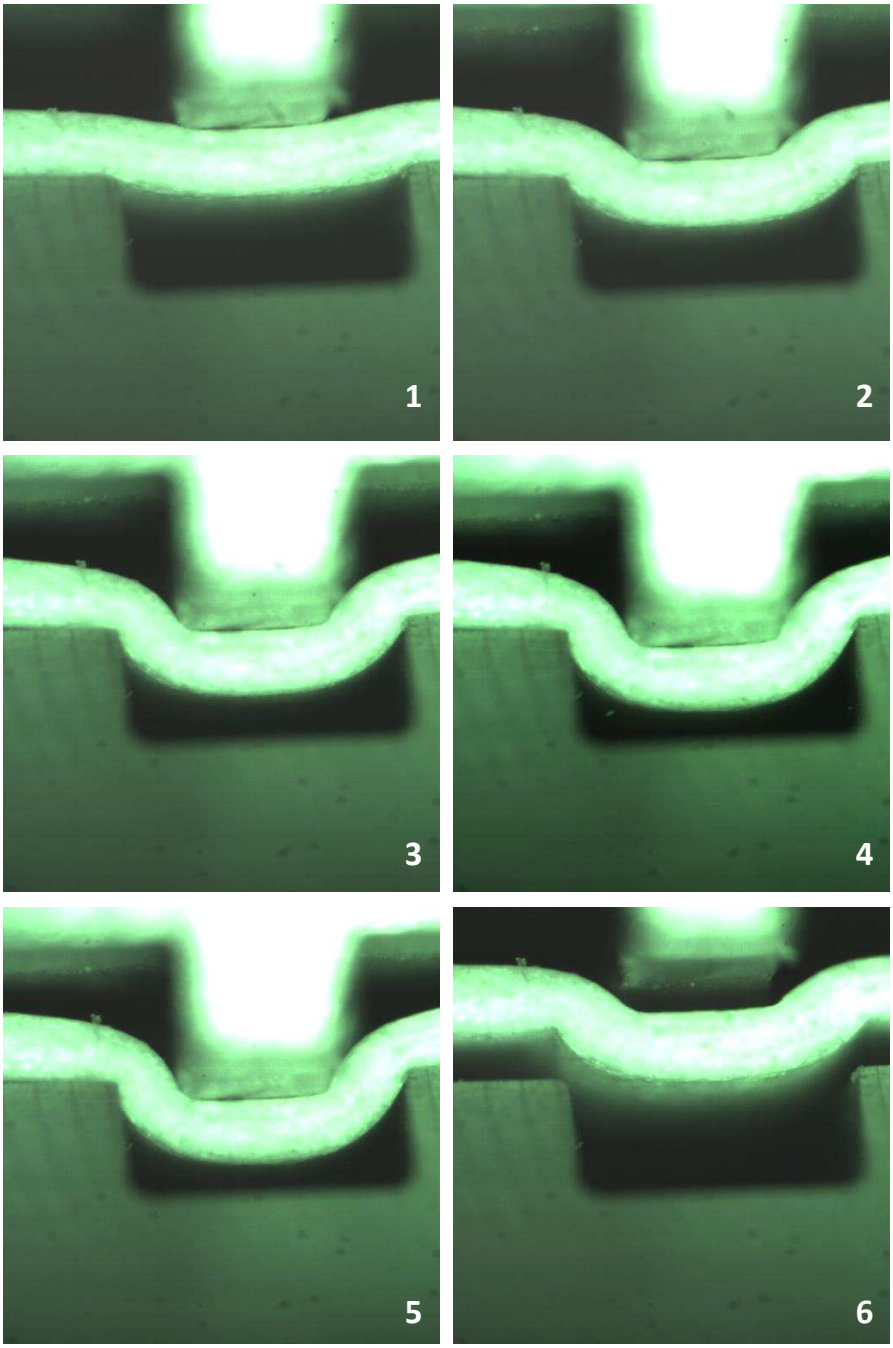

D.6 Paperboard F, inside

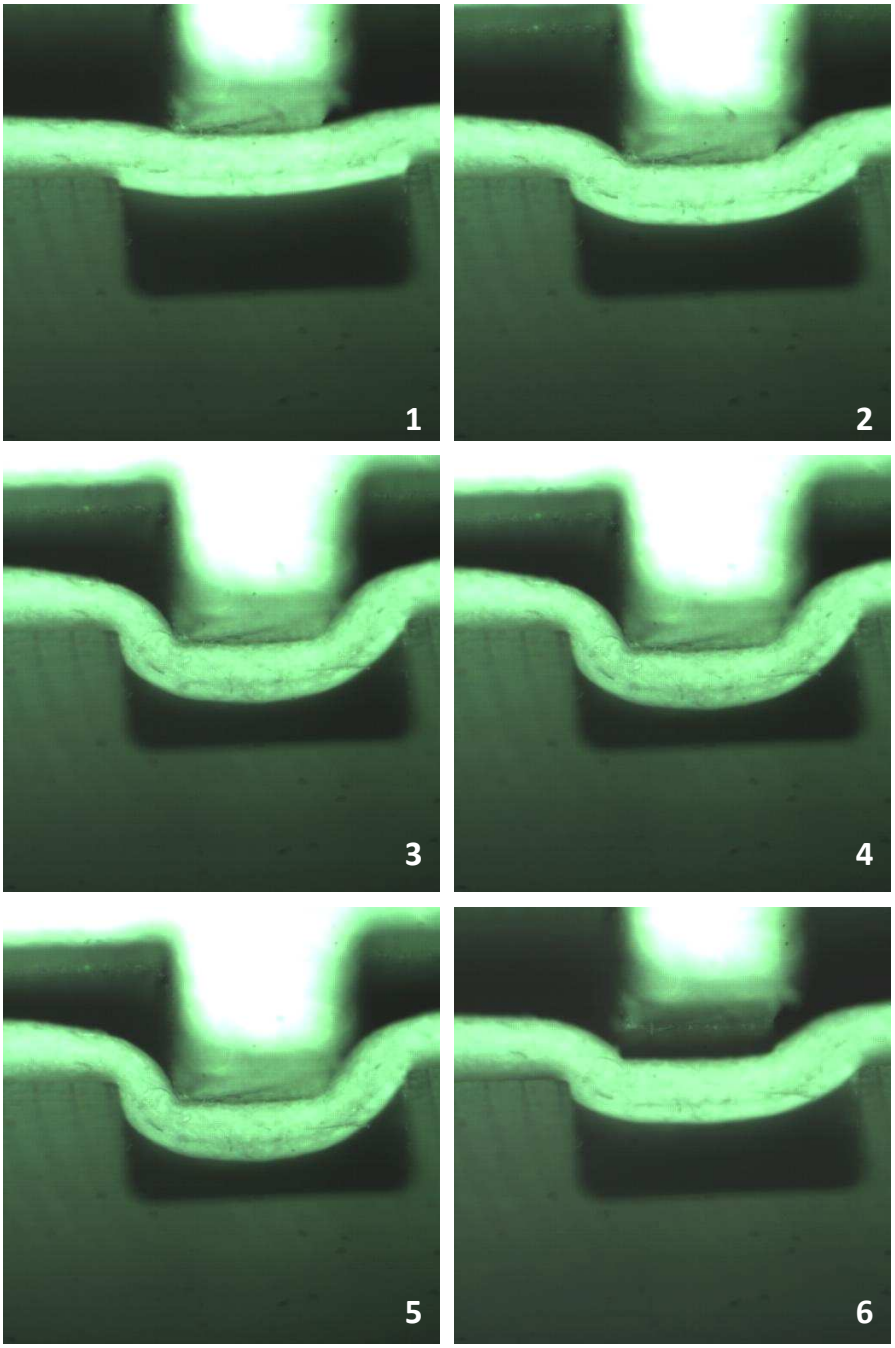

Appendix E Straight creases: *Photos of folding process*

E.1 Paperboard D, outside

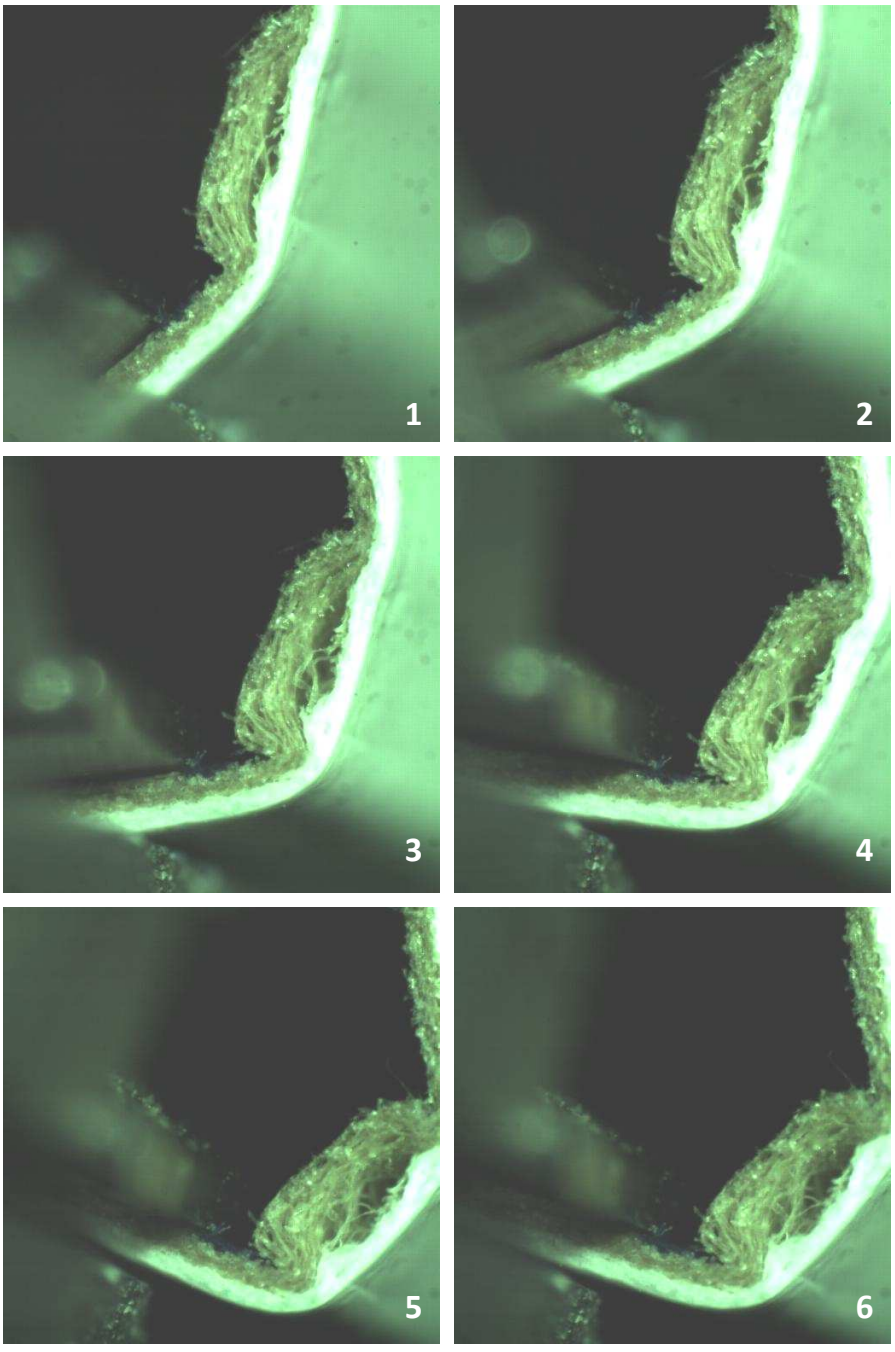

E.2 Paperboard D, inside

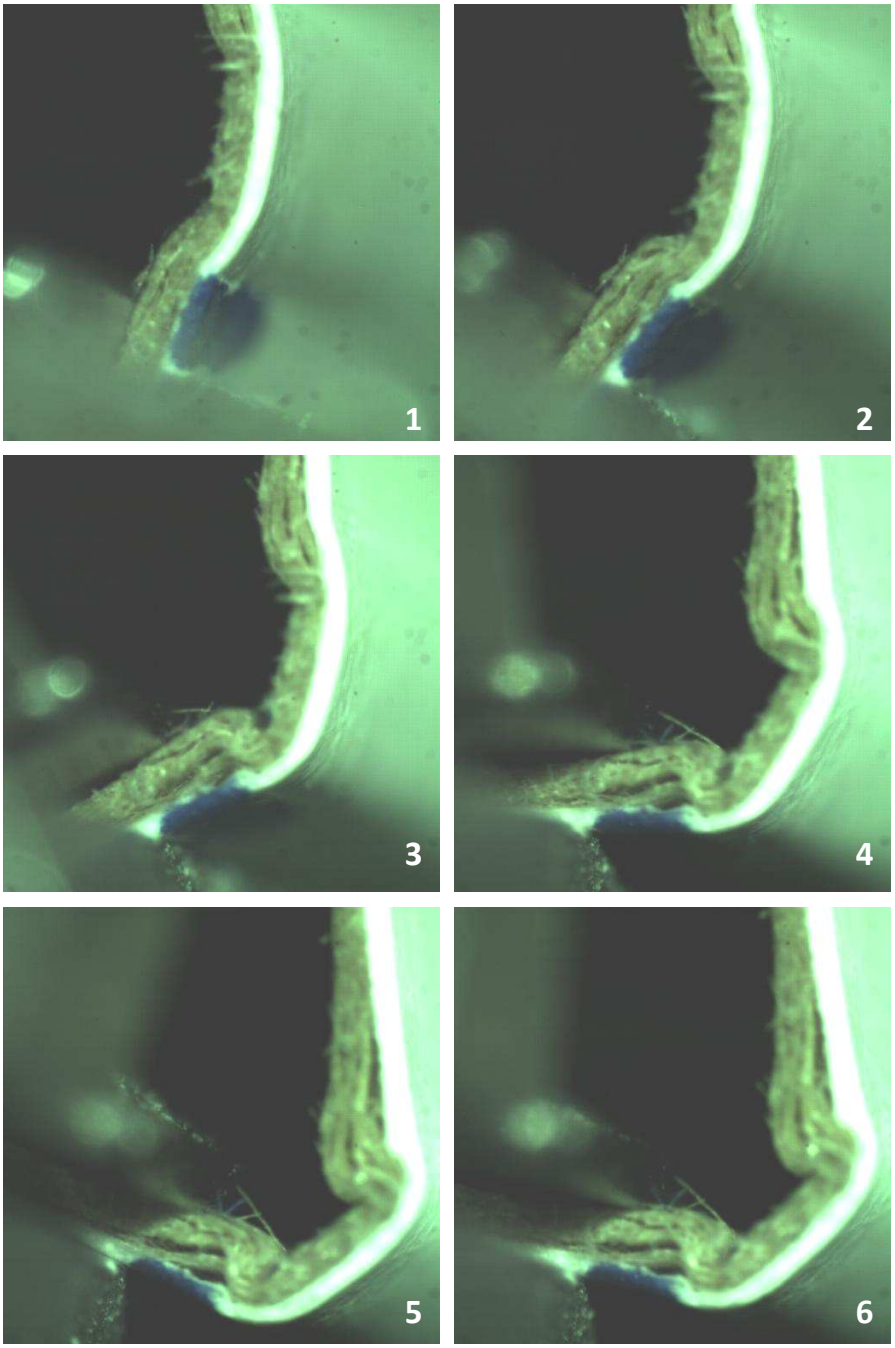

E.3 Paperboard E, outside

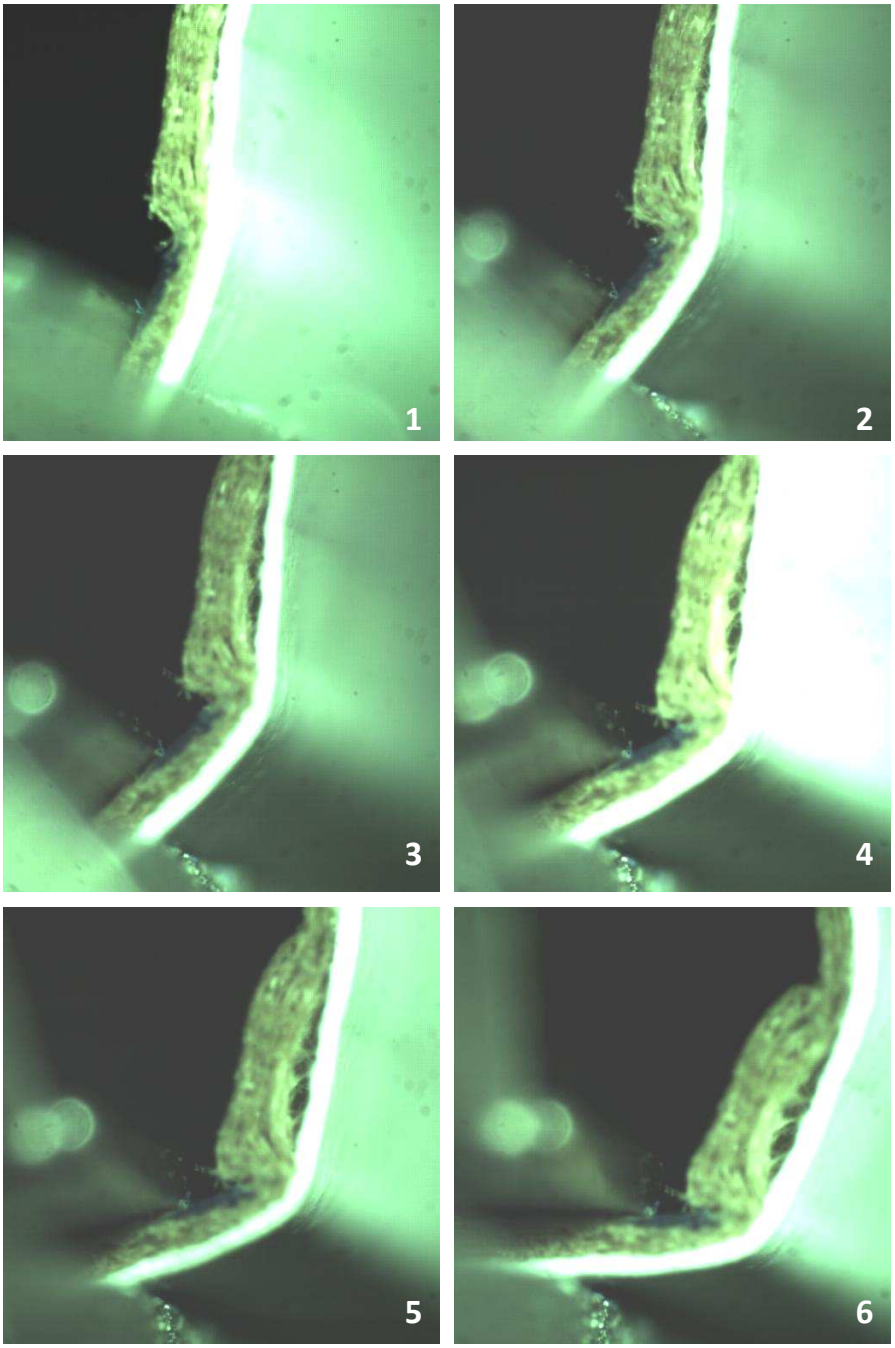

E.4 Paperboard E, inside

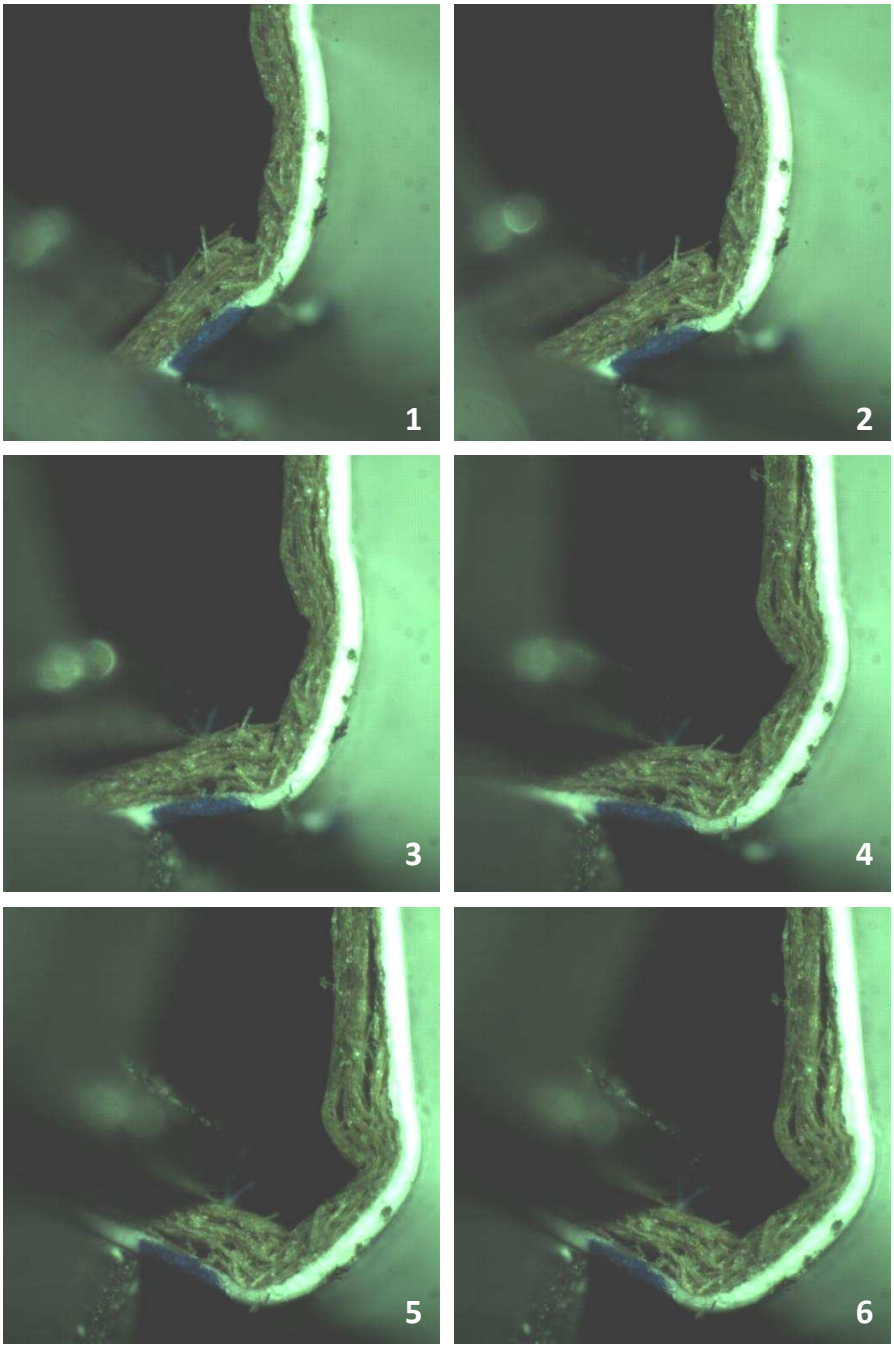

E.5 Paperboard F, outside

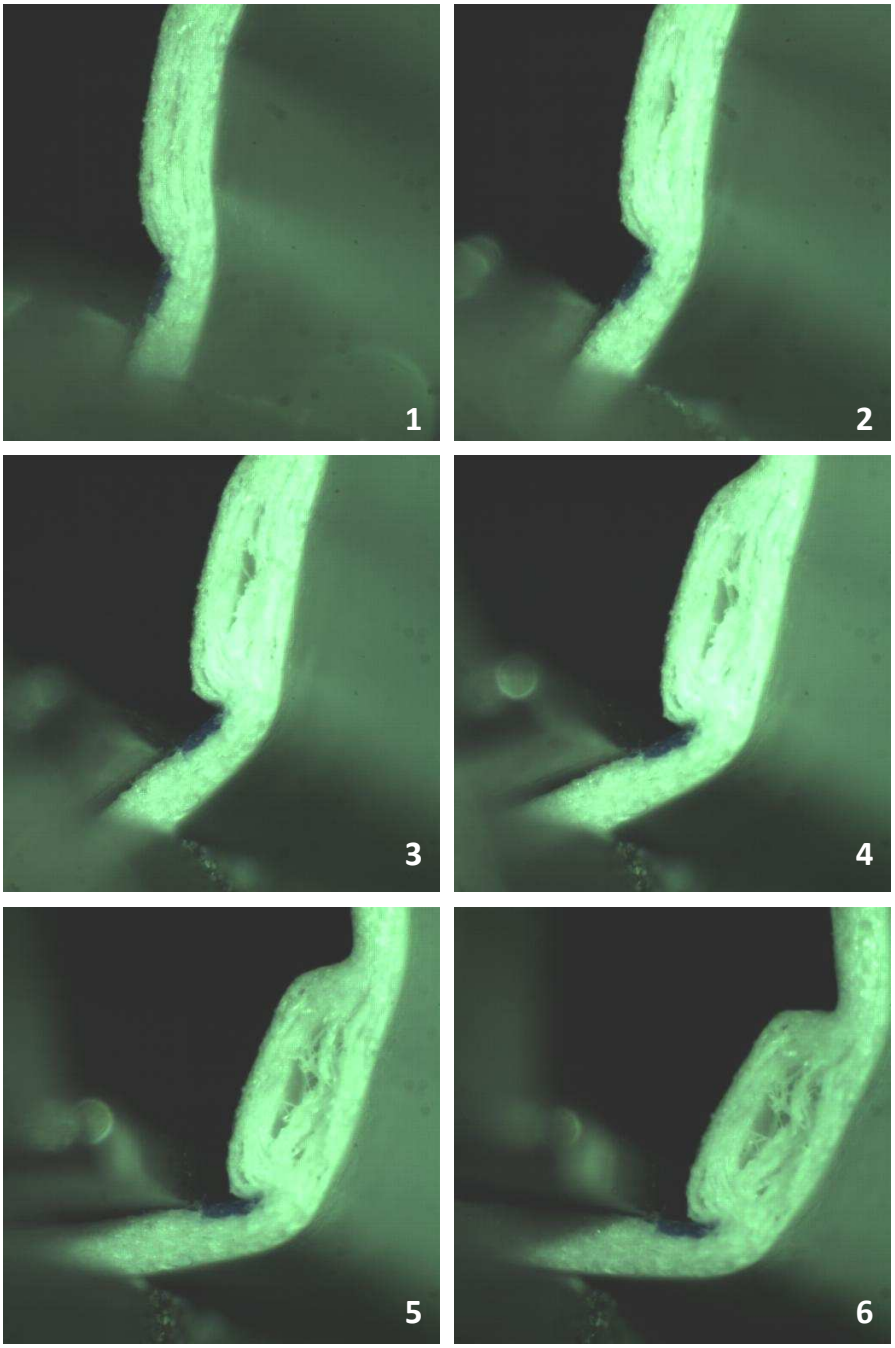

E.6 Paperboard F, inside

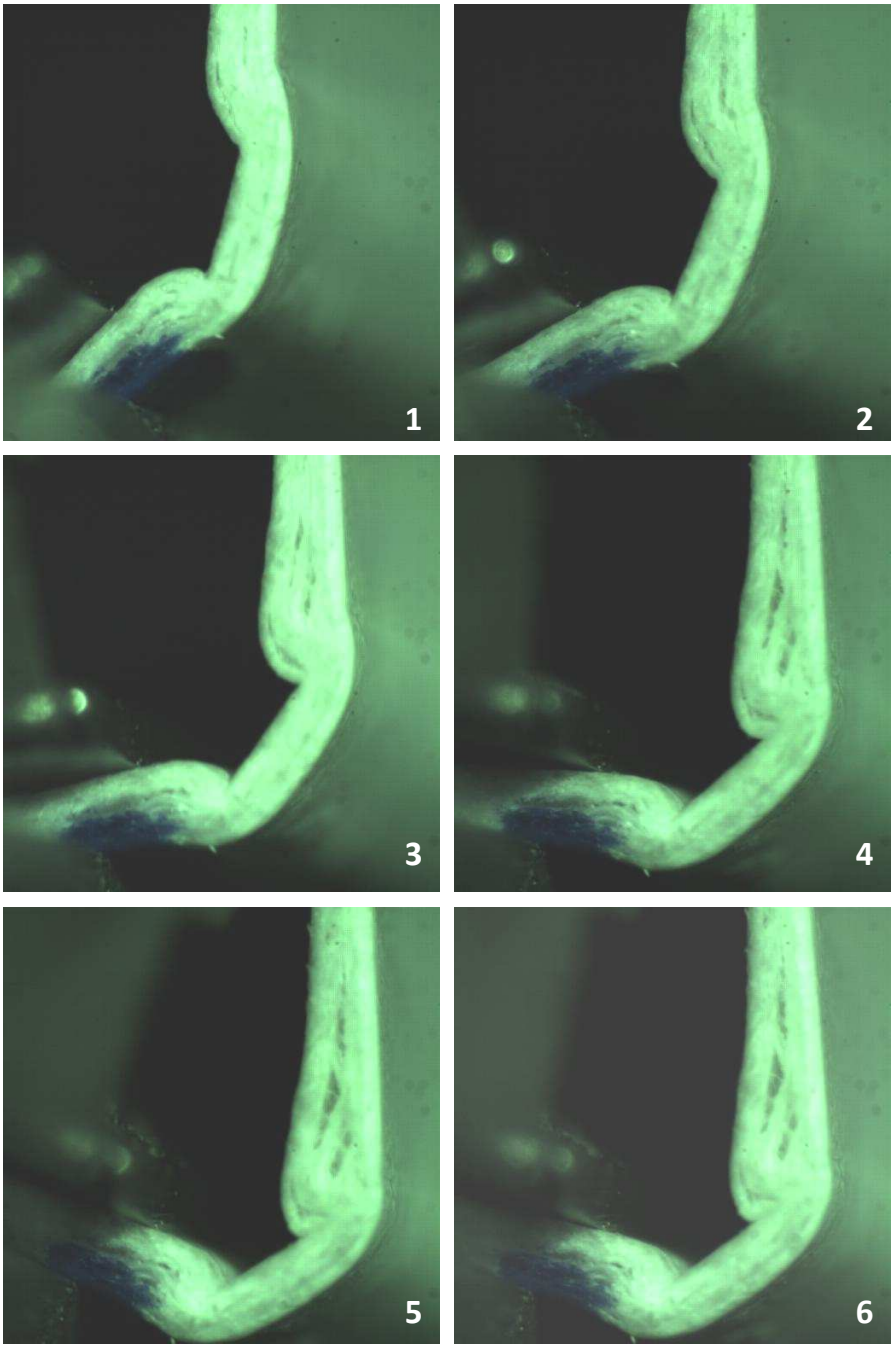

Appendix F 250 Base crease pattern: *MODDE Worksheet*

F.1 Worksheet, paperboard

Test Number	Crease Depth [mm]	Paperboard	Crease Side
1	0.23	A	Inside
2	0.28	A	Outside
3	0.18	B	Outside
4	0.13	B	Outside
5	0.23	A	Outside
6	0.18	B	Outside
7	0.18	A	Inside
8	0.18	B	Outside
9	0.13	B	Inside
10	0.18	B	Inside

F.2 Numerical values of MODDE worksheet, paperboard

	CD					MD					
Test Number	Initial Stiffness [mN/deg]	RCS	Max. Force [N]	Energy [kJ]	Final angle [deg]	Initial Stiffness [mN/deg]	RCS	Max. Force [N]	Energy [J]	Final angle [deg]	RCS GM
1	71.9	0.68	1174	101.2	76.4	30.3	0.60	666	60.6	70.7	0.64
2	72.5	0.64	1152	100.5	77.9	28.2	0.60	627	61.1	77.0	0.62
3	90.2	0.67	1400	115.3	77.8	38.8	0.70	841	75.1	69.6	0.68
4	100.0	0.75	1526	127.6	78.7	42.9	0.75	903	78.5	69.9	0.75
5	76.9	0.69	1210	101.6	76.7	32.0	0.68	717	64.9	71.2	0.68
6	90.9	0.68	1408	115.2	78.0	38.9	0.71	845	80.8	77.7	0.69
7	78.2	0.71	1267	105.5	76.3	34.3	0.69	713	61.0	71.9	0.70
8	85.7	0.65	1346	116.5	78.7	36.4	0.67	809	72.7	71.6	0.66
9	96.7	0.69	1499	128.7	79.5	40.1	0.72	914	84.9	72.8	0.70
10	102.0	0.77	1601	132.4	80.3	43.6	0.78	986	87.7	73.2	0.77

F.3 Worksheet, packaging material

Test Number	Crease Depth [mm]	Paperboard	Crease Side
1	0.13	A	Inside
2	0.18	B	Outside
3	0.18	A	Inside
4	0.20	A	Outside
5	0.13	B	Outside
6	0.18	B	Outside
7	0.18	B	Outside
8	0.08	B	Inside
9	0.13	B	Inside
10	0.23	A	Outside

F.4 Numerical values of MODDE worksheet, packaging material

	CD					MD					
Test Number	Initial Stiffness [mN/deg]	RCS	Max. Force [N]	Energy [kJ]	Final angle [deg]	Initial Stiffness [mN/deg]	RCS	Max. Force [N]	Energy [J]	Final angle [deg]	RCS GM
1	113.9	0.82	2049	175.2	73.2	50.6	0.78	1229	125.7	72.7	0.80
2	131.2	0.82	2338	199.9	76.2	56.6	0.81	1377	140.4	70.8	0.81
3	116.8	0.85	2173	180.4	73.1	54.5	0.83	1301	132.8	72.7	0.84
4	121.2	0.80	2162	187.9	73.8	53.6	0.79	1260	132.0	69.1	0.79
5	137.8	0.87	2558	214.2	76.3	61.5	0.85	1481	152.5	71.5	0.86
6	134.5	0.79	2419	206.2	76.7	59.8	0.83	1469	147.3	72.0	0.81
7	135.1	0.80	2390	208.6	77.1	58.1	0.81	1466	150.1	72.4	0.80
8	139.9	0.86	2618	222.5	76.4	61.6	0.89	1546	167.7	74.7	0.87
9	139.6	0.85	2682	221.9	75.6	59.7	0.84	1495	162.3	73.1	0.84
10	120.7	0.80	2126	189.5	75.7	50.7	0.77	1263	133.1	72.9	0.78

Appendix G 250 Base crease pattern: *MODDE Coefficient plots, paperboard*

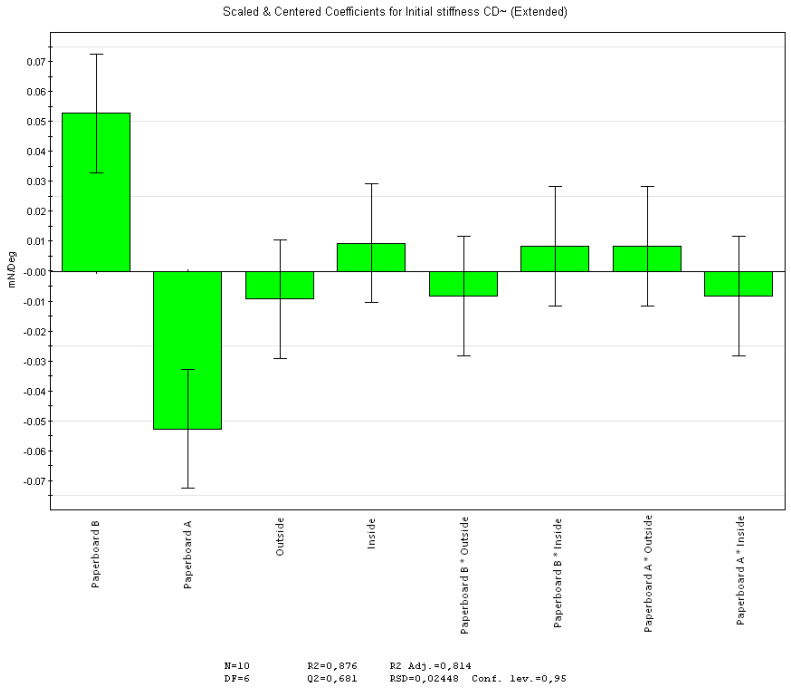

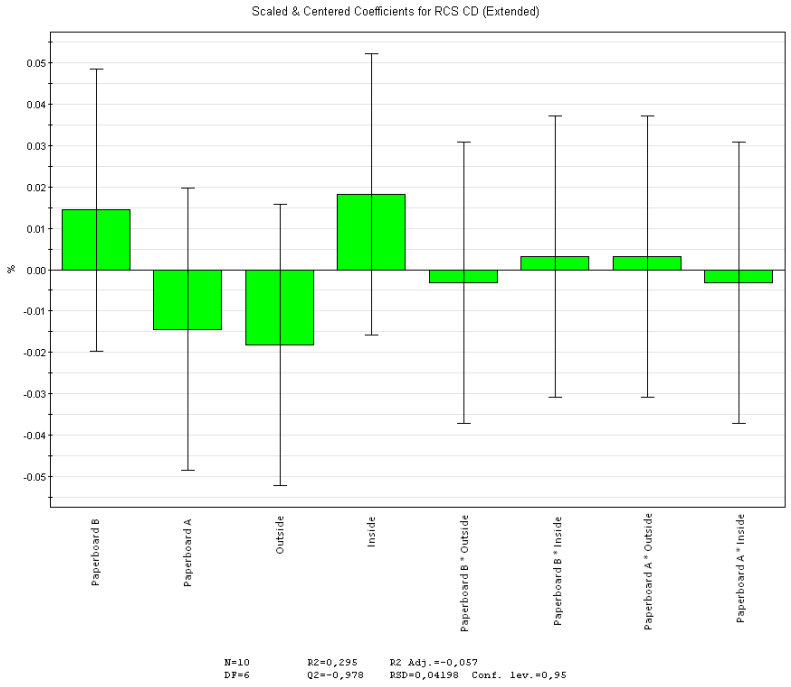

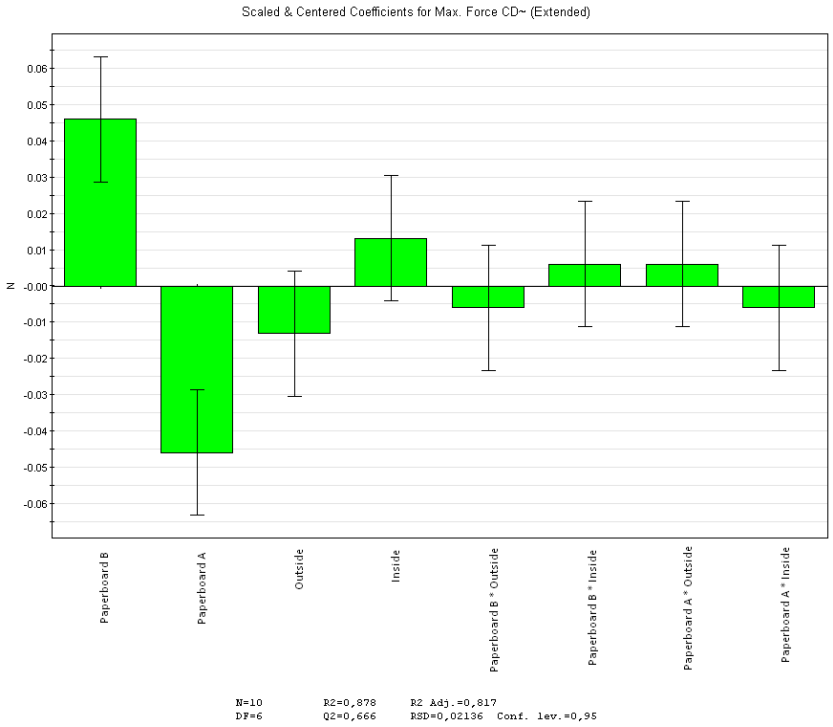
Scaled & Centered Coefficients for Max. Force CD~ (Extended)
N
0.06
0.05
0.04
0.03
0.02
0.01
-0.00
-0.01
-0.02
-0.03
-0.04
-0.05
-0.06
Paperboard B
Paperboard A
Outside
Inside
Paperboard B * Outside
Paperboard B * Inside
Paperboard A * Outside
Paperboard A * Inside
N=10 R2=0,878 R2 Adj.=0,817
DF=6 Q2=0,666 RSD=0,02136 Conf. lev.=0,95

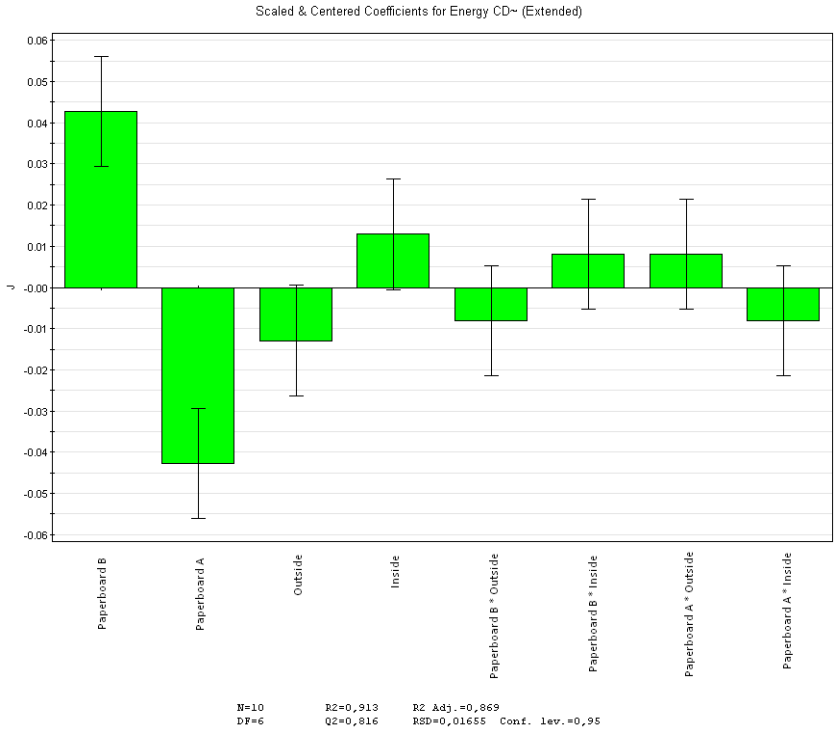
Scaled & Centered Coefficients for Energy CD~ (Extended)
J
0.06
0.05
0.04
0.03
0.02
0.01
-0.00
-0.01
-0.02
-0.03
-0.04
-0.05
-0.06
Paperboard B
Paperboard A
Outside
Inside
Paperboard B * Outside
Paperboard B * Inside
Paperboard A * Outside
Paperboard A * Inside
N=10 R2=0,913 R2 Adj.=0,869
DF=6 Q2=0,816 RSD=0,01655 Conf. lev.=0,95

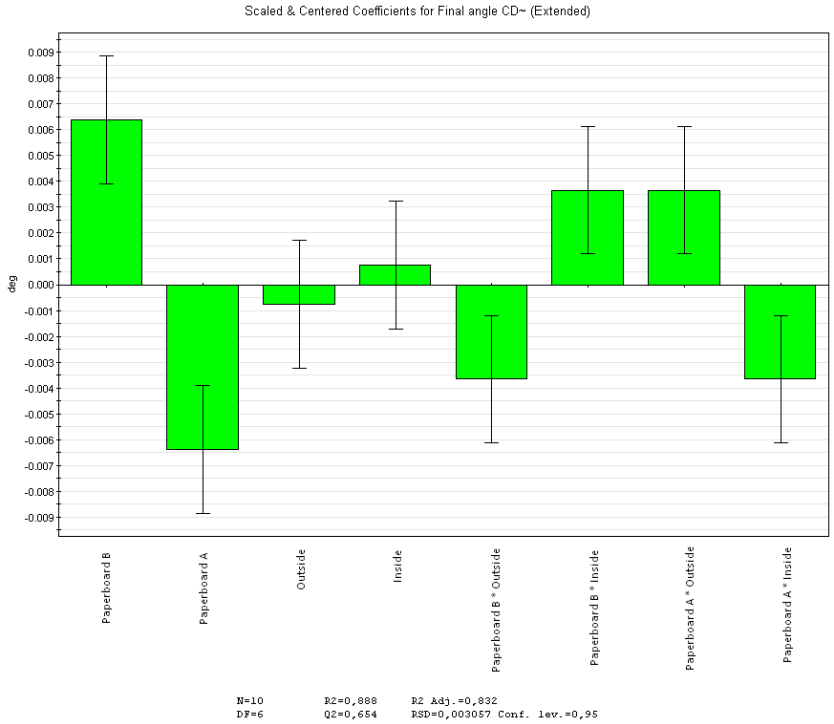
Scaled & Centered Coefficients for Final angle CD~ (Extended)
deg
0.009
0.008
0.007
0.006
0.005
0.004
0.003
0.002
0.001
0.000
-0.001
-0.002
-0.003
-0.004
-0.005
-0.006
-0.007
-0.008
-0.009
Paperboard B
Paperboard A
Outside
Inside
Paperboard B * Outside
Paperboard B * Inside
Paperboard A * Outside
Paperboard A * Inside
N=10 R2=0,888 R2 Adj.=0,832
DF=6 Q2=0,654 RSD=0,003057 Conf. lev.=0,95

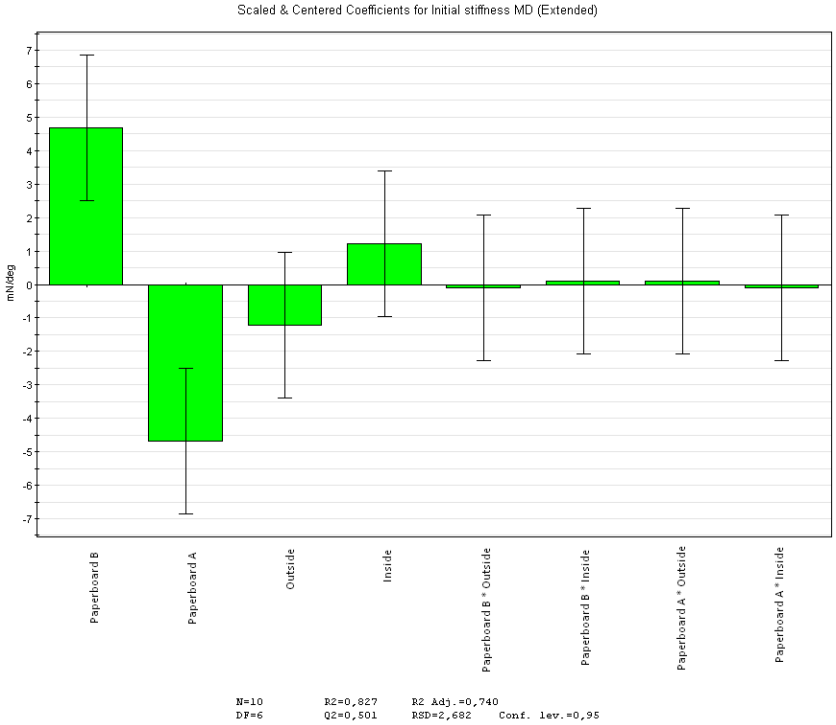
Scaled & Centered Coefficients for Initial stiffness MD (Extended)
mN/deg
7
6
5
4
3
2
1
0
-1
-2
-3
-4
-5
-6
-7
Paperboard B
Paperboard A
Outside
Inside
Paperboard B * Outside
Paperboard B * Inside
Paperboard A * Outside
Paperboard A * Inside
N=10 R2=0,827 R2 Adj.=0,740
DF=6 Q2=0,501 RSD=2,682 Conf. lev.=0,95

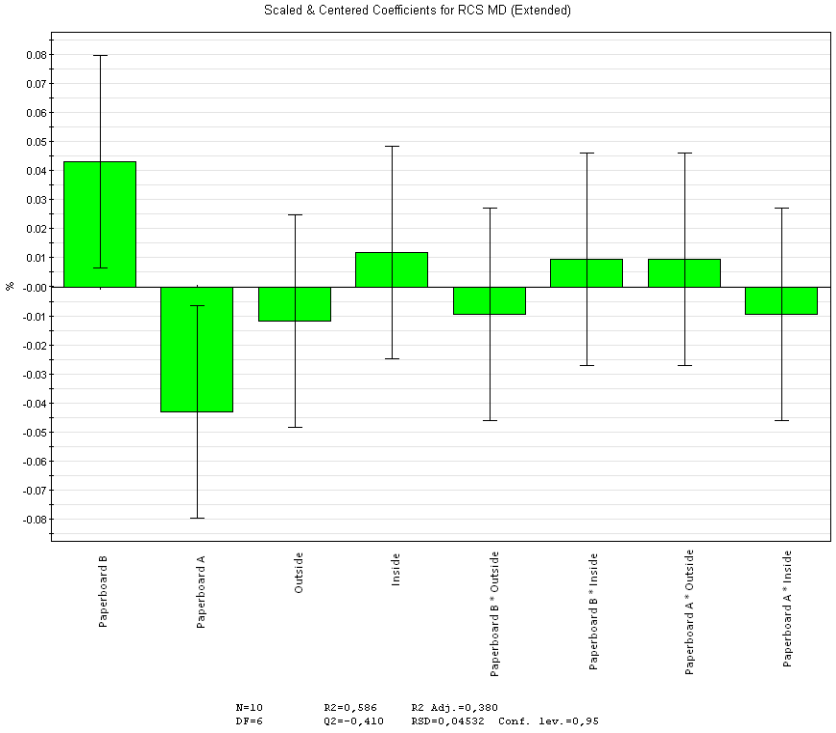
Scaled & Centered Coefficients for RCS MD (Extended)
%
0.08
0.07
0.06
0.05
0.04
0.03
0.02
0.01
-0.00
-0.01
-0.02
-0.03
-0.04
-0.05
-0.06
-0.07
-0.08
Paperboard B
Paperboard A
Outside
Inside
Paperboard B * Outside
Paperboard B * Inside
Paperboard A * Outside
Paperboard A * Inside
N=10 R2=0,586 R2 Adj.=0,380
DF=6 Q2=-0,410 RSD=0,04532 Conf. lev.=0,95

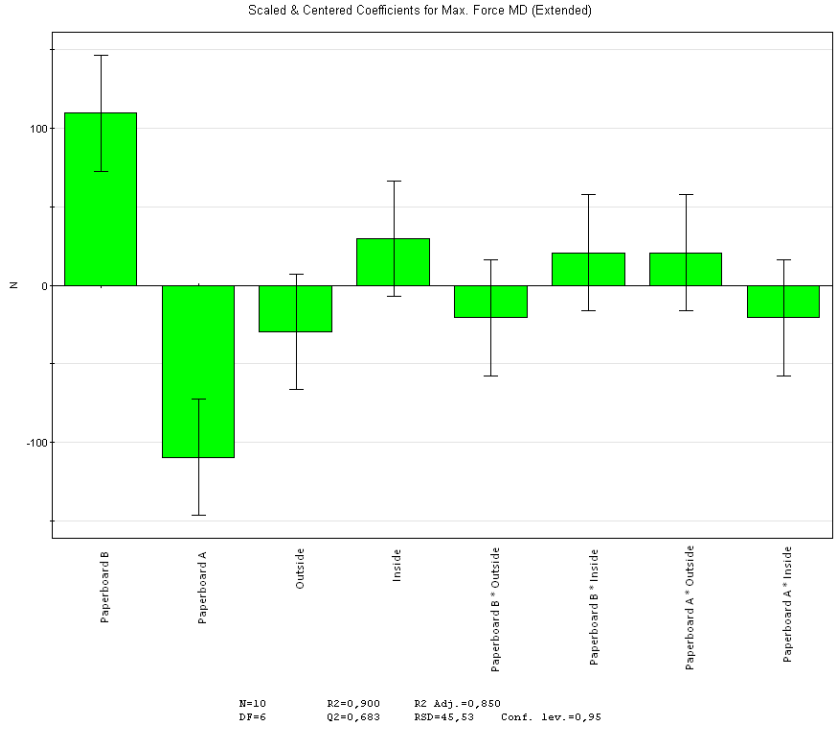
Scaled & Centered Coefficients for Max. Force MD (Extended)
N
100
0
-100
Paperboard B
Paperboard A
Outside
Inside
Paperboard B * Outside
Paperboard B * Inside
Paperboard A * Outside
Paperboard A * Inside
N=10 R2=0,900 R2 Adj.=0,850
DF=6 Q2=0,683 RSD=45,53 Conf. lev.=0,95

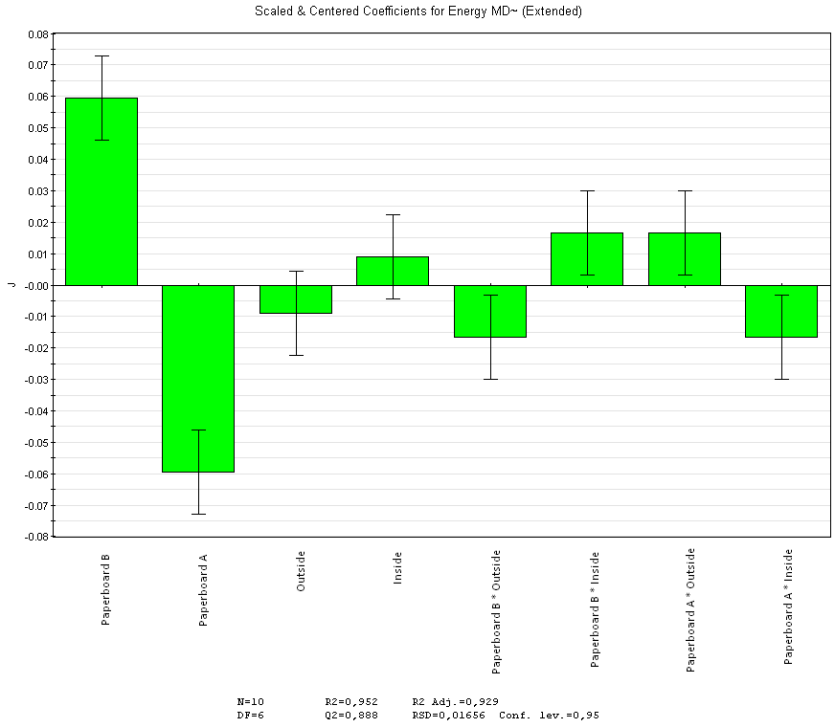
Scaled & Centered Coefficients for Energy MD~ (Extended)
J
0.08
0.07
0.06
0.05
0.04
0.03
0.02
0.01
-0.00
-0.01
-0.02
-0.03
-0.04
-0.05
-0.06
-0.07
-0.08
Paperboard B
Paperboard A
Outside
Inside
Paperboard B * Outside
Paperboard B * Inside
Paperboard A * Outside
Paperboard A * Inside
N=10 R2=0,952 R2 Adj.=0,929
DF=6 Q2=0,888 RSD=0,01656 Conf. lev.=0,95

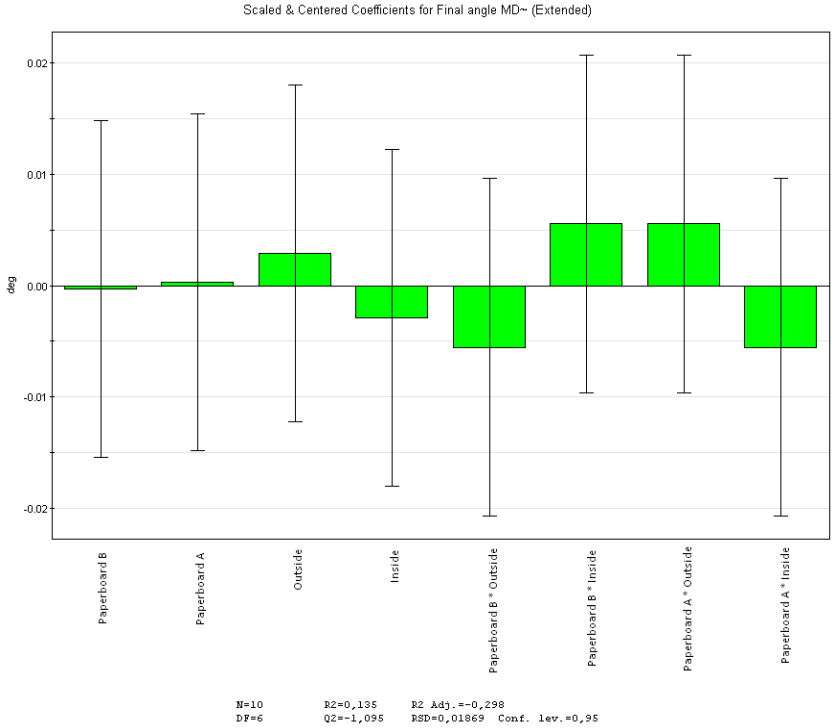
Scaled & Centered Coefficients for Final angle MD~ (Extended)
deg
0.02
0.01
0.00
-0.01
-0.02
Paperboard B
Paperboard A
Outside
Inside
Paperboard B * Outside
Paperboard B * Inside
Paperboard A * Outside
Paperboard A * Inside
N=10 R2=0,135 R2 Adj.=-0,298
DF=6 Q2=-1,095 RSD=0,01869 Conf. lev.=0,95

Appendix H 250 Base crease pattern: *MODDE Coefficient plots, packaging material*

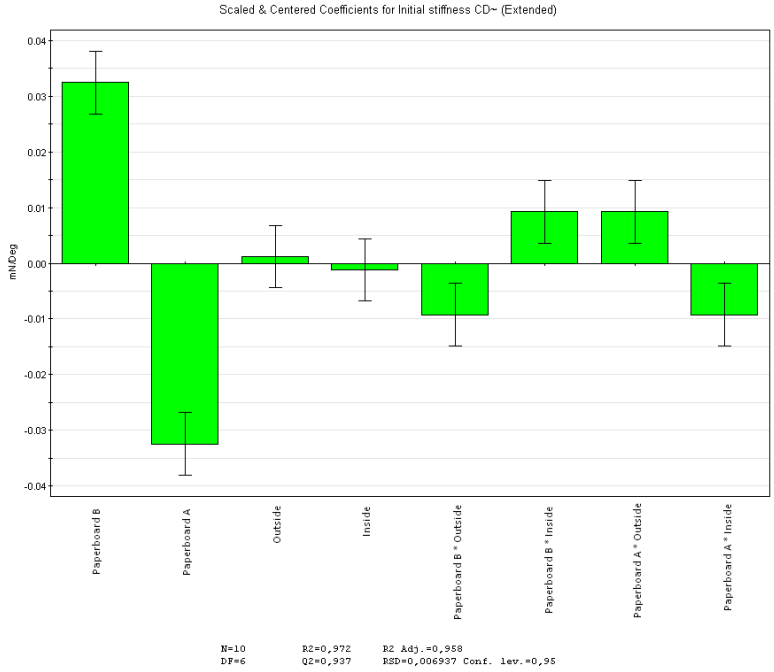

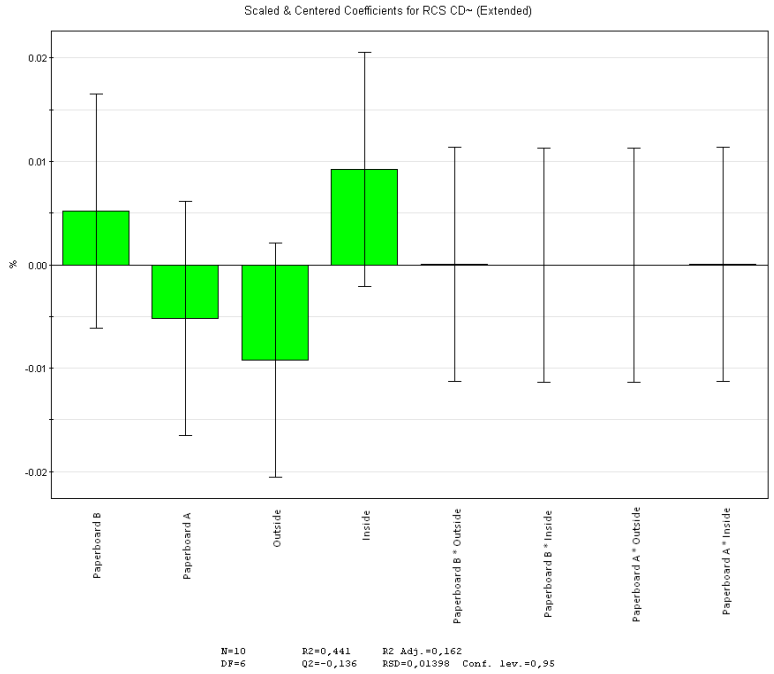

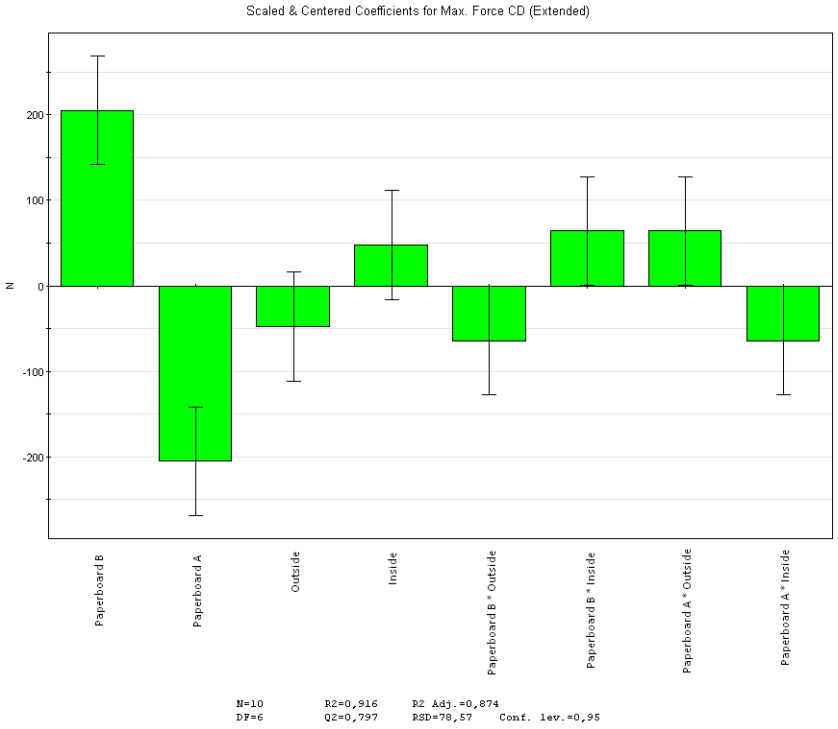
Scaled & Centered Coefficients for Max. Force CD (Extended)
N
200
100
0
-100
-200
Paperboard B
Paperboard A
Outside
Inside
Paperboard B * Outside
Paperboard B * Inside
Paperboard A * Outside
Paperboard A * Inside
N=10 R2=0,916 R2 Adj.=0,874
DF=6 Q2=0,797 RSD=78,57 Conf. lev.=0,95

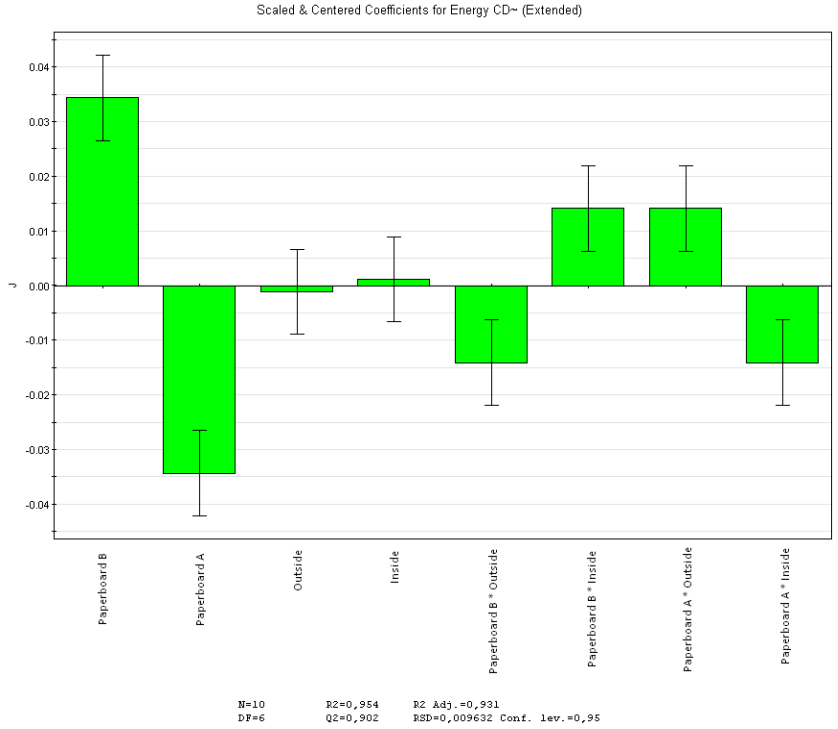
Scaled & Centered Coefficients for Energy CD~ (Extended)
J
0.04
0.03
0.02
0.01
0.00
-0.01
-0.02
-0.03
-0.04
Paperboard B
Paperboard A
Outside
Inside
Paperboard B * Outside
Paperboard B * Inside
Paperboard A * Outside
Paperboard A * Inside
N=10 R2=0,954 R2 Adj.=0,931
DF=6 Q2=0,902 RSD=0,009632 Conf. lev.=0,95

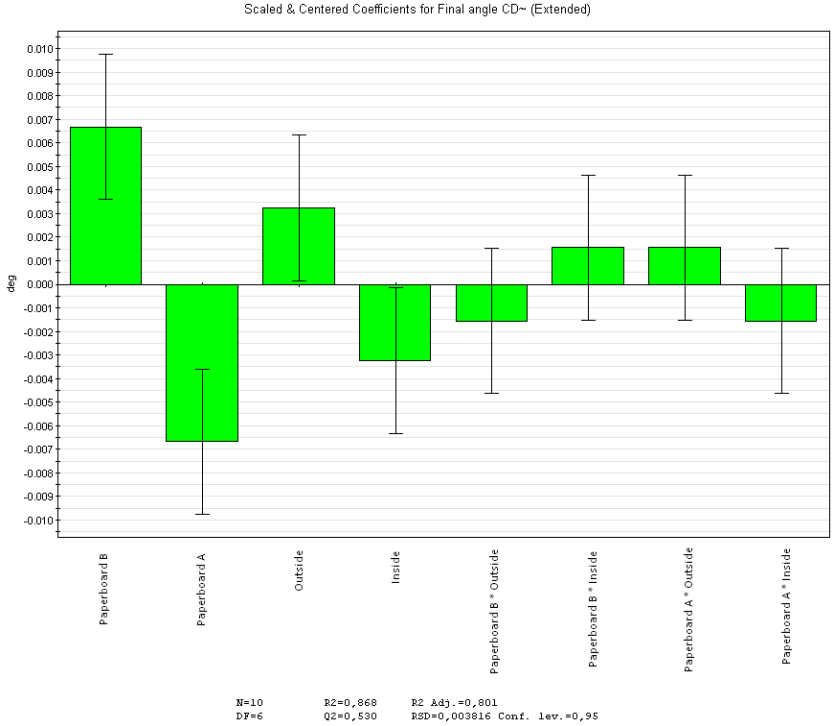
Scaled & Centered Coefficients for Final angle CD~ (Extended)
deg
0.010
0.009
0.008
0.007
0.006
0.005
0.004
0.003
0.002
0.001
0.000
-0.001
-0.002
-0.003
-0.004
-0.005
-0.006
-0.007
-0.008
-0.009
-0.010
Paperboard B
Paperboard A
Outside
Inside
Paperboard B * Outside
Paperboard B * Inside
Paperboard A * Outside
Paperboard A * Inside
N=10 R2=0,868 R2 Adj.=0,801
DF=6 Q2=0,530 RSD=0,003816 Conf. lev.=0,95

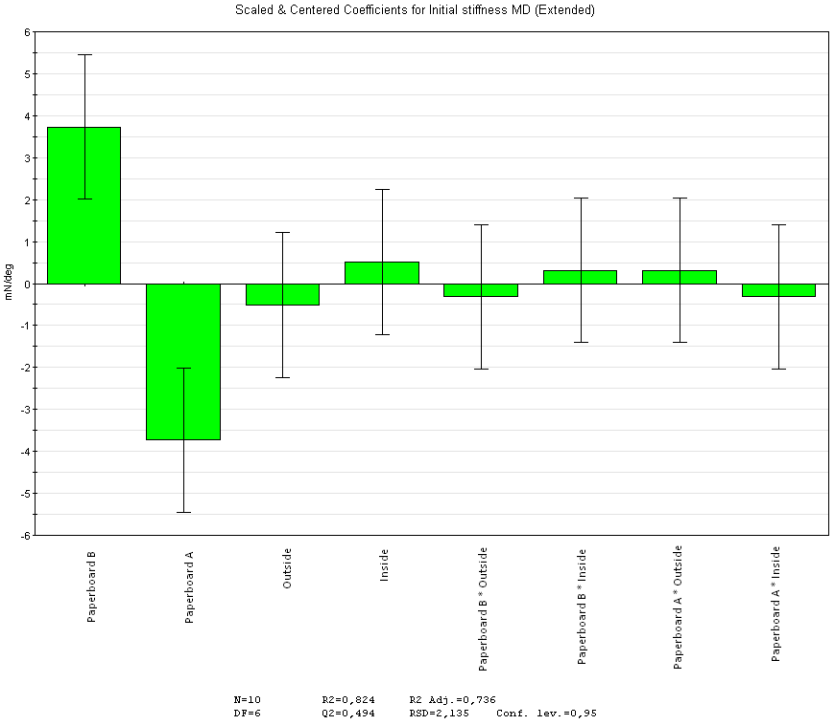
Scaled & Centered Coefficients for Initial stiffness MD (Extended)
mN/deg
6
5
4
3
2
1
0
-1
-2
-3
-4
-5
-6
Paperboard B
Paperboard A
Outside
Inside
Paperboard B * Outside
Paperboard B * Inside
Paperboard A * Outside
Paperboard A * Inside
N=10 R2=0,824 R2 Adj.=0,736
DF=6 Q2=0,494 RSD=2,135 Conf. lev.=0,95

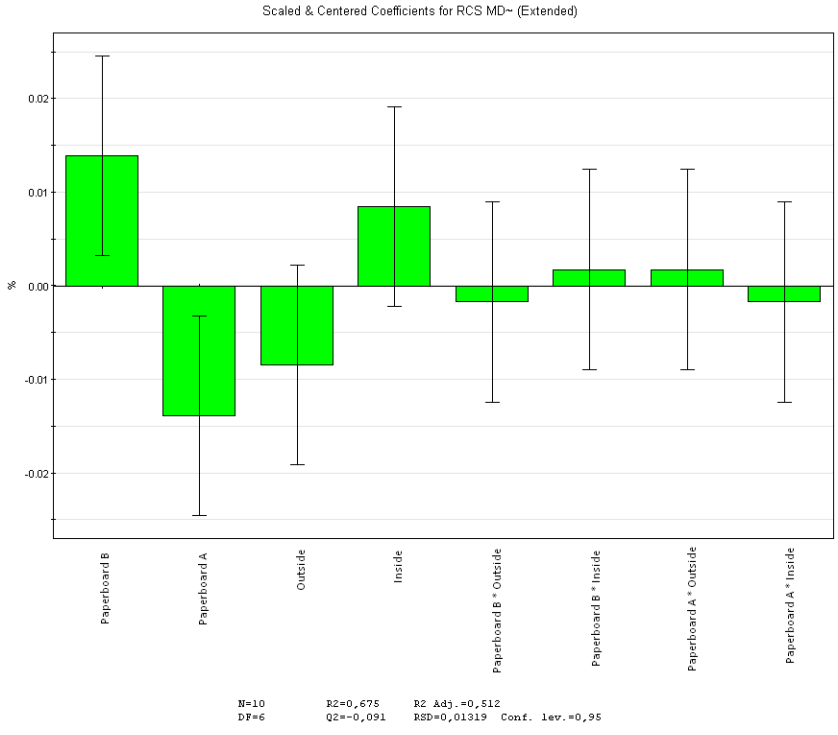
Scaled & Centered Coefficients for RCS MD~ (Extended)
%
0.02
0.01
0.00
-0.01
-0.02
Paperboard B
Paperboard A
Outside
Inside
Paperboard B * Outside
Paperboard B * Inside
Paperboard A * Outside
Paperboard A * Inside
N=10 R2=0,675 R2 Adj.=0,512
DF=6 Q2=-0,091 RSD=0,01319 Conf. lev.=0,95

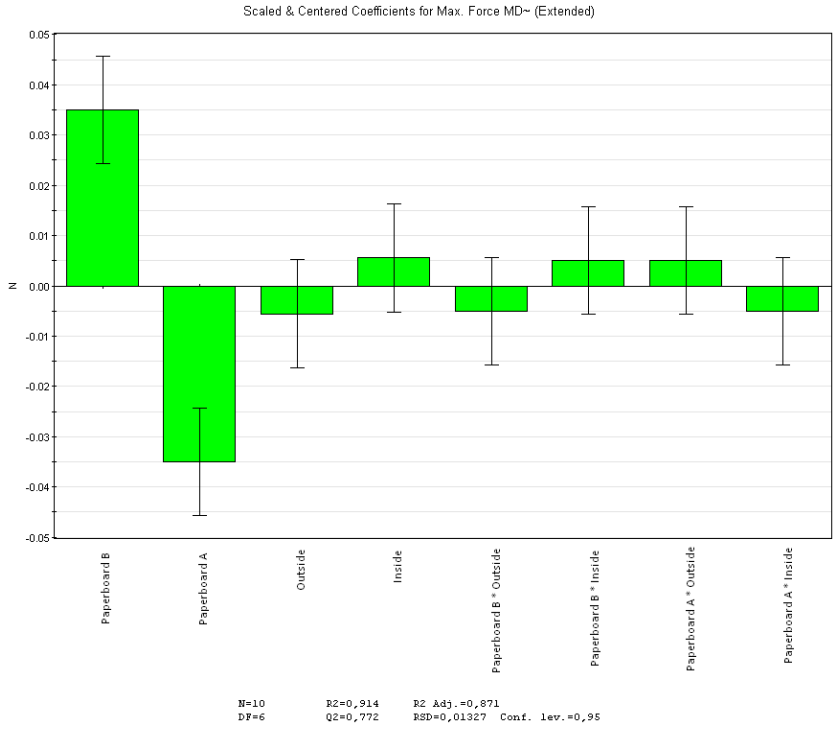
Scaled & Centered Coefficients for Max. Force MD~ (Extended)
N
0.05
0.04
0.03
0.02
0.01
0.00
-0.01
-0.02
-0.03
-0.04
-0.05
Paperboard B
Paperboard A
Outside
Inside
Paperboard B * Outside
Paperboard B * Inside
Paperboard A * Outside
Paperboard A * Inside
N=10 R2=0,914 R2 Adj.=0,871
DF=6 Q2=0,772 RSD=0,01327 Conf. lev.=0,95

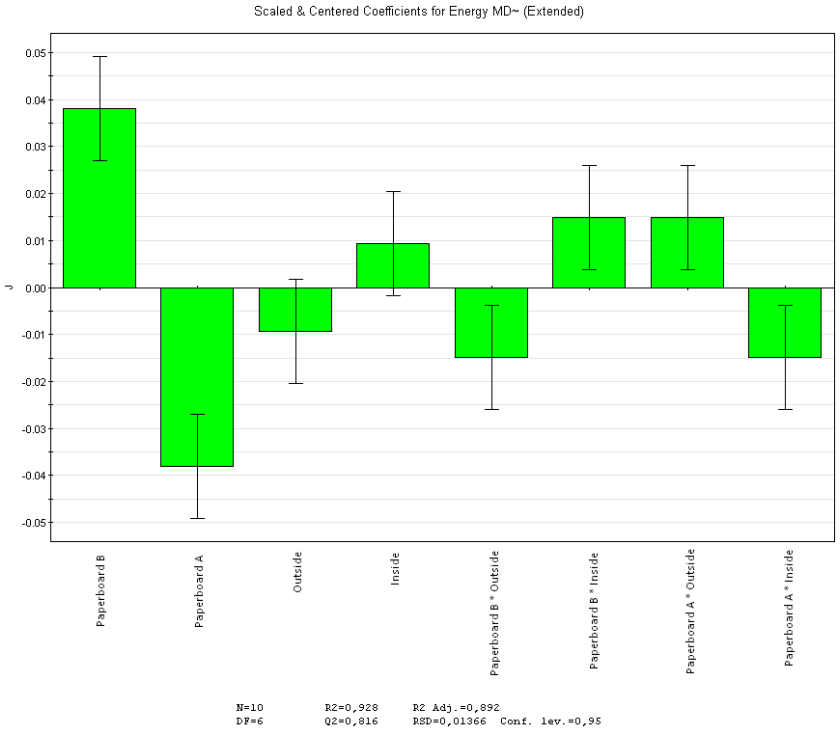
Scaled & Centered Coefficients for Energy MD~ (Extended)
J
0.05
0.04
0.03
0.02
0.01
0.00
-0.01
-0.02
-0.03
-0.04
-0.05
Paperboard B
Paperboard A
Outside
Inside
Paperboard B * Outside
Paperboard B * Inside
Paperboard A * Outside
Paperboard A * Inside
N=10 R2=0,928 R2 Adj.=0,892
DF=6 Q2=0,816 RSD=0,01366 Conf. lev.=0,95

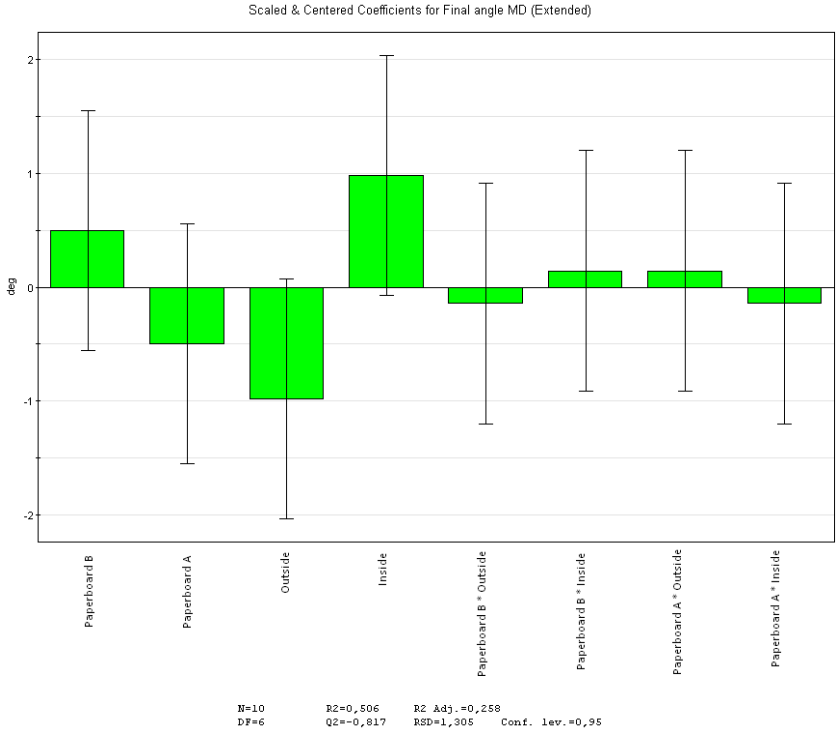
Scaled & Centered Coefficients for Final angle MD (Extended)
deg
2
1
0
-1
-2
Paperboard B
Paperboard A
Outside
Inside
Paperboard B * Outside
Paperboard B * Inside
Paperboard A * Outside
Paperboard A * Inside
N=10 R2=0,506 R2 Adj.=0,258
DF=6 Q2=-0,817 RSD=1,305 Conf. lev.=0,95

Appendix I 250 Base crease pattern: *Comparing inside and outside creasing*

I.1 Paperboard A, paperboard

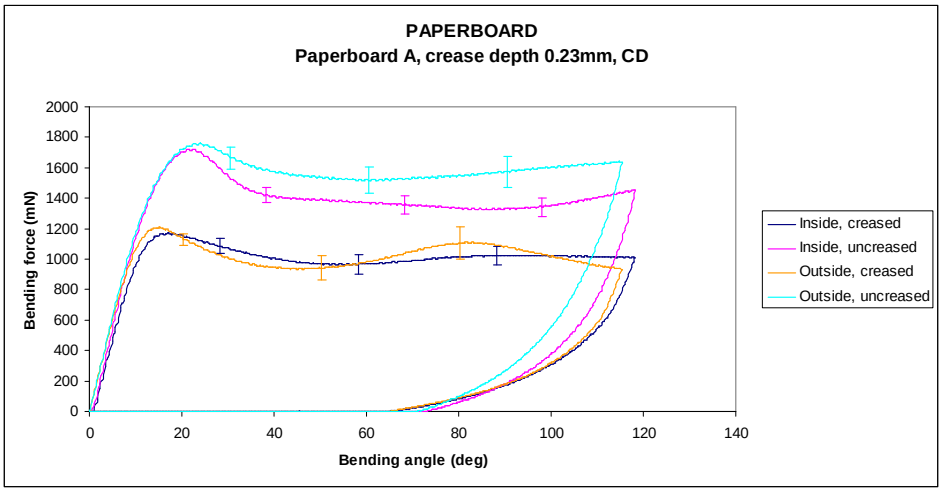

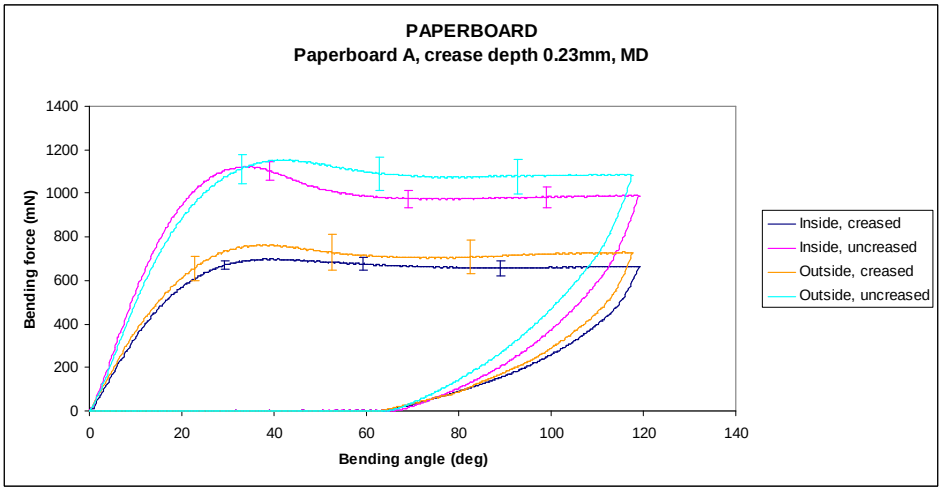

I.2 Paperboard B, paperboard

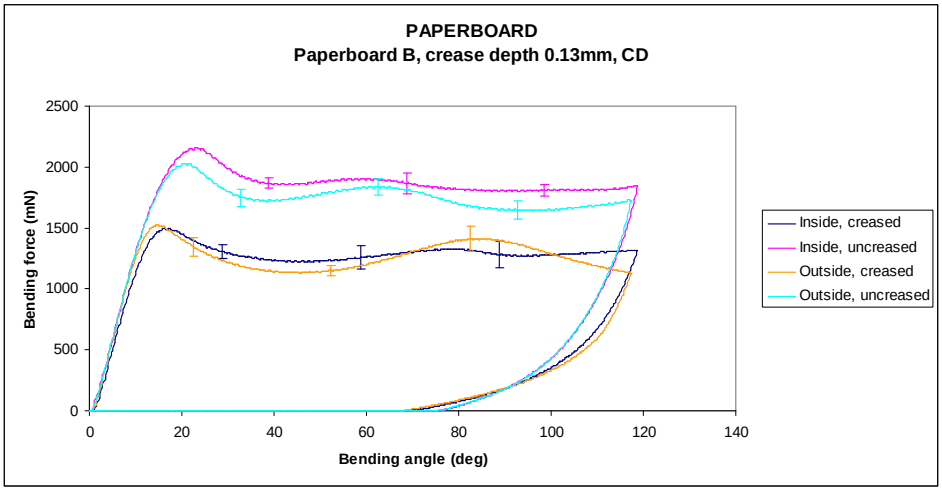

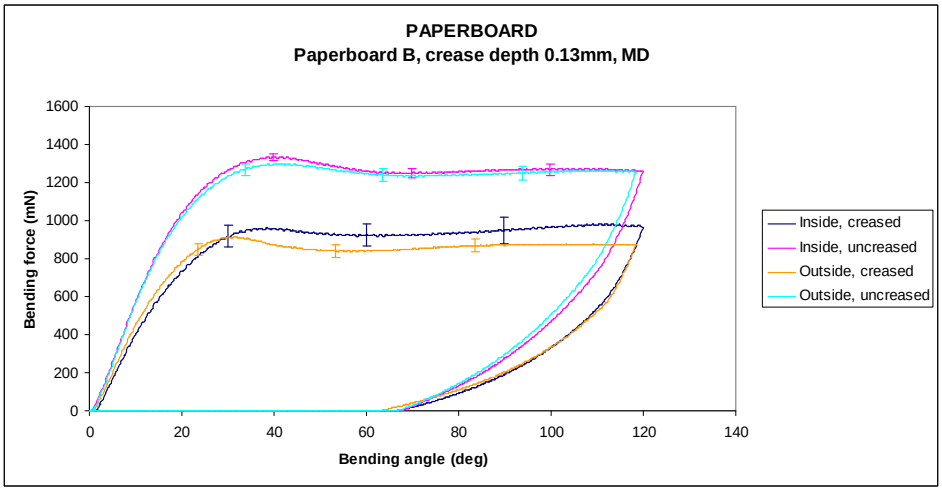

I.3 Paperboard A, packaging material

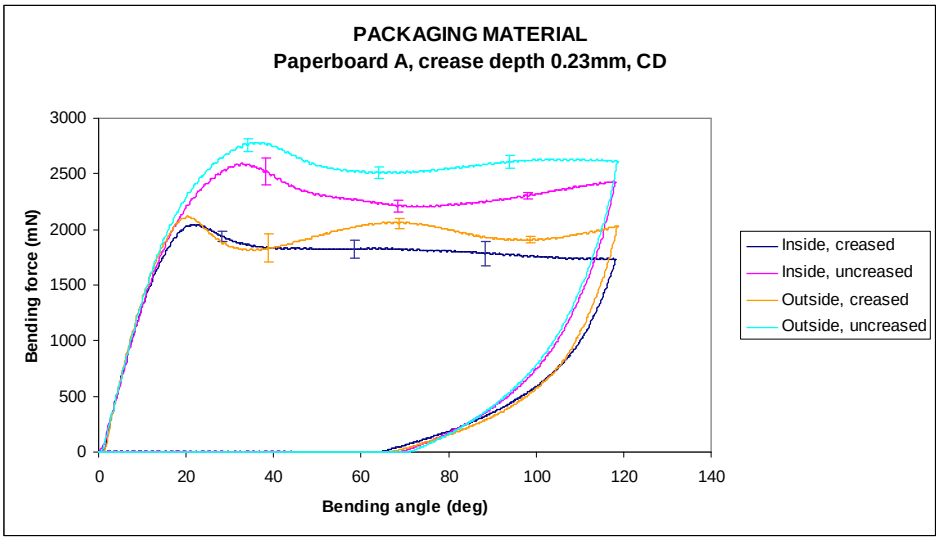

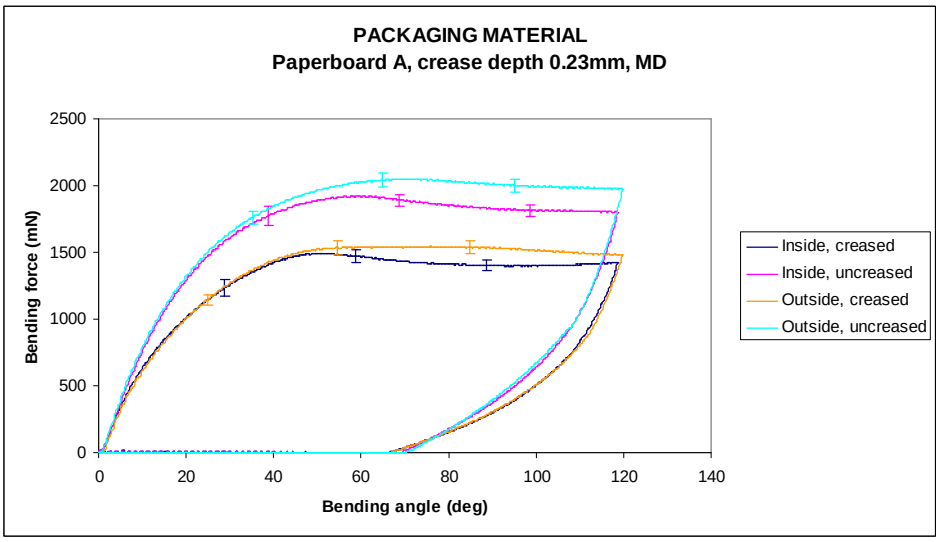

I.4 Paperboard B, packaging material

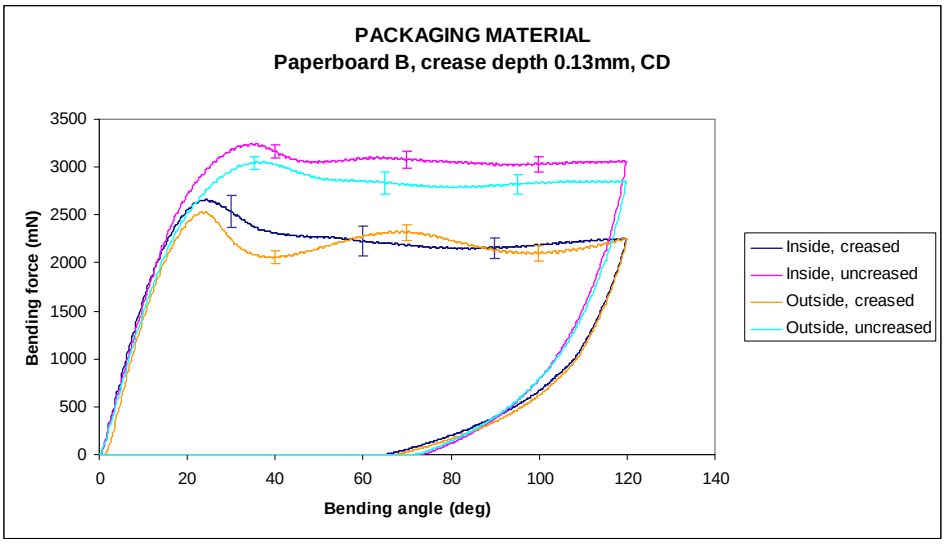

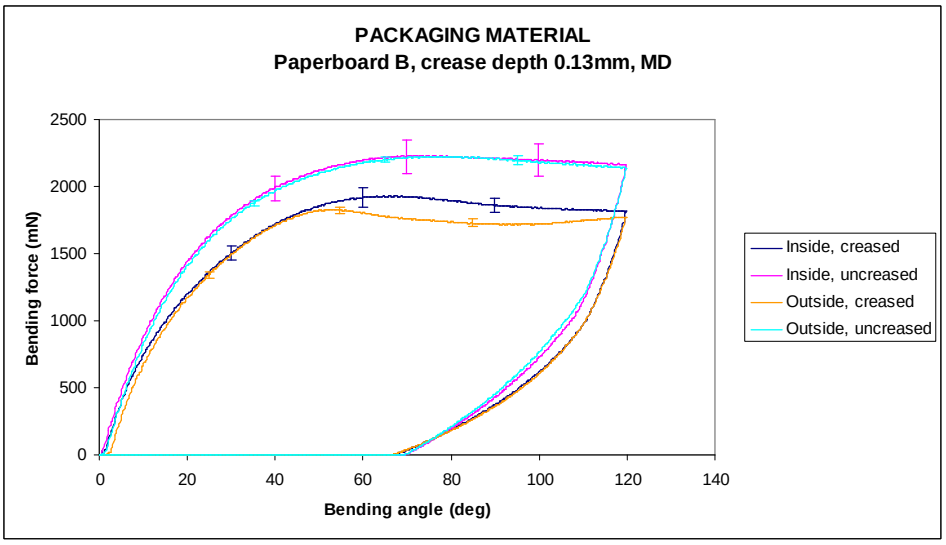

Appendix J Computer simulation: *Material Parameters*

J.1 Continuum model

Table J.1. Elastic parameters for anisotropic material

Ply	E_1	E_2	E_3	G_1	G_2	G_3	v_{12}	v_{13}	v_{23}
Top	7000	80	3000	80	1600	80	0	0.45	0
Middle	4000	60	1750	40	1000	50	0	0.45	0
Bottom	7000	80	3000	80	1600	80	0	0.45	0

Table J.2. Plastic parameters for isotropic material in 45° direction

Ply	σ^0	σ^f	ε^f
Top	25	45	0.010
Middle	15	30	0.015
Bottom	25	45	0.010

Table J.3. Potential for Hills's yield surface

Ply	P_{11}	P_{22}	P_{33}	P_{12}	P_{13}	P_{23}
Top	1	0.5	0.45	0.2	0.2	0.6
Middle	1	0.5	0.45	0.2	0.2	0.6
Bottom	1	0.5	0.45	0.2	0.2	0.6

J.2 Cohesive model

Table J.4. Interface properties

Notation	Interface
K_{md}	1000
K_{cd}	1000
K_{zd}	400
S_{md}	0.35
S_{cd}	1.2
S_{zd}	1.2
δ_f	10
α	0.20

Appendix K Computer simulation: *Comparing simulation models*

To get a good simulation model several models are tried to see which resembles the experimental values best. The original crease model is made by Mikael Nygårds [24] and is used with some smaller changes. Unfortunately due to the fact that MODDE was used when making the experiments the crease depth 0.2mm and the web tension 1.5kN/m with the crease geometry Straight4 are not available from all paperboards. Therefore the simulations are compared with experimental values from the crease geometry of Straight5 but with the crease depth of 0.2mm and web tension 1.5kN/m.

K.1 Creasing

The same crease model is the starting point for all folding models. The male and female dies are both made of rigid bodies. A closer description of the model can be seen under Simulation model in 5.2.1 in the main report.

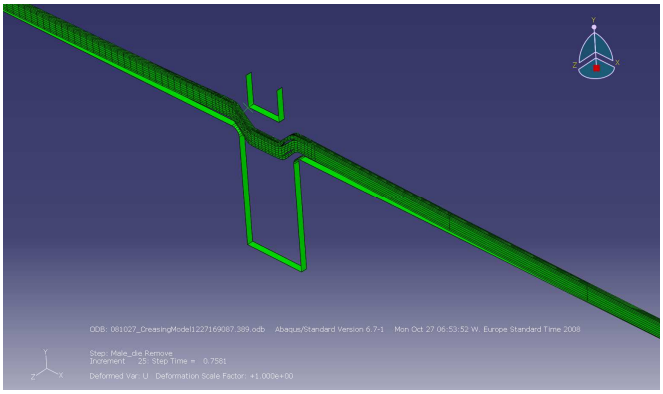

Figure K.1. Creasing of paperboard

The crease curve for all the folding models should hence look as the one below.

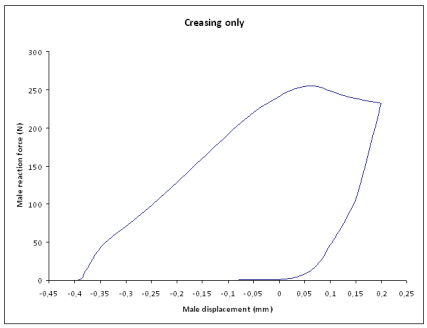

Figure K.2. Creasing of paperboard

K.2 Folding

There are several folding models described below.

K.2.1 Constraints

This is a model where the load cell and the clamp are made with constraints and boundary conditions. The nodes on the right side where the clamp of the L&W are located, are not allowed to move, this is enforced by boundary conditions in any direction or angle. The nodes 10 mm on the left side of the crease where the load cell should be in an L&W are tied to the center of rotation by a constraint. The center of rotation is then the point that rotates and the load cell nodes follow. This model can be folded to 120 deg but will not unfold after the fold.

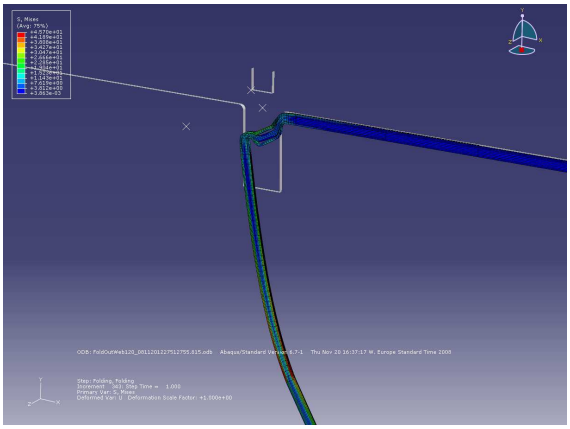

Figure K.03. Folding using constraints and boundary conditions

K.2.2 Moving load cell

In this model the clamp and the load cell are made up of rigid surfaces to look more as the experimental set up. But opposite to the real experimental set up the load cell is here rotating around the center of rotation. The reference point of the load cell is in the center of rotation. This model can only rotate 58 degrees before crashing if one uses full integration on the continuum elements, when using reduced integration the paperboard will fold around the load cell as well as the center of rotation.

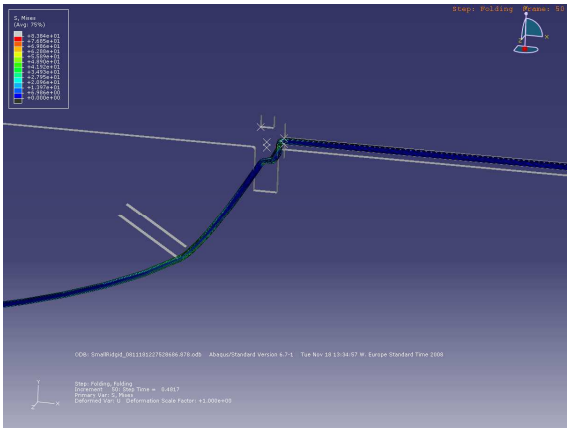

Figure K.4. Folding with a rotating load cell

K.2.3 Moving clamp

This is a similar model to the one above; the clamp and the load cell are both made of rigid bodies. But here the clamp is rotating around the center of rotation. The reference point of the clamp is in the center of rotation. This is the model that looks most like the experimental set up. Here full integration of the element are used, this influences the crease as well as the fold so the bottom right elements have a lot of plastic deformation and would probably crack in real life, this might also be the reason that it has a higher male reaction force in the last part of the crease operation. In this folding model the force in the reference point on the load cell is used instead of the moment in the center of rotation.

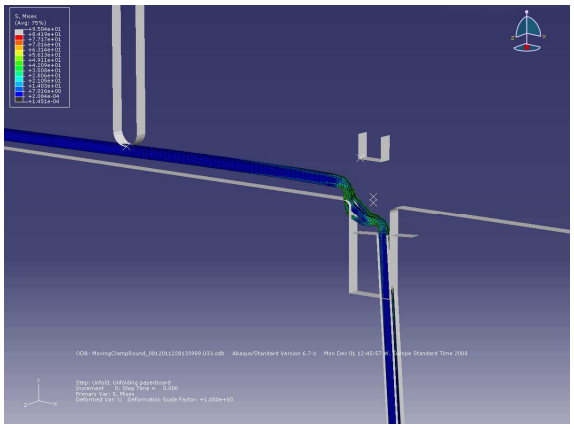

Figure K.5. Folding with a rotating clamp

K.3 Comparing models

Comparing the different simulations to experimental values to see what model works best.

K.3.1 Creasing

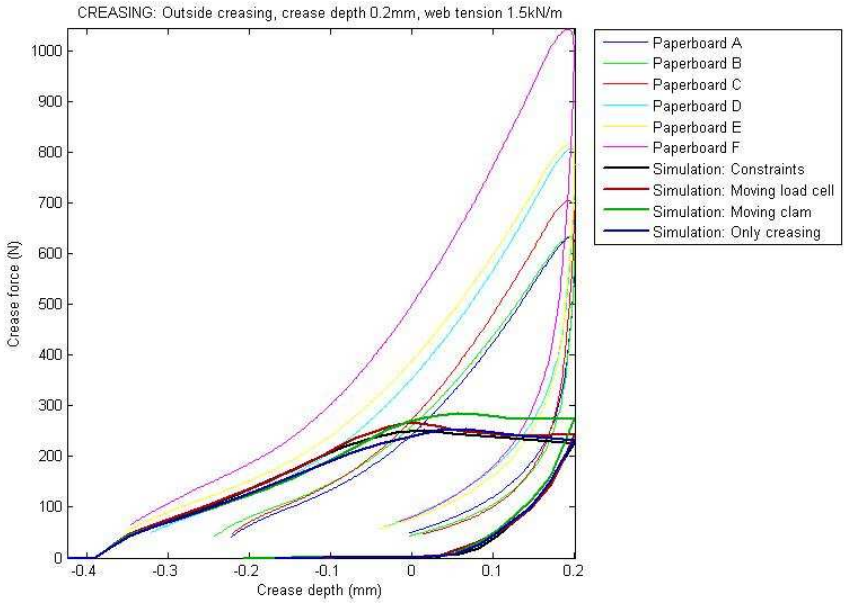

Figure K.6. Comparing creasing of all different paperboards and simulations at the crease depth 0.2mm and the web tension 1.5kN/m.

As can be seen in Figure K.6 all the simulation models are quite similar as they should be since they are all from the same model the only difference is the folding constraints that might affect the creasing. For example moving clamp uses with full integration on the continuum elements, this is possibly the reason for this curve being a bit higher than the other curves. The model corresponds well with earlier tests as can be seen in *Creasing of paperboard* [4] Even though the simulation of the creasing do not show the maximum reaction force they are still good models to predict the behavior and should show if there is a difference between inside and outside creasing.

K.3.2 Folding

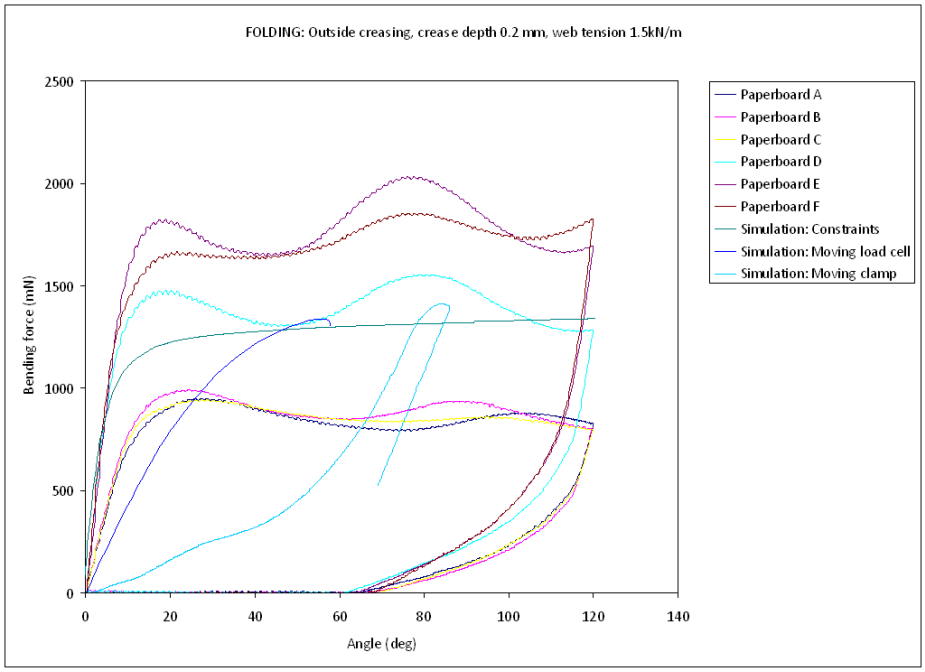

Figure K.7. Comparing folding of all different paperboards and simulations at the crease depth 0.2mm and the web tension 1.5kN/m. Constraints and Moving load cell are both scaled down with 1/10 to fit the plot.

As can be seen in Figure K.7 the simulation that best describes the folding is the one using constraints. Both constraints and moving load cell has to be scaled down with 1/10 to fit the plot. The curve showing the force from the moving clamp is quite different from the others. This might have to do with the fact that the force is taken from the load cell instead of the center of rotation. Between the center of rotation and the load cell there should not be a difference in force, but looking at the curve there seems to some kind of energy loss in the material.

K.4 Conclusion

Use the model with constraints and boundary conditions, since this is the model with the best resemblance to the experimental values.

Appendix L Computer simulation: *Comparing simulation results with experimental results*

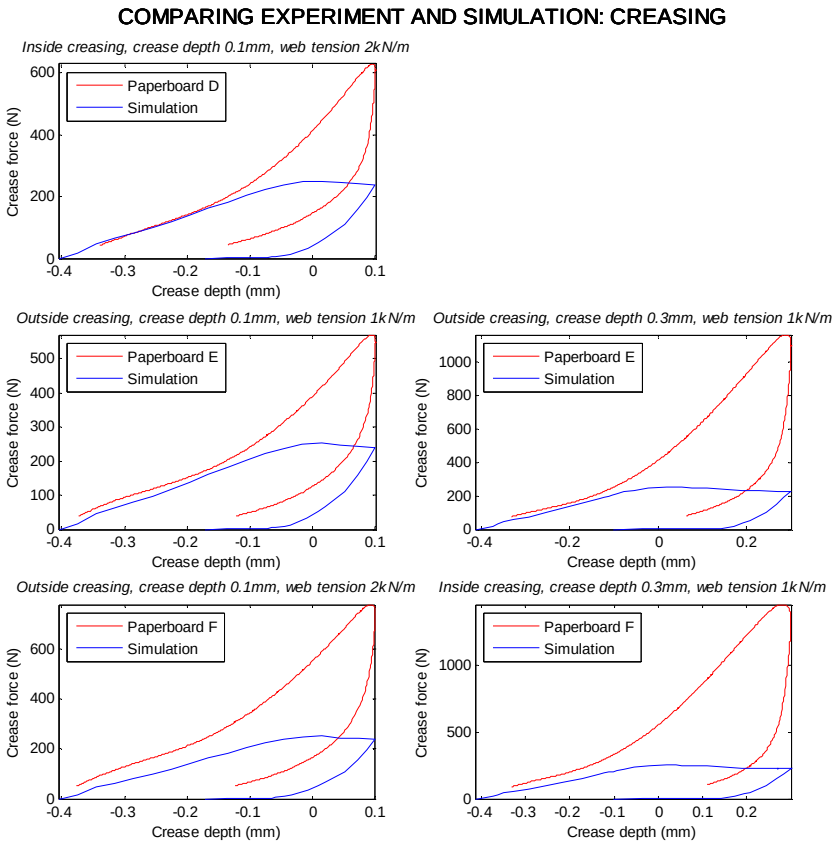

COMPARING EXPERIMENT AND SIMULATION: FOLDING

Inside creasing, crease depth 0.1mm, web tension 2kN/m

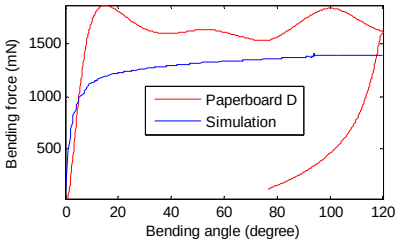

Outside creasing, crease depth 0.1mm, web tension 1kN/m

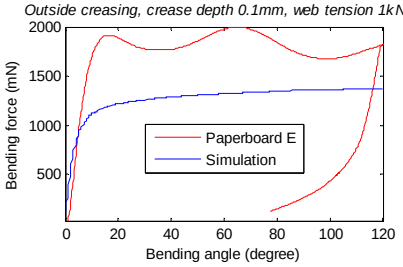

Outside creasing, crease depth 0.3mm, web tension 1kN/m

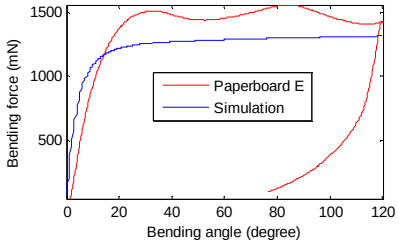

Outside creasing, crease depth 0.1mm, web tension 2kN/m

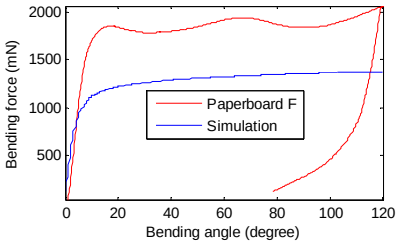

Inside creasing, crease depth 0.3mm, web tension 1kN/m

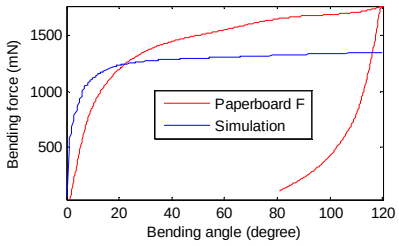

Appendix M Computer simulation: *Comparing Inside vs. Outside creasing*

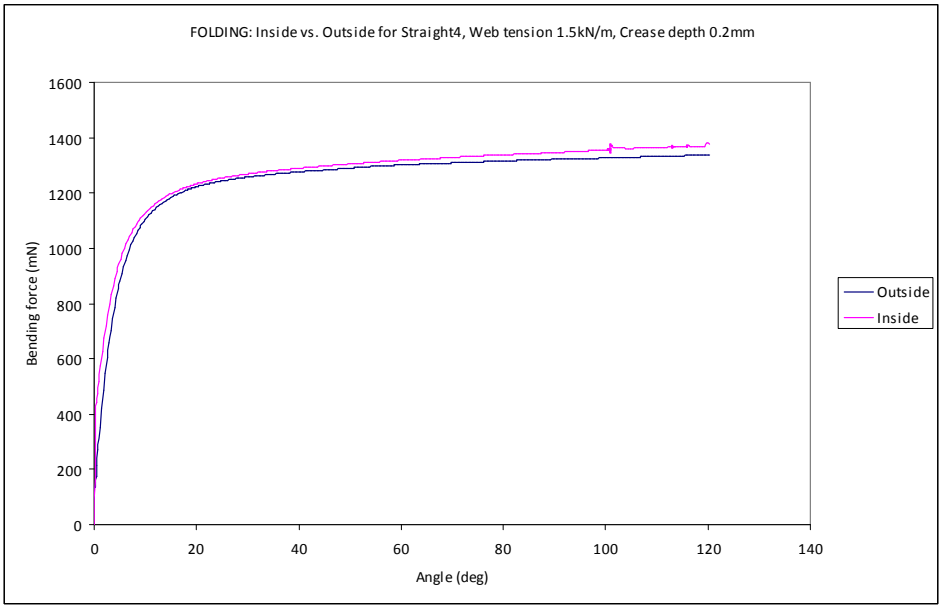

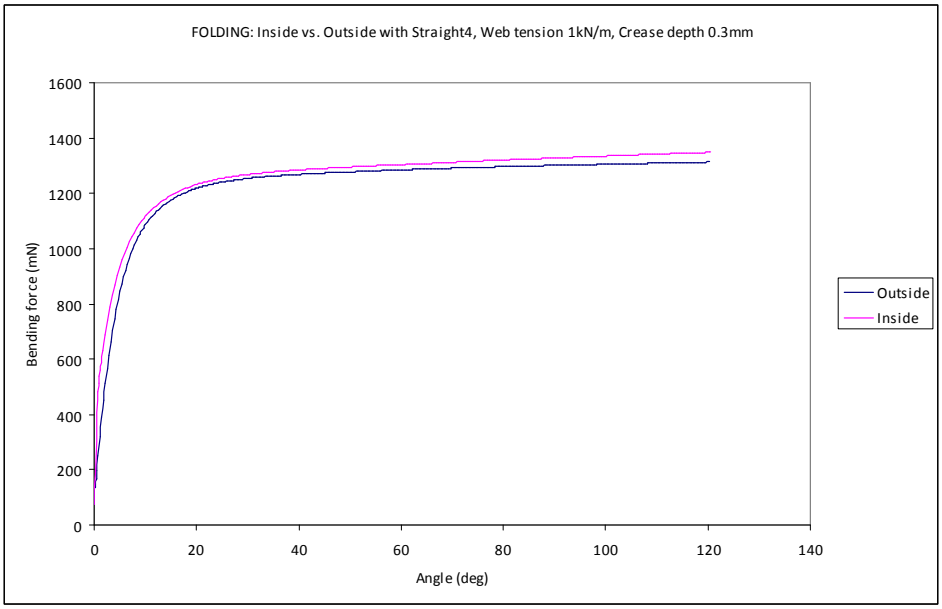

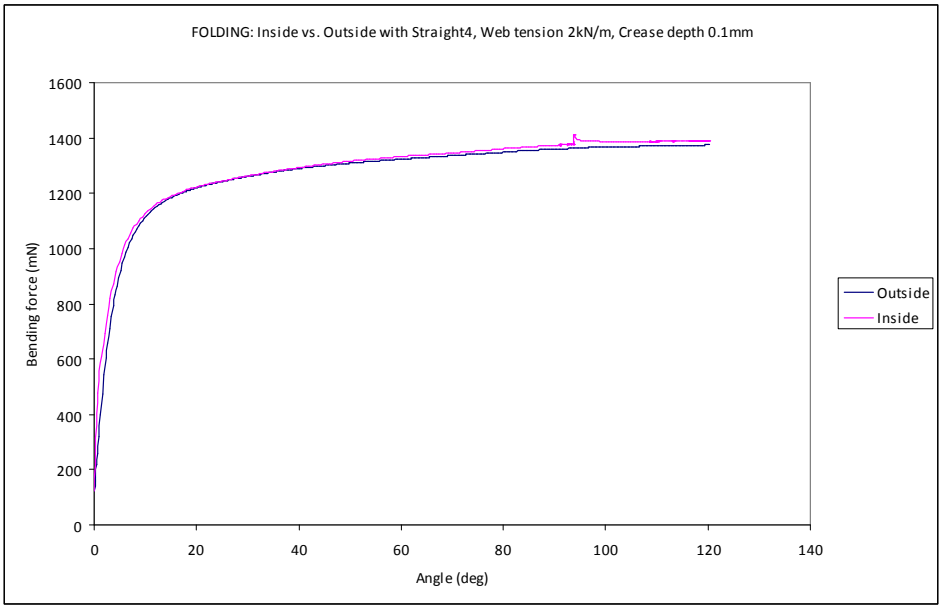
FOLDING: Inside vs. Outside with Straight4, Web tension 2kN/m, Crease depth 0.1mm
Bending force (mN)
1600
1400
1200
1000
800
600
400
200
0
0
20
40
60
80
100
120
140
Angle (deg)
Outside
Inside